Universidade de Aveiro
2016

Departamento de Engenharia de Materiais e Cerâmica

MOHAMMADMEHDI SHABANI

Tribossistemas de revestimentos multicamada de diamante CVD micro/nanocristalino

Tribosystems based on multilayered micro/nanocrystalline CVD diamond coatings

Universidade de Aveiro
2016

Departamento de Engenharia de Materiais e Cerâmica

MOHAMMADMEHDI SHABANI

Tribossistemas de revestimentos multicamada de diamante CVD micro/nanocristalino

Tribosystems based on multilayered micro/nanocrystalline CVD diamond coatings

Tese apresentada à Universidade de Aveiro para cumprimento dos requisitos necessários à obtenção do grau de Doutor em Ciência e Engenharia de Materiais, realizada sob a orientação científica do Doutor Rui Ramos Ferreira e Silva, Professor Associado do Departamento de Engenharia de Materiais e Cerâmica da Universidade de Aveiro e co–orientação do Doutor Filipe José Alves de Oliveira, Investigador Principal do Laboratório Associado CICECO–Instituto de Materiais de Aveiro, da Universidade de Aveiro.

Apoio financeiro da FCT (bolsa MULTIDIACOAT–PTDC/EME–TME/100689/2008) e projeto Pest–C/CTM/LA0011/2013.

To My Family

o júri

presidente

Professor Doutor José Carlos Esteves Duarte Pedro
professor catedrático da Universidade de Aveiro

Professor Doutor Albano Augusto Cavaleiro Rodrigues de Carvalho
professor catedrático da Faculdade de Ciências e Tecnologia da Universidade de Coimbra

Professor Doutor Rui Ramos Ferreira e Silva
professor associado da Universidade de Aveiro

Professor Doutor José Manuel Ramos Gomes
professor associado da Escola de Engenharia da Universidade do Minho

Professor Doutor Victor Fernando Santos Neto
professor auxiliar convidado da Universidade de Aveiro

Professor Doutor Cristiano Simões Abreu
professor adjunto do Instituto Superior de Engenharia do Porto

acknowledgments

Firstly, I would like to express my special appreciation and gratitude to my supervisor Prof. Rui Silva and co–supervisor Dr. Filipe Oliveira for the continuous support and their patience during my PhD study. I am thankful to FCT (Fundação para a Ciência e a Tecnologia) for financial support of MULTIDIACOAT–PTDC/EME–TME/100689/2008 project and also the strategic project (PEST–C/CTM/LA0011/2013), financed by national funds through FCT/MCTES (PIDDAC) and co–financed by the European Regional Development Fund (ERDF) through the COMPETE–Operational Programme Competitiveness Factors. Many thanks to Dr. Cristiano Abreu and Prof. José Gomes for the tribology facilities in University of Minho. Also many thanks to Dr. João Miguel Carrapichano for the sealing tests. I am grateful to my colleagues Dr. Ermelinda Salgueiredo, Dr. Miguel Ângelo Neto, Dr. Flávia Almeida and Dr. Diogo Mata who helped me during my PhD study. I am thankful to Dr. António José Fernandes and the group of Prof. Florinda Costa for Raman measurements in the Physics Department of Aveiro University. I am grateful to DURIT company: the owner, Dr. Joaquim Sacramento, Dr. Eduardo Soares and the company staff for the machining process. Thanks to the colleagues in Electron Microscopy Service, Marta Ferro and Bruno Almeida for their training and the technicians of Materials and Ceramic Engineering Department of Aveiro University for their assistance. Last but not the least, I am grateful to my family for all the supports during my life.

palavras–chave

Multicamadas; HFCVD; Diamante micro/nanocristalino; Nitreto de silício; Tribologia; Ferramentas de corte; Anéis para empanques mecânicos

resumo

A combinação das características do diamante microcristalino (MCD) e nanocristalino (NCD), tais como elevada adesão do MCD e a baixa rugosidade superficial e baixo coeficiente de atrito do NCD, é ideal para aplicações tribológicas exigentes. Deste modo, o presente trabalho centrou–se no desenvolvimento de revestimentos em multicamada MCD/NCD. Filmes com dez camadas foram depositados em amostras de cerâmicos de Si_3N_4 pela técnica de deposição química em fase vapor assistida por filamento quente (HFCVD). A microestrutura, qualidade do diamante e adesão foram investigadas usando técnicas como SEM, AFM, espectroscopia Raman, DRX, indentação Brale e perfilometria ótica 3D. Diversas geometrias para aplicações distintas foram revestidas: discos e esferas para testes tribológicos à escala laboratorial, e para testes em serviço, anéis de empanques mecânicos e pastilhas de corte para torneamento.

Nos ensaios tribológicos esfera–sobre–plano em movimento recíproco, sob 10–90% de humidade relativa (RH), os valores médios dos coeficientes de atrito máximo e em estado estacionário são de 0,32 e 0,09, respetivamente. Em relação aos coeficientes de desgaste, observou–se um valor mínimo de cerca de $5{,}2\times10^{-8}$ $mm^3N^{-1}m^{-1}$ para valores intermédios de 20–25% de RH. A humidade relativa tem um forte efeito sobre o valor da carga crítica que triplica a partir de 40 N a 10% RH para 120 N a 90% de RH. No intervalo de temperaturas 50–100 ° C, as cargas críticas são semelhantes às obtidas em condições de baixa RH (~10–25%).

A vida útil das ferramentas com revestimento de dez camadas alternadas MCD/NCD e 24 µm de espessura total no torneamento de um compósito de matriz metálica Al– 15 vol% Al_2O_3 (Al–MMC) é melhor do que a maioria das ferramentas de diamante CVD encontradas na literatura, e semelhante à maioria das ferramentas de diamante policristalino (PCD). A formação de cratera ocorre por desgaste sucessivo das várias camadas, atrasando a delaminação total do revestimento de diamante do substrato, ao contrário do que acontece com os revestimentos monocamada.

Os anéis de empanque testados com biodiesel apresentaram coeficientes de desgaste ($4{,}1\text{x}10^{-10}$ $mm^3N^{-1}m^{-1}$) duas ordens de grandeza menores do que em ensaios esfera–sobre–plano em movimento recíproco ($k = 5{,}0\text{x}10^{-8}$ $mm^3N^{-1}m^{-1}$), mas não foi possível obter vedação completa devido a sobreaquecimento do fluido. Esta condição foi obtida com água sob pressão, para condições P.V na gama 0,72–5,3 $MPa.ms^{-1}$. Um coeficiente de atrito em estado estacionário de ~ 0,04 e um valor de coeficiente de desgaste de $6{,}0\text{x}10^{-10}$ $mm^3N^{-1}m^{-1}$, característico de um regime desgaste ultra–suave, revelam o alto desempenho deste tribossistema.

keywords

Multilayer; HFCVD; Micro/nanocrystalline diamond; Silicon nitride; Tribology; Cutting tools; Mechanical seal rings

abstract

The combination of the characteristics of microcrystalline diamond (MCD) and nanocrystalline diamond (NCD) varieties, such as high adhesion of MCD and low surface roughness and low friction coefficient of NCD, is ideal for highly–demanding tribological applications. The main objective of this study was thus the development of multilayered MCD/NCD coatings for such purpose. Single layer and tenfold multilayer coatings were grown onto Si_3N_4 ceramic samples by the hot–filament CVD (HFCVD) process and their microstructure, diamond quality and adhesion were investigated using SEM, AFM, Raman spectroscopy, XRD, Brale indentation and 3D optical profilometry. Several geometries for distinct applications were then coated: discs and balls for lab–scale tribological testing, mechanical seal rings and cutting inserts for in–service testing.

For the ball–on–flat reciprocating tests in the 10–90% relative humidity (RH) range the average values of the maximum and steady–state friction coefficients are 0.32 and 0.09, respectively. Regarding the wear coefficient of the discs, a valley–shaped evolution is observed within the same RH range, with a minimum of about 5.2×10^{-8} $mm^3N^{-1}m^{-1}$. Humidity has a strong effect on the value of the critical load that triples from 40 N at 10% RH to 120 N at 90% RH. In the 50–100 °C range the critical loads are similar to those attained under dry conditions (≤ 25% RH).

The tool life of a 24 µm thick tenfold multilayered MCD/NCD coated insert in the turning of an Al–15 vol.% Al_2O_3 metal matrix composite (Al–MMC) is better than most reported CVD diamond systems, behaving as well as most PCD tools. Crater wear occurs by successive wear of the layers, delaying total delamination of the diamond coating from the substrate, unlike what would happen with monolayer coatings.

Under biodiesel lubrication seal rings present wear coefficients ($4.1x10^{-10}$ $mm^3N^{-1}m^{-1}$) two orders of magnitude lower than the reciprocating sliding ball–on–flat experiments ($k = 5.0x10^{-8}$ $mm^3N^{-1}m^{-1}$), but no full sealing was possible due to overheating of the fluid. This condition was only attained with pressurized water, for P.V conditions in the range 0.72–5.3 $MPa.ms^{-1}$. A steady state friction coefficient value of ~0.04 and a wear coefficient value of $6.0x10^{-10}$ $mm^3N^{-1}m^{-1}$, characteristic of an ultra–mild wear regime, reveal the high performance of this tribosystem.

Contents **Page**

List of Figures **Page**

List of Tables **Page**

Nomenclature

AFM – atomic force microscopy

Al–MMC – Aluminum metal matrix composite

BOD – ball–on–disc

BOF – ball–on–flat

c–BN – cubic boron nitride

CFRP – carbon fiber reinforced polymers

CIP – cold isostatic pressing

CMCs – ceramic matrix composites

COF – coefficient of friction

CVD – chemical vapor deposition

DOC – depth of cut

DLC – diamond like carbon

EDS – energy dispersive X–ray spectroscopy

G band – crystalline graphite

GFRP – glass fiber reinforced polymers

HFCVD – hot filament chemical vapor deposition

HV – Vickers hardness

IF – indentation fracture

MCD – microcrystalline diamond

ML – multilayer

MMCs – metal matrix composites

NCD – nanocrystalline diamond

PCD – polycrystalline diamond

PMCs – polymer matrix composites

P.V – effective pressure× linear velocity capability

PVD – physical vapor deposition

RMS – root mean square

SEM – scanning electron microscopy

SENB – single edge notch beam

SEPB – single edge pre–cracked beam

SL– single layer

XRD – X–ray diffraction

UNCD – ultrananocrystalline diamond

f – feed rate

F – applied load for ring–on–ring configuration

F_f – feed force

F_c – cutting force

F_{DOC} – depth–of–cut force

k – wear coefficient

K_{1C} – fracture toughness

L – working distance

P – effective pressure

r – ball radius

R_a – mean surface roughness

RH – relative humidity

R_q – root mean square

T – temperature

T_{fil} – filament temperature

T_{sub} – substrate temperature

v – cutting speed

V – linear velocity

W – applied load for ball–on–flat configuration

W_c – critical load

X – sliding distance

μ – friction coefficient

ω – angular velocity

Introduction

In this introduction the motivation and objectives of the PhD study are presented. The thesis organization is also outlined.

Advances in techniques for the deposition and processing of coatings have allowed the design and manipulation of materials with unique properties that are often unreached in the bulk form. High–performance superhard diamond coatings offer great potential for tribological applications due to their superior characteristics, not typically found in conventional coatings. The protection they afford can improve the lifetime of components and they have attracted great interest for industrial applications.

During the last decades, interest in producing high–quality, adherent and smooth diamond coatings on metallic and ceramic substrates for use in various engineering applications has been overwhelming. The reason for the interest are the properties of diamond, i.e. high hardness, stiffness, and thermal conductivity, as well as biocompatibility and inertness in corrosive media. Hot–filament CVD process (HFCVD), one of the most important technological developments in the past decades, makes possible the production of high–quality diamond coatings to enhance the wear and abrasion performance of the coated substrates.

The combination of the characteristics of microcrystalline diamond (MCD) and nanocrystalline diamond (NCD) varieties, such as high adhesion of MCD and low surface roughness and low friction coefficient of NCD, is ideal for highly–demanding tribological applications. The present PhD study relates to the development of tribosystems based on multilayer MCD/NCD coatings grown on silicon nitride (Si_3N_4) ceramic substrates using HFCVD process. Several geometries for distinct applications were coated: discs and balls for lab–scale tribological testing; mechanical seal rings and cutting inserts for in–service testing.

The present PhD thesis is composed of six distinct chapters. The first chapter describes the state of the art on the tribological performance of CVD diamond coatings and their application in machining of metal matrix composite (MMC) materials and as mechanical seal rings in industrial equipment to prevent the leakage of fluids.

The second chapter includes the details about: (i) fabrication and surface pre–treatments of Si_3N_4 ceramic substrates; (ii) deposition of micro– and nanocrystalline diamond films via a home–made HFCVD reactor as well as their main microstructural and physical characterization techniques; (iii) experimental details on the tribological tests of diamond–coated Si_3N_4 discs and balls and of the Si_3N_4 mechanical seal rings; (iv) Si_3N_4 cutting inserts fabrication, diamond coating and parameters of the turning tests of an Al–based metal matrix composite (Al–MMC) workpiece.

The third chapter contains the experimental results about Si_3N_4 ceramic substrate characterization and of the as–deposited diamond coatings by means of scanning electron microscopy (SEM), Raman spectroscopy, X–ray diffraction (XRD). atomic force microscopy (AFM) and adhesion assessment by Brale indentation testing.

The fourth chapter deals with the experimental results and discussion about the tribological behavior of multilayered MCD/NCD coatings in self–mated configuration where the effect of temperature and relative humidity are evaluated. In addition, the tribological behavior of the diamond coatings under biodiesel lubricated conditions is studied.

The fifth chapter covers the results and discussion about of the selected applications: turning inserts and mechanical seal rings. The first part of this chapter covers the machining performance in the turning of an Al–15%Al_2O_3 metal matrix composite (MMC). In the second part, the tribological behavior of mechanical seal rings under biodiesel lubrication and the full sealing conditions of pressurized water are described.

Finally, the sixth chapter includes the main conclusions of the present PhD study as well as suggestions of future work.

Chapter 1

Bibliographic overview

The literature review of this PhD study is here presented. This chapter starts with a brief introduction about hard and superhard coating materials. Then, the tribological performance of CVD diamond coatings is overviewed. The next part is about the application of CVD diamond coatings in machining, namely of metal matrix composite (MMC) materials. The last part of this chapter is devoted to another application of CVD diamond coatings: mechanical seals widely used in industrial pumps, compressors and mixers to prevent the leakage of fluids.

1.1. Hard and superhard coatings

In the field of coatings, hard (20 GPa < Vickers hardness < 40 GPa) and superhard (Vickers hardness > 40 GPa) coatings have received large attention because of a variety of applications for protection of bulk materials and components. Materials protection by hard coatings is one of the most important means of materials performance improvement. Hard materials for coatings can be categorized in three main groups depending on the chemical bonding characteristics: metallic hard materials (carbides, borides, and nitrides of transition metals), ionic hard materials (oxides of Al, Zr, Ti), and covalent hard materials (carbides, borides and nitrides of Al, Si, B, and also diamond). Among these, cubic boron nitride (c–BN), diamond–like carbon (DLC) and diamond are known as superhard materials [1]. Figure 1 shows a distribution of hard coating materials in terms of chemical bonding.

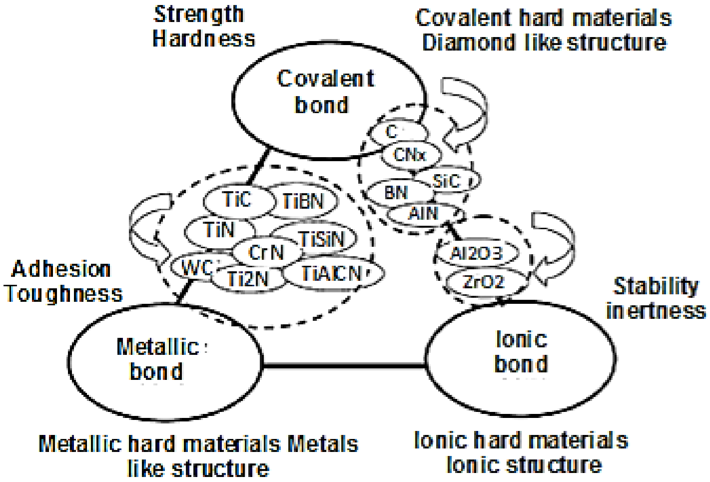

Figure 1. Hard materials categories in terms of chemical bonding [1].

The most important feature of hard protective coatings is to decrease wear and, as a result, increase the tool lifetime. So it is important to know which mechanism cause wear (abrasion, adhesion, corrosion, high temperature, etc.) in order to find the adequate coating for the desired process. A combination of well–defined coating properties can provide possibilities for new technical processes, e.g. low coefficient of friction and resistance against high temperatures enables dry machining without use of cooling–lubricating liquids.

Development of hard protective coatings started in early 1960 with chemical (CVD) and physical (PVD) vapour deposition techniques. Some PVD forms which are being used nowadays involve magnetron sputtering, evaporation by laser, cathode arc and electron beam. Depositions are made under very low level vacuum ($<10^{-6}$ torr), substrate temperature varying from room temperature up to 500°C, and coating thickness of a few micrometres. Transition metal nitrides, like titanium nitride (TiN), titanium aluminium nitride (TiAlN), chromium nitride (CrN) and zirconium nitride (ZrN), are among the most useful materials used as protective coatings due to their high hardness, wear resistance and thermal stability. PVD techniques represent a very interesting and convenient route to realize and optimize multilayered structures of such compounds with a reliable control of thin film thickness, microstructure and composition,

Since the late 1960s, CVD technologies have advanced from single layer to multilayer versions combining TiN, TiCN, TiC, Al_2O_3, DLC and diamond, among others. CVD coatings combine high temperature and medium temperature processes in complex cycles that produce excellent wear resistant coatings [2]. Aiming at coating optimization for mechanical applications, both coating material (e.g., nitride, carbide, oxide etc.) and coating structure (single layer, multilayer, gradient composition layer etc.) have to be considered [3].

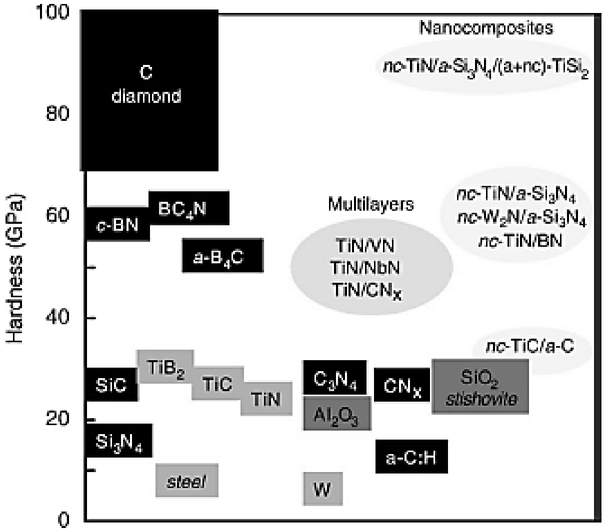

Figure 2. Schematic representation of the different classes of hard materials: covalent, metallic, oxide type and nanocomposites [4].

With advances in the last two decades, CVD and PVD processes have been widely used to deposit hard, super hard, soft and combining hard/soft coating materials for applications such as dies, cutting tools and biocompatible devices used in medical applications [5]. Figure 2 shows the schematic representation of the different classes of hard materials as a function of their hardness.

1.2. Tribology of multilayered micro and nanocrystalline CVD diamond coatings

The historical development for tribological films and solid lubricant coatings is represented in Figure 3 [6]. Important aspect besides the material and production process that can influence on wear and friction behaviour of tribological coatings is the design of the coatings. It can differ from single component to multicomponent multilayer, through nanostructure, superlattice, and gradient to adaptive coatings.

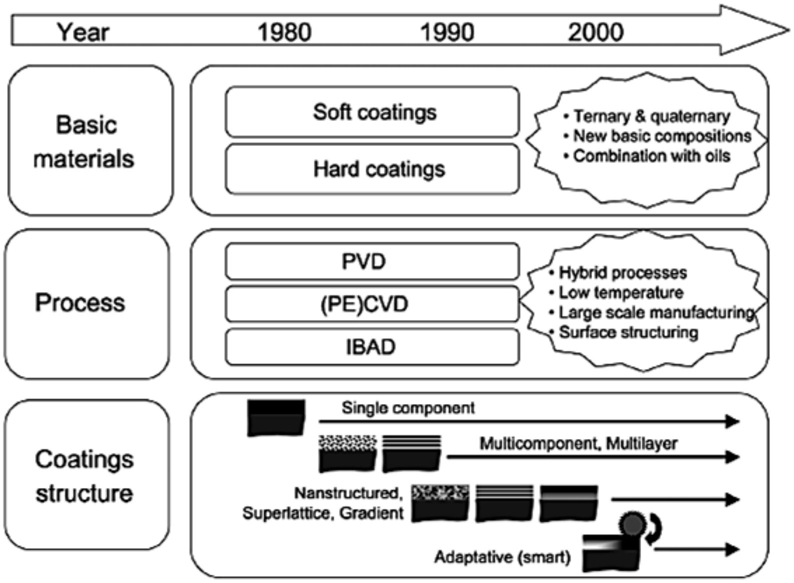

Figure 3. Historical development of tribological coatings and solid lubricant films [6].

Single component tribological coatings belong to the first generation of tribological coatings, most of them obtained by PVD and CVD. Multilayer and multicomponent of metal/ceramic and ceramic/ceramic tribological coatings belong to the second generation of tribological coatings such as Ti/TiN and DLC/WC, TiC/TiN. Third generation belongs to graded, nanostructured and superlattice type coatings such as TiAlN with the addition of yttrium or chromium and WC/DLC/WS_2 nanocomposite coatings exhibiting self–adaptation [6].

Concerning multilayer systems, multilayers can be divided as isostructural and non–isostructural depending on whether the constituent materials have the same structure or not [7]. Non–isostructural multilayer coatings combine materials which form thermodynamically stable interfaces, e.g. metal/ceramics [8] and nitride/nitride multilayers [9]. For isostructural multilayer coatings, epitaxial accommodation at the interfaces leads to the growth of superlattice when the individual layer thickness is of the size of lattice dimension. Then the coating is considered as a new material as demonstrated for AlN/CrN [9]. By applying multilayer tribological coatings on substrate surface, it is possible to enhance the tribological properties by (i) increasing the coating/substrate adhesion, (ii) improving the load support, (iii) reducing the surface stresses and, (iv) enhancing resistance to crack propagation [10].

Mechanisms for toughening layered ceramic coatings such as TiC/TiB_2 or TiN/(Ti(C,N) include as shown in Figure 4: (i) crack splitting at the boundaries of small sized grains, (ii) crack deflection at the interface between layers, (iii) reduction of stress concentration by interface opening, and (iv) plastic deformation at the interface for energy dissipation and stress relaxation [11]. Additionally, a tough multilayered coating can have high hardness and elastic modulus which can facilitate crack stopping and strain relaxation of the coated surface. Also it is proposed that shear strength of coatings can be increase by alternating layer of high and low elastic modulus. This phenomenon relates to prevention of dislocation formation and mobility by differences in elastic modulus between layers in a multilayer coating design.

Hall–Petch strengthening (grain size effect) can also be one of the reasons for strength increment in multilayer thin coatings in a nanometric scale [11]. Hall–Petch behavior is related to dislocations pile–up at grain boundaries. This pile–up at grain boundaries prevents dislocations movement. For materials with a fine grain structure there are many grain boundaries which block the movement of dislocations across the grain boundaries. In polycrystalline multilayer, the grain size decreases with the decrease in layer thickness. The effect of an increased strengthening with decrease in grain size d_g is described by the well–known Hall–Petch equation.

$$Y = Y_0 + k_{HP}\, d_g^{-0.5} \qquad (1)$$

where Y is the enhanced yield stress, Y_0 is the yield stress for a single crystal, and k_{HP} is a constant and d is the grain size.

Another factor is Orowan strengthening. Orowan strengthening is due to dislocations in layered materials being effectively pinned at the interfaces**.** As a result, the dislocations are forced to drop out along the layers. Forcing a dislocation to drop out in a layered material requires an increase in the applied shear stress. This additional shear stress would be expected to increase as the film thickness is reduced [5].

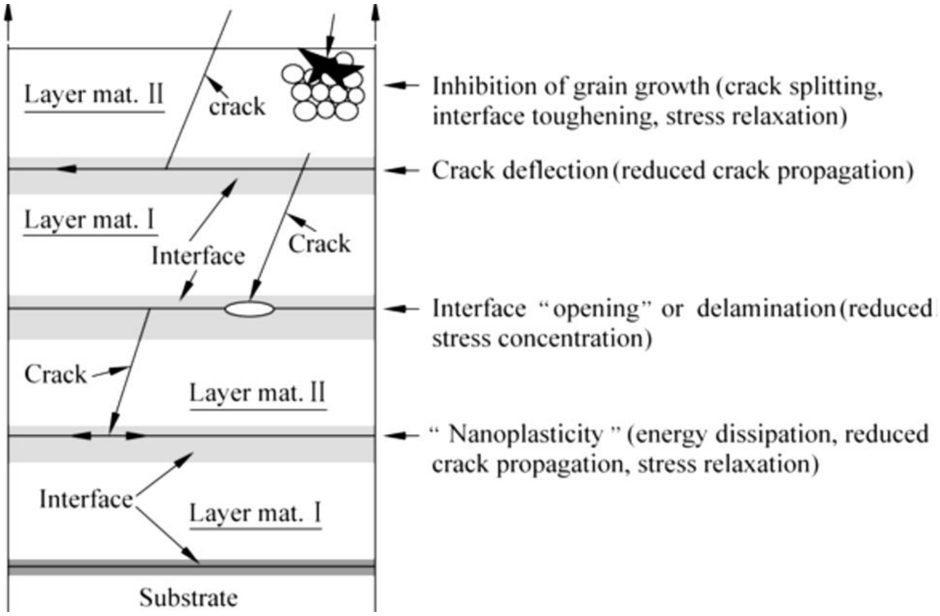

Figure 4. Mechanisms of toughness enhancement in hard ceramic multilayers [11].

As discussed previously, by applying a multilayer coating design, increments in toughness and hardness are expected and in some cases higher value of elastic modulus. So, multilayer films have obvious advantages over homogeneous films. By considering the advantages of multilayer coating design, we wish to use multilayer micro– and nanocrystalline diamond (MCD/NCD) deposited via home–made HFCVD process on silicon nitride ceramic substrate, which can be used for wear and tribological applications such as cutting inserts and mechanical seal rings. Although the adhesion of microcrystalline diamond is high and acceptable to substrate surface, the major problem of microcrystalline diamond is that it produces rough surfaces on the workpiece materials. However, microcrystalline diamond can be used as first (adhesion) layer to the substrate surface [12] in multilayered coatings. Moreover, although microcrystalline diamond has excellent wear resistance, its fracture toughness is not so high [13]. This characteristic can be related to the structure of the microcrystalline diamond film which grows into a columnar shape and during mechanical or tribological applications, the cracks can easily propagate in the column direction of microcrystalline diamond films [13].

As mentioned previously, diamond is a unique material with some exceptional optical, mechanical, thermal and electrical properties. Particularly due to some superior properties of diamond such as extreme hardness, highest bulk modulus, highest thermal conductivity, superior wear resistance, low coefficient of friction and chemical inertness, makes it a preferred candidate for tribological applications in the form of diamond coatings. In addition to being the hardest material, diamond provides some of the lowest friction coefficients to sliding tribological interfaces when tested in ambient conditions. This combination of extreme hardness, superior wear resistance and very low friction makes the diamond ideal for a wide range of tribological applications [12,14,15].

For tribological applications such as cutting tools, mechanical seal rings, or even in optics and microelectronics, it is very important to grow diamond film layers with a smooth surface [15]. Two of the important properties of NCD films are surface smoothness and formation of a thin continuous film without voids and non–uniformities [16]. Studies indicate that the microcrystalline diamond (MCD) films produced by conventional CVD processes exhibit the columnar structures of coarse crystals and thus rough surface, which easily leads to a high friction coefficient during sliding [17–19]. Thus, the trend to adjust the deposition process is developed to decrease the size of diamond crystals. Such process can avoid the columnar structure and therefore smoothen the surface [20]. In addition, the multilayer films show some desirable properties, such as high adhesion strength and low internal stress [21,22] which indicate that the multilayer films, including multilayer diamond coating, are a promising method to improve the mechanical properties of films, as shown schematically in Figure 5.

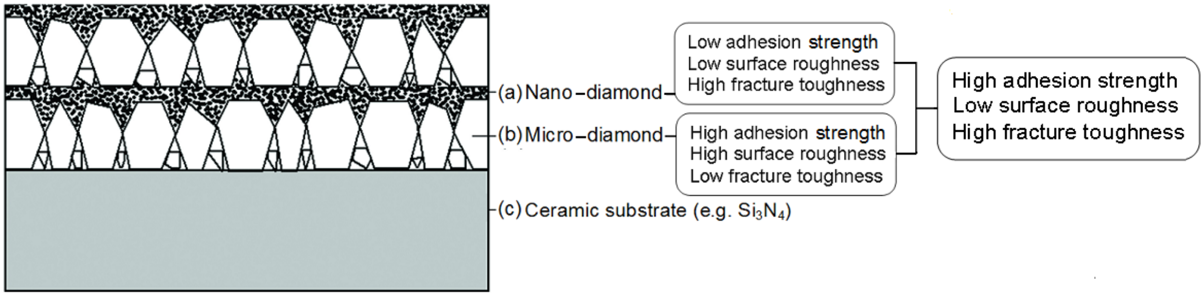

Figure 5. Schematic diagram of improvement of tribological properties of coated ceramic surface by applying a multilayer micro– and nanocrystalline diamond (MCD/NCD) coating [22].

Silicon nitride (Si_3N_4) is one of the promising structural ceramic substrates for wear resistant applications. In addition, silicon nitride is a proper substrate for diamond growth due to the low coefficient of thermal expansion mismatch to the diamond, which results in a significant adhesion improvement between the diamond coatings and silicon nitride ceramic substrates [23–25].

Self–mated diamond–on–diamond tribosystems are remarkable because the sliding friction coefficient is nearly the same with or without an organic lubrication fluid. That behavior is because of the high hardness of diamond, and as a result, high local pressure in the contact areas cause the lubrication fluid to be completely compressed on for low to medium sliding velocity ranges. In addition, diamond surfaces are usually passivated by hydrogen or oxygen, and are relatively inert [26]. So that property not only makes the diamond as a great potential replacement material in many tribological applications, but also it can be used to reduce friction in severe chemical medium in which conventional fluid lubrication could not be useful [27].

Some of the other factors that influence the friction and wear behavior of diamond are contact pressure, surface roughness, crystallographic orientation, and the presence or formation of gaseous, liquid, solid and transfer films on the sliding surface. The effect of counterface on friction and wear was evaluated using various counterbodies such as SiC, Si_3N_4, 100Cr6 steel, 440C steel and Al_2O_3 balls [28–31]. Regarding CVD diamond against different ceramic counterbodies, Zeiler et al. [32] investigated the tribological performance of CVD diamond coatings against Al_2O_3, SiC, Si_3N_4 and ZrO_2 ceramic counterbodies. Polycrystalline diamond coatings were grown on Ti–6Al–4V alloy through microwave plasma chemical vapor deposition (MPCVD). They found that the diamond coatings on Ti–6Al–4V alloy decreases wear and friction significantly compared with uncoated self–mated Ti tribo–systems. Moreover, polishing of the CVD diamond coatings improved the wear behavior than the non–polished CVD diamond surfaces. Al_2O_3 and Si_3N_4 demonstrated very good wear and very low friction behavior against as–deposited CVD diamond compared to SiC and ZrO_2 ceramic counterfaces.

Using different tribo–test environments for CVD diamond coatings, Miyoshi and coworkers [33] studied the tribological properties of CVD diamond, DLC and c–BN films in sliding contact with CVD diamond in ultrahigh vacuum, dry nitrogen, humid air, and water. A comparative study of the tribological performance of as–deposited, fine–grain diamond, and surface–modified coarse–grain diamond films by means of mechanical polishing and nitrogen ion implantation was carried out. The surface roughness of the tested coatings was in the range 6–37 nm. The coatings were deposited on silicon, silicon nitride and silicon carbide substrates. The tribological tests were accomplished at room temperature on a unidirectional rotating apparatus with sliding speeds in the range 31 to 107 mm/s. In those tests, fine–grained CVD diamond and surface–modified CVD diamond were made to slide against CVD diamond pins having the radius of 1.6 mm, under an applied load of 0.49 N. The steady state friction coefficient and wear rate of fine–grain and polished coarse–grain CVD diamond films were measured for all tested environments. Selected results of fine–grain CVD and surface–modified CVD diamond are illustrated in Figure 6. Similar studies were accomplished regarding the effect of different tribological test environments on wear and friction of CVD diamond coatings [34–37].

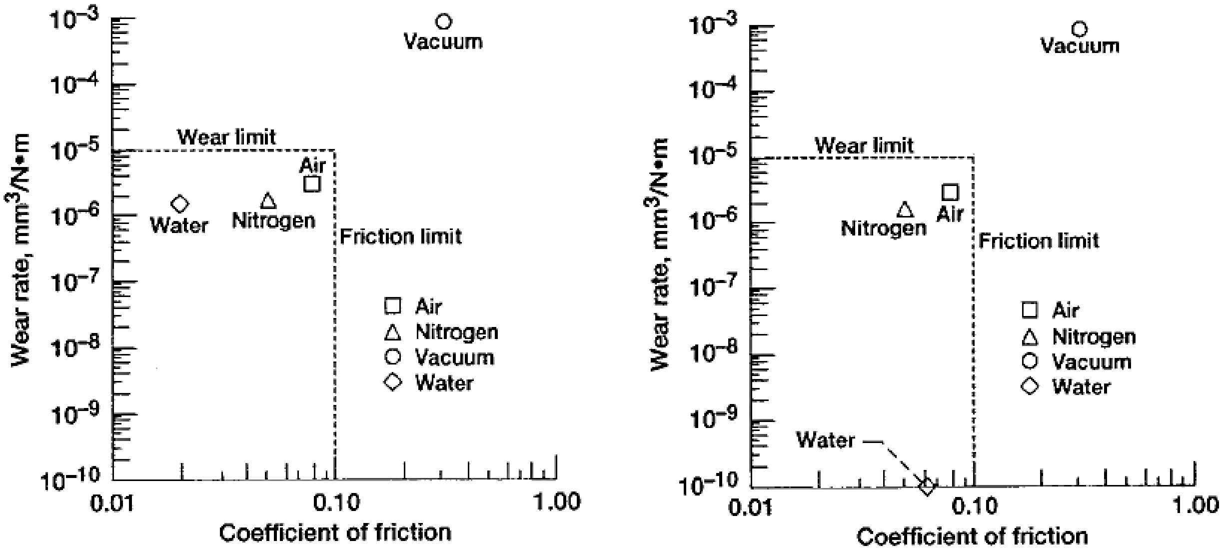

(a) (b)

Figure 6. Coefficients of friction and wear rates of (a) fine–grain CVD diamond film in sliding contact with CVD diamond pins and (b) coarse–grain CVD diamond film in sliding contact with CVD diamond pins in humid air, dry nitrogen, ultrahigh vacuum, and water [33].

The friction behavior of polycrystalline diamond films against a variety of the counterbodies is controlled by surface roughness of the coated substrate. For self–mated diamond sliding, the coefficient of friction initially is high normally above 0.1 but it decreases as the surface of the coating becomes smooth until it stabilizes at a value below 0.1 which depends on the original surface roughness. The wear of the film is decreased when the roughness and friction is reduced. For diamond on non–diamond counterbodies, the friction depends on the formation of a transfer layer in the first steps of the wear test. For instance, the initial friction between rough diamond coatings and a sapphire counterface is about 0.2, but rapidly increases to 0.6 when a thick transfer layer formed at the interface between film and counterbody [38].

The wear mechanism of diamond films in a friction process such as reciprocating ball–on–flat sliding wear tests has attracted of much scientific and technological interest. Reciprocating sliding wear is a relative cyclic motion with small amplitude that occurs between two surfaces in contact. Sliding wear combines the most of the wear mechanisms, like abrasive, adhesive, oxidative and fatigue. In addition, sliding wear can be easily realized on hard surfaces with minimal energy input into the friction surfaces, since the wear is concentrated in a small contact area between them [18].

The sliding wear of diamond coatings takes place by micro–fracture of the tips of contacting asperities which leads to the smoothness of the coating. In this situation normally the wear rates are low but rapid increments can occur when the coating detached from the substrate. The durability of the coatings is often poor because the frequent stress to the coating conducts to the interfacial defects propagation and coating detachment from the substrate. In this situation, stability and structure improvement of the interface is needed in order to successfully use diamond coatings in tribological applications [38].

Self–mated diamond coatings including individual microcrystalline diamond (MCD) and nanocrystalline diamond (NCD) based tribosystem have been studied in several works in different wear conditions i.e. wear environment, applied loads, sliding distance and temperature [20,23,39–43].

Regarding grain size effect, Abreu et al. [23] studied the grain size effect on self–mated CVD diamond dry tribosystems. Dense silicon nitride substrates were fabricated by pressureless sintering and diamond coated by microwave plasma chemical vapor deposition. The deposition time varied between 1 and 10 h in order to investigate the effect of the diamond grain size and film thickness on the tribological behavior of self–mated CVD diamond coatings on silicon nitride. Reciprocating dry sliding ball–on–flat wear tests were performed in air up to 16 h, at room temperature, with normal applied load from 10 to 105 N. The stroke and frequency of the sliding tests were kept constant with values of 6 mm and 1 Hz, respectively. Low friction value of $\mu = 0.03$ was obtained in steady state situation and a mild wear mode was gained for the longer runs, with the wear coefficient values around 10^{-8} $mm^3N^{-1}m^{-1}$. Their work showed that the larger grain size and thicker diamond films present smaller compressive residual stresses less than 1 GPa because of the proper in–depth accommodation of the contact pressure which causes delay in film delamination to much higher applied loads (105 N) than the thinner, small grain sized coatings, grown for 1 h that fail under applied normal load of 35 N.

Lei and coworkers [39] investigated the tribological behavior of micro and nanocrystalline diamond films in dry sliding and water lubricating condition. Micro and nanocrystalline diamond coatings were deposited on WC–Co balls and flat specimens using the HFCVD method. They found that the main wear mechanism of the tested tribosystems may be a dominant abrasive wear mode induced by self–polishing or micro–abrasion. In ambient air, the stable coefficient of friction of all tested contacts was in the range of 0.053–0.062, while under water lubrication, the value drop into the scope of 0.023–0.025. The origin of decreased friction coefficient in HFCVD diamond tribosystem under water lubrication is attributed to the effect of water on the formed graphic material (sp^3 to sp^2) and the chemisorbing of diamond surface with H_2O, hydrogen or hydroxyl ions.

Friction and wear performance of HFCVD nanocrystalline diamond coated silicon nitride ceramics was evaluated by Abreu et al. [40]. Silicon nitride ceramics were chosen as substrates because of chemical and thermal compatibility to the diamond which cause the proper nanocrystalline diamond film adhesion to the substrate. Nanocrystalline diamond coatings were grown by hot–filament chemical vapor deposition using $Ar/H_2/CH_4$ gas mixtures. The tribological assessment of homologous pairs of nanocrystalline diamond films was accomplished using reciprocating ball–on–flat tests using nanocrystalline diamond–coated Si_3N_4 plates and balls. The initial coefficient of friction raised up to 0.7, then shortly decreased to the very low friction coefficients values of 0.02–0.03. The threshold load before the diamond film delamination obtained to a value of 40 N and the mild wear regime of $k= 10^{-7}$ $mm^3N^{-1}m^{-1}$ for self–mated dry sliding conditions was achieved.

In other study, Abreu and coworkers [41] studied the enhanced performance of HFCVD nanocrystalline diamond self–mated tribosystems by plasma pretreatments on silicon nitride substrates. Monolayer nanocrystalline diamond films were deposited by the hot–filament chemical vapor deposition on hydrogen plasma pretreated silicon nitride substrates. The friction and wear behavior of self–mated nanocrystalline diamond films in unlubricated sliding and high applied loads up to 90 N was performed by reciprocation ball–on–flat configuration in ambient temperature. The reciprocating tests showed the initial high friction coefficient which related to the surface roughness of nanocrystalline diamond coatings. Shortly, a steady state regime installs, with low friction coefficient values of 0.01–0.04. They found that a polishing wear mechanism controls the material loss which is responsible for mild wear coefficients of $k= 10^{-7}$ $mm^3N^{-1}m^{-1}$. The hydrogen etching causes the film adhesion improvement compared to the non–etched surfaces which was confirmed by the high threshold loads of 60 N before the film delamination.

Tribological testing of self–mated nanocrystalline diamond coatings on Si_3N_4 ceramics was carried out by Abreu and coworkers [20]. Microwave plasma–assisted chemical vapor deposition of nanocrystalline diamond was obtained by $Ar/H_2/CH_4$ gas mixtures on Si_3N_4 discs and ball substrates. The tribological tests of the monolayer nanocrystalline diamond coated Si_3N_4 substrates were performed in the self–mated pairs without lubrication for evaluation of the friction and wear. Friction coefficient value shortly after a sharp peak which reached a maximum around 0.44 in applied load of 35 N decreased to 0.02 in the steady state situation. The wear coefficient values of $k= 1\times10^{-8}\ mm^3N^{-1}m^{-1}$ for the self–mated monolayer nanocrystalline coatings were obtained which revealed the mild wear regime. The main wear mechanism was found to be self–polishing induced by micro abrasion of diamond coated surfaces.

Other work for self–mated diamond tribosystem was accomplished by Abreu et al. [42] which used CVD diamond water lubricated tribosystems for high load planar sliding. The microwave plasma chemical vapor deposition was used to coat diamond film onto Si_3N_4 substrates from CH_4–H_2 gas mixtures during 2.5 h, resulting in a film thickness around 15 μm. Self–mated planar reciprocating sliding ball–on–flat wear tests were performed up to 16 h and 690 m of sliding distance with normal applied load from 70 N to 160 N. The worn surfaces demonstrate polished surface caused by diamond abrasion on the counterbody surface. A steady state sliding regime observed during the wear test with a very low friction coefficient of 0.04–0.05 and a wear coefficient of about $10^{-8}\ mm^3N^{-1}m^{-1}$.

Using water lubrication in a self–mated nanocrystalline diamond coatings, Abreu and coworkers [43] tested self–mated diamond tribosystem of HFCVD nanocrystalline diamond coatings in the presence of water. Nanocrystalline diamond coatings of 20 μm thickness were deposited via hot–filament chemical vapor deposition on silicon nitride ceramic substrates. The water lubricated self–mated nanocrystalline diamond tribosystem was examined in a ball–on–flat tribometer. They observed a very low friction coefficient values of $\mu= 0.02$–0.05 combined with a high wear resistance of $k= 10^{-9}$–$10^{-8}\ mm^3N^{-1}m^{-1}$ for the wear conditions up to the 85 N threshold load before the diamond coating detachment.

Multilayered micro and nanocrystalline diamond (MCD/NCD) system takes advantage of both microcrystalline and nanocrystalline diamond layers. Several investigations on multilayered diamond coating on WC–Co substrates consisting of alternating layers of micro and nanocrystalline diamond coatings are reported with low surface roughness, good adhesion and low friction coefficient [44–49].

On silicon nitride substrates, Salgueiredo et al. [50] studied the SiC particle erosive–induced wear of mono, bi and multilayered diamond composite coatings grown by HFCVD. They found that the multilayered diamond coatings revealed the best erosive resistance and that the damage occurred by gradual loosening of material from the outer layer after longer testing time which was attributed to the micro/nanocrystalline diamond interfaces that deflected cracks and prevented crack propagation.

Using environmentally–friendly lubricants in a self–mated diamond tribosystem, Almeida and coworkers [51] evaluated enhancing the tribological performance under biodiesel lubrication using CVD diamond Si_3N_4 coated parts. Two types of coatings were tested: (i) a single layer (SL) of microcrystalline diamond (MCD) and (ii) a multilayered (ML) system made of three bilayers of MCD/nanocrystalline diamond (NCD). Their results show among the tested diamond coating types, the microcrystalline (MCD) single layered coatings (SL) presents a higher initial COF peak (0.30–0.35 with SL against 0.15 with ML) due to the intrinsic higher surface roughness of MCD. However, once running–in is attained, the SL leads to an optimal friction performance with its surface presenting plateaus and valleys capable of interacting positively with the lubricant.

In other study related to self–mated tribosystems, Salgueiredo et al. [52] carried out self–mated tribological systems based on multilayer micro/nanocrystalline CVD diamond coatings. Bi– and fourfold layer of micro and nanocrystalline diamond films were deposited onto silicon nitride substrate. All coatings present a total film thickness in the 10–12 μm range, for comparison purposes. Tribological tests were carried out with a reciprocating sliding configuration without lubrication. Fourfold composite coatings exhibited a superior critical load before delamination (130–200 N), when compared to the mono (60–100 N) and bilayer coatings (110 N). Regarding the friction behaviour, a short time initial high friction coefficient was followed by low friction regimes between 0.02 and 0.09. Their findings showed that for the multilayer composite coating, the top nanocrystalline diamond layer wears out progressively performing a sacrificial role, while the underneath harder microcrystalline diamond layer keeps the residual stresses at low levels.

Regarding adhesion strength assessment for different diamond coating architectures, Salgueiredo and coworkes [53] accomplished a comparative study of different combinations of microcrystalline and nanocrystalline diamond morphologies (monolayers, bi–, tri– and fourfold layer) coated via HFCVD technique on silicon nitride ceramic substrates. The diamond multilayer morphology and the structural quality investigated by SEM, AFM and UV–Raman spectroscopy. They found that by using the multilayer design, starting with a microcrystalline adherent layer on Si_3N_4 ceramic substrates and ending with a nanocrystalline smooth layer at the top, it was possible to keep the surface roughness at a low mean surface roughness (R_a) level of ~ 90 nm. The fourfold multilayer configuration permitted achieving 10 μm thick diamond coatings that tolerate an indentation load of 800 N with a Brale cone, before film spalling off. This behaviour is determined by the high bonding strength of the initial microcrystalline layer on the Si_3N_4 ceramic substrate. Moreover, they concluded that a set of advantages for the micro and nanocrystalline multilayer design for mechanical applications is obvious. It provides a smooth end surface when the top coating is of the nanocrystalline diamond type, which is particularly relevant for tribological applications that require high load bearing capacity and low frictional loss.

In other work, the tribological behaviour of Si_3N_4 substrates coated with monolayer–micrometric, monolayer–submicrometric and multilayer–micrometric HFCVD diamond coatings was investigated by Chen et al. [54]. The coating thicknesses in each case was ~13–16 μm for monolayer–micrometric diamond coatings, ~ 10–12 μm for monolayer–submicrometric diamond coatings, and ~ 22–24 μm for multilayer–micrometric diamond coatings. Tribological properties were studied by sliding tests in ambient air under unlubricated condition using a reciprocating ball–on–flat configuration and commercial uncoated Si_3N_4 ceramic balls of 4 mm diameter were used as counterbodies. Their results showed the friction of coefficients of 0.127, 0.076 and 0.071 for the with monolayer–micrometric, monolayer–submicrometric and multilayer–micrometric coated Si_3N_4 substrates in steady state regime, respectively. The reduction of friction coefficient for the multilayer micrometric coated Si_3N_4 substrates was related to the high purity diamond crystals of the multilayer micrometric coatings. In addition, differences of the friction coefficient between multilayer micrometric and monolayer submicrometric coated Si_3N_4 substrates were very small, although multilayer micrometric diamond coatings demonstrate higher wear resistance than the monolayer submicrometric diamond coatings, which results from the decrease in the hardness of the monolayer submicrometric diamond coatings.

Regarding alternating diamond layers coated hardmetal substrates, Dumpala and coworkers [55] evaluated the growth and characterization of integrated nano– and microcrystalline dual layer composite diamond coatings on WC–Co substrates. Hot filament chemical vapor deposition was employed to deposit diamond coatings on WC–Co substrates. Two types of coatings were grown for performance comparison and the diamond coatings were: (i) integrated composite diamond (ICD) coating, and (ii) microcrystalline diamond (MCD) coating. ICD coating was grown on WC–Co substrate by integrating the microcrystalline diamond (MCD) and nanocrystalline diamond (NCD) layers with the transition layer. This ICD coating was deposited in three steps: a) MCD layer for 6 h, b) transition layer (MCD to NCD) for 2 h and c) NCD layer for 6 h. Microcrystalline diamond (MCD) coating was grown for 12 h. Total coating thickness for ICD coating and MCD coating was ∼ 10.2 μm and 4.3 μm, respectively. Tribological tests were performed using a ball–on–disc type linear reciprocating under dry conditions. Uncoated silicon nitride (Si_3N_4) and silicon carbide (SiC) ceramic balls of 6 mm diameter were used as counterbody with a normal load of 10 N. Their results indicated that the integrated composite diamond (ICD) coatings have low and stable friction coefficient of ~ 0.06 against Si_3N_4 ceramic that after a sliding distance of 100 m in comparison with microcrystalline diamond (MCD) coatings showed friction coefficient more than 0.1.

In the present work, the concept is to use the advantages of both micro– and nanocrystalline diamond on silicon nitride (Si_3N_4) ceramic substrates and evaluate these advantages in a multilayer coating design for specific tribological applications such as mechanical seals and cutting tools.

1.3. Diamond cutting tools

Regarding to cutting tools market, Figure 7(a) and (b) illustrate the estimated main used cutting tools in the USA and worldwide in 1998 and 2005 [56].

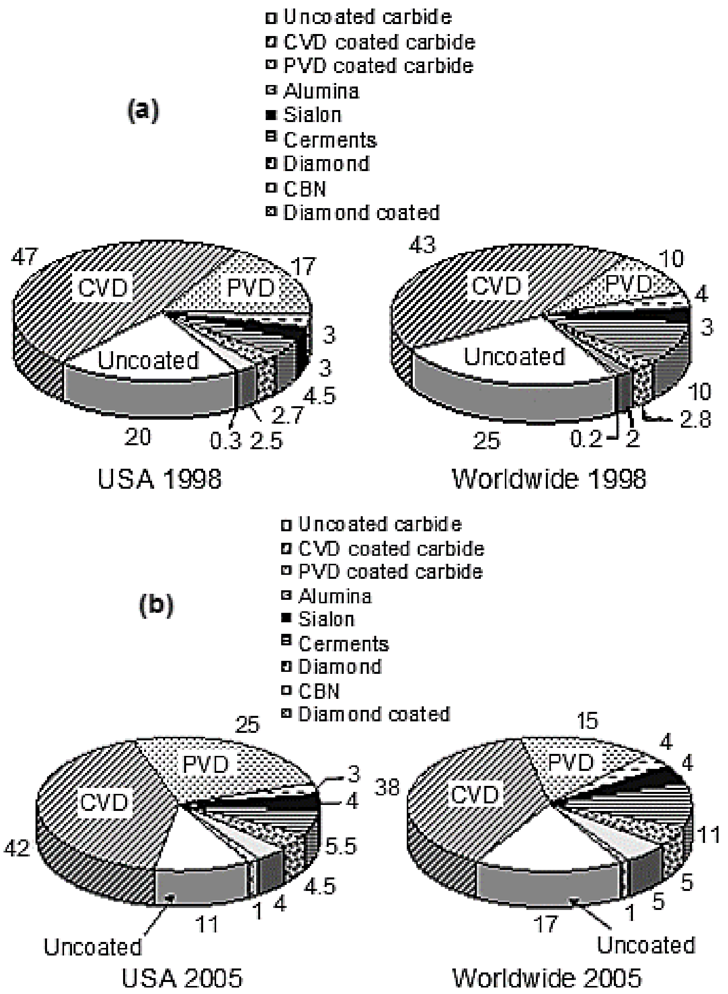

Figure 7. Estimated main used cutting tool materials in USA and in worldwide for (a) 1998 and (b) 2005 [56].

By comparing the trends, it can be implied that PVD coated cutting tools had the highest growth in cutting tools industry, while CVD coated cutting tools had the highest contribution for cutting tools materials. Moreover, the contribution of uncoated carbide tools is reduced in 2005 compared to 1998, which resulted in tendency to CVD and PVD coated cutting tools.

There are several parameters which can influence on cutting performance of the cutting tools in machining processes of the workpiece materials as demonstrated in Figure 8.

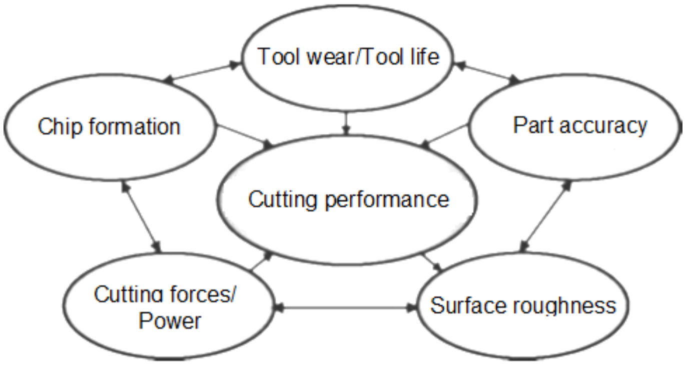

Figure 8. Representation of the factors influencing the cutting performance of tools during turning [57].

In the particular case of machining metal matrix composites (MMCs), the stresses on the cutting edge are mainly due to the mechanical and thermal loads. Mechanical loads are created because of: (i) considerable abrasion through contact with particulate or fiber ceramic reinforcement, (ii) high dynamic loads appeared via the reinforcement impacts at the cutting edge and (iii) alternating stress represented from inhomogeneity of the workpiece material. In addition, thermal loads are generated by high local temperature generated by intensive microcontact between the cutting edge and ceramic reinforcements. Figure 9 shows the tribological system in the machining of metal matrix composites (MMCs) [58].

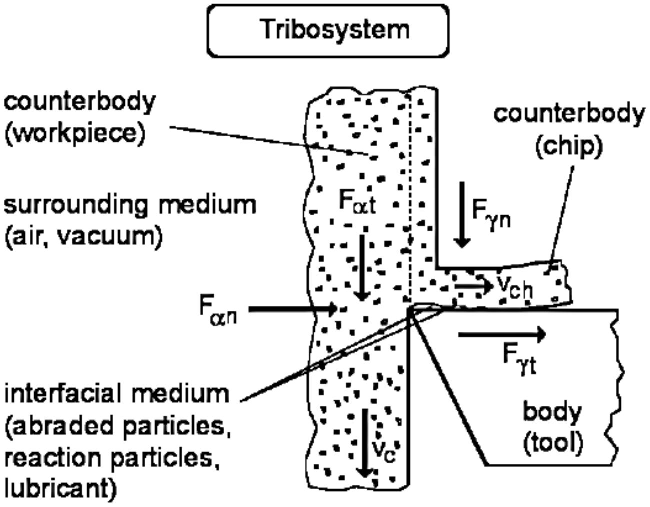

Figure 9. Tribological system in the machining of metal matrix composites (MMCs) [58].

CVD diamond in the forms of PCD and CVD coated cutting tools can be used for the machining of MMCs. In this section, the use of diamond in the form of polycrystalline diamond (PCD) and chemically vapor deposited diamond (CVD) for cutting applications are overviewed.

1.3.1. Polycrystalline diamond (PCD) cutting tools

Synthetic polycrystalline diamond (PCD) tools are composed of synthetic and very tough micro diamond particles which are kept together by a metal binder that is mostly selected from transition metals group in periodic table such as Co, Ni or their alloys. PCD tools are produced by sintering of diamond particles under high pressure and temperature conditions, and consist of maximum of 15% of transition metal binder. During the sintering process of PCD, the holes between diamond particles are filled with cobalt binder. The binder helps PCD to obtain higher fracture toughness when comparing to single crystal diamond. Generally, PCD tools are used as an insert or tip that is brazed to the cutting tool, which is mostly made of WC–Co cemented carbide. PCD–tipped cutting tools are conventionally used where very high surface finishing and long tool life are necessary. PCD–tipped tools are widely used for other machining operations like turning and milling. PCD is commonly used in the industry to machine non–ferrous materials like Al–Si, Al alloys, and metal matrix composites (MMCs) because of favorable mechanical properties [59–61]. Figure 10 shows some examples of PCD–tipped inserts for turning and finishing operations. Processing and production of PCD tools have high costs and are also time consuming, so an alternative for PCD is CVD diamond that can coat the cutting tools and substitute it in wear and tribological applications.

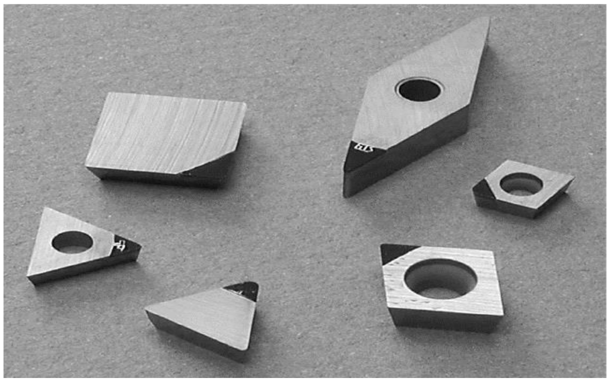

Figure 10. Some examples of PCD–tipped inserts for turning and finishing operations [62].

Regarding PCD cutting tools, Lin et al. [63] studied the machinability of a silicon carbide reinforced aluminum metal matrix composite material. Duralcan (A359–20 vol.% SiC) used as the workpiece material and PCD inserts were employed for turning tests in v = 300, 500, 700 $m.min^{-1}$, f = 0.1, 0.2, 0.4 $mm.rev^{-1}$ and DOC = 0.5 mm. They observed that flank wear happened due to abrasion between the tool and workpiece material. In addition, by increasing the speed turning with PCD tool, wear was found to increase with increasing cutting speed and feed. Moreover, uniform distribution of SiC particle reinforcements inside Al matrix caused to discontinuous chip formation during turning tests of A359–20 vol.% SiC.

Davim and Baptista [64] evaluated relationship between cutting force and PCD cutting tool wear in machining silicon carbide reinforced aluminum. An A356–20 vol.% SiC MMC was selected as the workpiece material. The turning process was performed using PCD cutting tool at v = 250–500 $m.min^{-1}$, f = 0.05–0.2 $mm.rev^{-1}$ and DOC = 1 mm in lubricated conditions. The main wear mechanism was flank wear of tool due to the abrasion between SiC reinforcements and cutting tool. Cutting forces increased with cutting time gradually. Cutting, feed and depth forces increased with flank wear increasing.

In other work, Muthukrishnan and coworkers [65] investigated machinability issues in turning of Al–SiC (10p) metal matrix composites using PCD cutting tools. The turning conditions were: v = 200–400 $m.min^{-1}$, f = 0.075 $mm.rev^{-1}$ and DOC = 0.5 mm and the turning tests were carried out under dry machining conditions. They observed the wear is predominantly due to the abrasive action of the SiC on the tool flank. Higher cutting speeds result in relatively easier removal of the hard SiC particles caused better surface finish. Moreover, power consumption became less at higher cutting speeds.

El–Gallab et al. [66] performed the turning of Al–20 SiC metal matrix composite particulate metal–matrix composites using triangular Al_2O_3–TiC ceramic, TiN–coated carbide and polycrystalline diamond (PCD). The turning conditions for TiN–coated carbide and Al_2O_3–TiC ceramic tools were: v = 248 $m.min^{-1}$, f = 0.2 $mm.rev^{-1}$ and DOC = 0.5, while for PCD tool were: v = 670; 894 $m.min^{-1}$, f = 0.25; 0.45 $mm.rev^{-1}$ and DOC = 1.5; 2.5 mm. Their work demonstrated that polycrystalline diamond tools (PCD) exhibited higher tool life compared to TiN–coated carbide and Al_2O_3–TiC ceramic tools. Moreover, two last tools suffered from extreme edge chipping and crater wear during the machining of the Al–20 SiC metal matrix composite.

In other study, D´Errico and R. Calzavarini [67] carried out the turning of Al–based metal matrix composites of Al6061–10 vol.% SiC and A359–20 vol. % SiC using uncoated WC–Co tool, PCD, some CVD diamond (20–50 μm) directly coated WC–Co tools and a 500 μm brazed CVD thick diamond. The turning conditions for Al6061–10 vol.% SiC were: v = 250; 300 $m.min^{-1}$, f = 0.4 $mm.rev^{-1}$ and DOC = 1.5 mm, while for A359–20 vol. % SiC were: v = 250–500 $m.min^{-1}$, f =

0.1–0.4 mm.rev^{-1} and DOC = 1.5 mm. Their results exhibited that the deposition of CVD diamond coatings increase more than 100% the cutting performance of uncoated WC–Co cutting tool, but still the problems related to direct diamond coated tools should be solved. Moreover, brazed thick diamond behaves well for turning of A359–20 vol. % SiC and even in some turning conditions can compete with PCD tools.

Durante and coworkers [68] examined aluminum–based MMC machining with PCD and diamond–coated cutting tools. The workpiece materials were Al–10% Al_2O_3, Al–20% Al_2O_3 and Al–20% SiC. The turning conditions were: v = 500 m.min^{-1}, f = 0.4 mm.rev^{-1} and DOC = 1.5 mm in emulsion 5% lubricant. Moreover, PACVD diamond–coated WC–Co tools with thicknesses of 10 and 15 μm and in turning of Al–10% Al_2O_3, Al–20% Al_2O_3 and Al–20% SiC in turning conditions of v = 250–500 m.min^{-1}, f = 0.4 mm.rev^{-1} and DOC = 1.5 mm in 5% emulsion lubricant. In addition, CVD diamond coated WC–Co tools with thickness of 30 μm used for the turning of Al–20% SiC workpiece in v = 300 m.min^{-1}, f = 0.1– 0.3 mm.rev^{-1} and DOC = 1 mm in dry conditions. The results indicated CVD diamond coated WC–Co cutting tools increases the tool life, but the main problem of CVD diamond coated tools are coating detachment of cutting tools even in lubrication conditions and also PCD tools showed higher tool life of almost twice compared to the CVD diamond coated tools.

1.3.2. CVD diamond–coated cutting tools

Figure 11 compares the CVD deposition conditions with those of PVD technology for the coating of cutting tools, where it is shown that CVD needs higher pressures and temperatures than PVD.

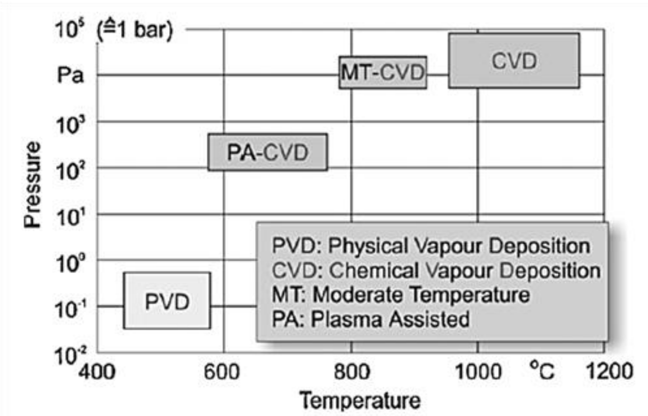

Figure 11. Coating deposition technologies for cutting tools [69].

In addition, Figure 12 represents and compares the possible substrate materials, applications and coating materials which are often deposited by PVD and CVD processes. Diamond–like carbon (DLC) and diamond coatings have received considerable research efforts on the development of various tool materials [70–76]. Diamond coated tools are economically attractive alternatives to their PCD counterparts because they offer an advantage in the fabrication of cutting tools with complex geometry, e.g. drill bits. Figure 13 represents a wide variety of diamond coated cutting tools, including PCD and CVD brazed thick films.

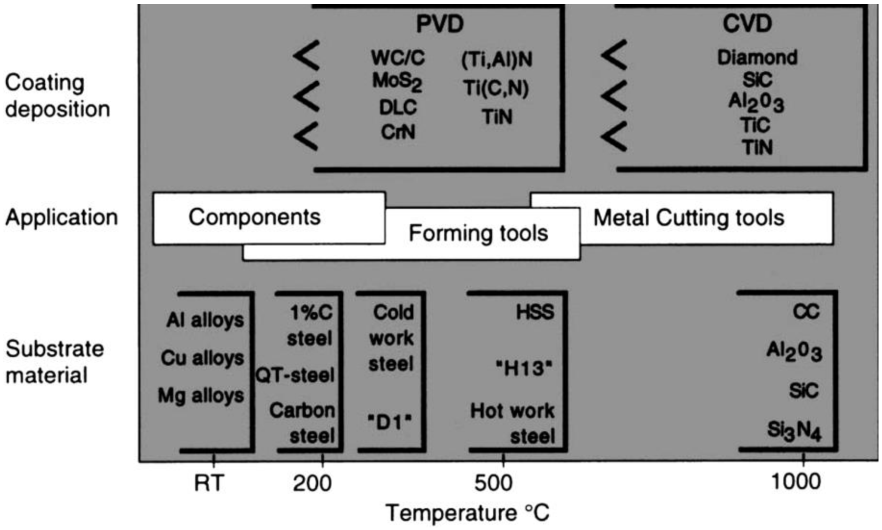

Figure 12. Typical temperature limits of potential substrate materials compared to typical working temperatures of applications and deposition temperatures of PVD and CVD coating processes [77].

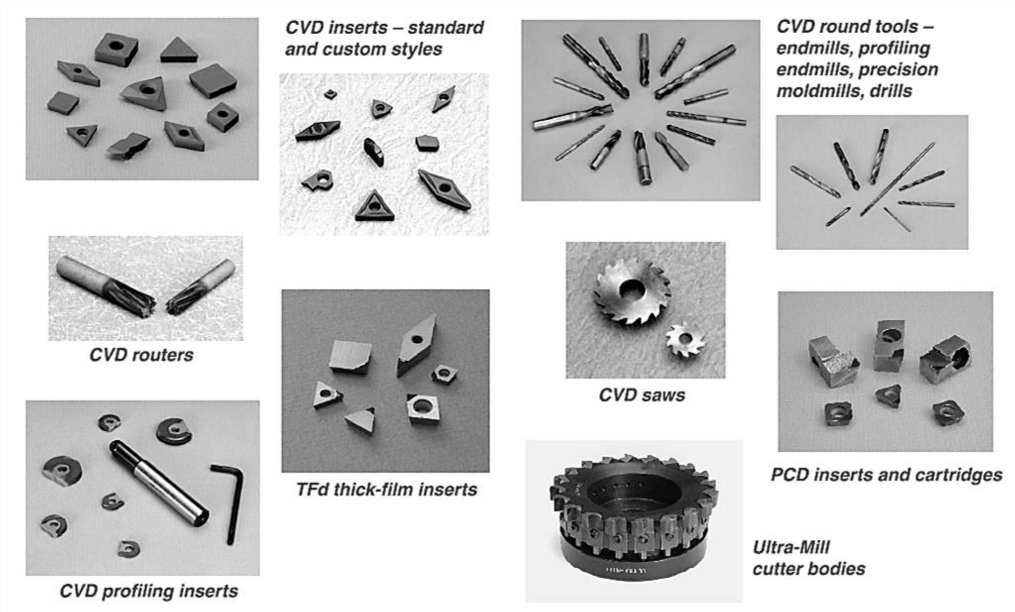

Figure 13. Wide variety applications of diamond–coated cutting tools [78].

Microwave CVD (MPCVD), hot–filament CVD (HFCVD), combustion synthesis, and plasma arc are some of the CVD techniques there are widely used for diamond deposition on cutting tool materials [69,72–75,79]. Regarding the classification of difficult–to–machine materials, they fall into three categories, namely: (i) hard materials (Ti alloys, Ni alloys, ceramics, Co–Cr, hardened steels); (ii) ductile materials (polymers, Mg alloys, low carbon steels) and (iii) non homogeneous materials such as polymer matrix composites (PMCs), metal matrix composites (MMCs) and, ceramic matrix composites (CMCs). A variety of non–ferrous difficult–to–machine workpiece materials have been machined by chemically vapor deposited diamond. They include aluminum–silicon alloys, carbon fiber reinforced polymers (CFRP), glass fiber reinforced polymers (GFRP) and different metal matrix composites (MMCs) [71,75**]**.

Chen et al. [80] assessed the cutting performance of double layers of micro and nanocrystalline diamond coated silicon nitride inserts in the machining of aluminium–silicon alloy. Double layers of micro and nanocrystalline diamond coatings were grown on Si_3N_4 inserts through hot–filament CVD with a total thickness of 12–14 μm. Double–layer structure of micro and nanocrystalline diamond was obtained by the deposition of the rough microcrystalline diamond layer and then the smooth fine–grained nanocrystalline diamond layer. For comparison, the uncoated Si_3N_4 insert and monolayer nanocrystalline and monolayer microcrystalline coated inserts were also tested in their work. The dry turning conditions of Al–Si alloy were at 350 $m.min^{-1}$ of cutting speed (v), 0.4 mm of cutting depth (DOC), and 0.1 $mm.rev^{-1}$ of feed rate (f). Their work showed that the double micro and nanocrystalline diamond–coated silicon nitride insert has the best cutting behavior showing a very low flank wear.

In other work, Kopf and coworkers [81] investigated the diamond coated cutting tools for machining of non–ferrous metals and fiber reinforced polymers. Hot filament CVD process was used for the diamond growth on WC–Co cutting tools. Turning conditions of carbon fiber reinforced polymers (CFP) with 50% carbon fibers were: cutting speed (v) = 100 $m.min^{-1}$, depth of cut (DOC) = 3 mm and feed rate (f) = 0.4 $mm.rev^{-1}$. Diamond coating with the thickness of 9 μm showed better tool life than diamond coating with the thickness of 6 μm and PCD cutting tool. In addition, glass fiber reinforced polymers (GFRP) with 77% of glass fibers were turned with a cutting speed (v) of 350 $m.min^{-1}$, depth of cut (DOC) of 1 mm and feed rate (f) of 0.1 $mm.rev^{-1}$. The results indicated that diamond coating with the thickness of 25 μm showed better tool life than diamond coating with the thickness of 15 μm and PCD cutting tool. Moreover, Al–20Si cast alloy were tested in turning conditions of: cutting speed (v) = 400 m.min^{-1}, depth of cut (DOC) = 2 mm and feed rate (f) = 0.2 mm.rev^{-1} by multilayer diamond–coated WC–Co cutting tool (M10 type). The turning results demonstrated the 20 μm multilayer diamond coating has better tool life than other multilayer thicknesses (6, 13, 18 μm) and monolayer diamond thickness of 2 μm and 6 μm.

Dumpala et al. [82] studied the wear performance of dual–layer graded composite diamond coated WC–Co cutting tools. Hot filament CVD diamond was used to deposit diamond coatings with coating thickness of ~ 10 μm on WC–Co cutting tool with three different coating morphologies: (i) monolayer microcrystalline diamond (MCD) coating; (ii) dual layer composite diamond coating; and (iii) dual–layer graded composite diamond coating with a transition layer between microcrystalline and nanocrystalline diamond. Also, uncoated and commercial TiN coated WC–Co cutting tools were evaluated and compared the cutting performance with diamond–coated WC–Co cutting tools. The wear performance of the diamond coated WC–Co cutting tools with various coating morphologies was investigated through of turning Al–30 vol.% SiC_p metal matrix composite workpiece material and compared with uncoated and TiN coated WC–Co tools. Turning tests were carried out under dry conditions using the following cutting conditions of: cutting speed (v) = 380 m.min^{-1}, feed rate (f) = 0.1 mm.rev^{-1} and depth of cut (DOC) = 1 mm. Their results showed that uncoated and TiN coated WC–Co inserts failed after turning for a very short time. This rapid wear of uncoated and TiN coated WC–Co cutting inserts could be attributed to the abrasive wear of the harder SiC particles. The dual–layer graded composite diamond (NCD/transition layer/MCD/WC–Co) and monolayer microcrystalline diamond (MCD) coated cutting tools demonstrated better cutting performance than composite diamond (NCD/MCD/WC–Co) coated WC–Co cutting tools. The weak cutting performance of the dual–layer composite diamond (deposited without diamond transition–layer) coated WC–Co cutting insert was attributed to the sharp interface between the nanocrystalline diamond (NCD) and microcrystalline diamond (MCD) layers. The improved tool life of the dual–layer graded composite diamond coated WC–Co cutting tool was related to the low surface roughness of nanocrystalline top layer and improved interfacial integrity of the nanocrystalline and microcrystalline diamond layers in a graded diamond composite coating.

Regarding thick diamond coated cutting tools, Almeida et al. [83] carried out the turning of hardmetal using thick diamond coated Si_3N_4 cutting inserts. Microwave plasma CVD diamond coated with the thickness of 150 μm grown on rectangle Si_3N_4 inserts. Three hardmetals with composition of WC–18Co (GD 40), WC–25Co (GD 50) and WC–27Co (GD 60) were chosen for turning process. The depth of cut (DOC) was constant at 0.2 mm for the three hardmetal grades, while the turning speed (v) and feed rate (f) were decreased from 30 m.min^{-1} and 0.15 mm.rev^{-1} for GD 50 and GD 60 to 20 m.min^{-1} and 0.1 mm.rev^{-1} for GD 40. Their results showed that the wear of the Si_3N_4 cutting inserts took place by microchipping of the CVD diamond which resulted in the abrasion of the rake and flank faces. Wear of Si_3N_4 cutting inserts changed the cutting edge geometry and increased by the cutting force increase. In addition, by performing the turning tests in lubricating conditions, due to the reduction of Co adhesion and enhancement of diamond debris removal from the Si_3N_4 cutting edges, cutting tool life increased.

Using different cutting angles of turning, Almeida and coworkers [84] investigated semi–orthogonal turning of hardmetal with CVD diamond and PCD inserts at different cutting angles. 400 µm thick MPCVD brazed diamond and PCD tools were employed in 0º rake angle and 11º clearance angle and –6º rake angle and 6º clearance angle for dry turning tests of WC–18Co at v = 20 m.min^{-1}, f = 0.1 mm.rev^{-1} and DOC = 0.02–0.05 mm. In roughing conditions, the 0º rake angle and 11º clearance angle inserts exhibited the best performance regarding the cutting forces, tool wear and workpiece surface quality. In addition, considerable differences were not observed between the 0º rake angle and 11º clearance angle and –6º rake angle and 6º clearance angle tools in the hardmetal finishing. Moreover, the PCD cutting tool was not able to cut an abrasive WC–18Co workpiece, not only because of its lower hardness but also due to the adhesion wear via the presence of the cobalt binder of the WC–18Co workpiece material and the PCD cutting tool.

A comparison has been accomplished by Castro et al. [85] on dry machining of silicon–aluminum alloys with CVD diamond brazed and directly coated Si_3N_4 ceramic tools. 12 µm thick MPCVD diamond directly coated Si_3N_4 cutting inserts and 300 µm thick CVD diamond brazed WC–Co were used for dry turning of Al–12 wt.% Si and Al–18 wt.% Si at v = 600 m.min^{-1}, f = 0.1 mm.rev^{-1} and DOC = 0.5 mm. Both tools i.e. 12 µm thick MPCVD diamond directly coated Si_3N_4 cutting inserts and 300 µm thick CVD diamond brazed WC–Co performed the turning of an Al–12 wt% Si alloy. 12 µm thick MPCVD diamond directly coated sharp Si_3N_4 cutting inserts performed better than chamfered edges because of lower cutting forces and lower and lower cutting tool wear. 300 µm thick CVD diamond brazed WC–Co tool could accomplish dry turning the Al–18 wt% Si alloy with the low flank wear resulted from diamond chipping.

Using different tool geometry, Almeida and coworkers [86] performed machining hardmetal with CVD diamond direct coated ceramic tools. 15 μm thick MPCVD diamond coated rectangular Si_3N_4 cutting inserts with three edge geometries of sharp, chamfer and hone for turning of WC–25 wt.% Co hardmetals. Turning conditions were: v = 15 $m.min^{-1}$, f = 0.03–0.3 $mm.rev^{-1}$ and DOC = 0.1–0.3 mm. Diamond coating detachment and edge fracture occurred for honed edge tools at all tested conditions. Flank wear were highest for the chamfered tools than for sharp tool edges Wear of the cutting edges increases by increasing the machining time or worse turning conditions. The cutting forces for the sharp edge were lowest and for honed edges were the highest in hardmetal turning with MPCVD diamond tools. Sharp edge tools film delaminated from the flank face during the turning tests of hardmetal without significant effect on the cutting tool performance.

Applying CVD diamonds with different surface roughness for cutting purposes, Almeida et al. [87] studied the machining behavior of silicon nitride tools coated with micro– (MCD), submicro– (SMCD) and nanometric– (NCD) HFCVD diamond crystallite sizes. HFCVD diamond coated Si_3N_4 with three morphologies and surface roughnesses of. 20, 42 μm thick MCD (RMS of 0.55, 0.78 μm) and 23, 50 μm thick SMCD (RMS of 0.18, 0.23 μm) and 13, 23 μm thick NCD (RMS of 0.18, 0.26 μm) were used for dry turning of WC–25Co at cutting speed (v) = 15 $m.min^{-1}$, feed rate (f) = 0.1 $mm.rev^{-1}$ and depth of cut (DOC) = 0.1 mm. Highest cutting forces and rake and flank wear belong to MCD and the lowest ones belong to SMCD coated Si_3N_4 inserts. Moreover, 23 μm sub–micrometric diamond (SMCD) coated Si_3N_4 inserts presented the best combination of types of wear and workpiece surface finishing.

Al–based metal matrix composite materials reinforced with ceramic particles such as SiC, Al_2O_3 have been attracted of much research during past decades due to their superior mechanical properties. Aluminum metal matrix composites (Al–MMCs) reinforced with ceramic particles are widely used for high performance applications like in automotive, aircraft, aerospace and military due to their improved physical and mechanical properties. Among the ceramic particle–reinforced Al matrix composites, Al_2O_3 particulate reinforced aluminum composites are the most famous kind of Al–MMCs. Al_2O_3 reinforced aluminum matrix composites have been mostly employed in automotive, aircraft industry and aerospace due to casting productivity, high strength to weight ratio, and proper tribological properties compared to the unreinforced alloys [88–90].

Although the combination of high strength, hardness and wear resistance of ceramic reinforcements in the ductile Al metal matrix enhance the mechanical properties of the composite material, but some problems of machining can arise of presence of ceramic reinforcements inside the metallic matrix. Machinability of metal matrix composites (MMCs) has received a broad attention due to the high tool wear raised form the presence of hard ceramic particle reinforcements. The final production processes like powder metallurgy, hot forging or casting are not enough to produce metal matrix composite to the designed dimensions and shapes, thus the machining is needed to attain desirable shapes and dimensions. The inherent abrasiveness of the hard and wear resistant ceramic particle reinforcements accelerate tool wear and reduce the tool life. Al–MMCs which were reinforced with Al_2O_3 particles are difficult to machine materials because of the excessive abrasiveness of Al_2O_3 ceramic reinforcements [91–94].

Regarding to CVD diamond coated cutting tools for turning of Al metal matrix composites; Chou et al. [95] studied the CVD diamond tool performance in metal matrix composite machining. Monolayer microcrystalline CVD diamond of 30 μm thickness coated triangle WC–6Co cutting inserts. A359–20SiC_p was as the workpiece material. The turning conditions were: cutting speed (v) = 1–6 $m.min^{-1}$, feed rate (f) = 0.05–0.3 $mm.rev^{-1}$ and depth of cut (DOC) = 2 mm. They found that tool wear is sensitive to cutting speed (v) and feed rate (f). Moreover, the main wear mechanism was coating failure because of high stresses due to the thermal expansion difference between the coating and cutting tool at high cutting temperatures.

CVD diamond coated cutting tools, due to easier productivity, coating of complex cutting edge geometries and lower cost, can be an alternative of PCD for turning of metal matrix composites. Their performance is a function of the cutting tool material and geometry, turning conditions, adhesion strength of diamond coating–cutting tool, diamond coating roughness and thickness, as is shown by the different results in Figure 14 [96].

This was also proved by Vandevelde et al. [97] who evaluated the cutting applications of DLC, hard carbon and diamond films. Uncoated WC–6 wt.% Co, diamond–like carbon (DLC), amorphous hard carbon, CVD diamond coatings and PCD tools were used for turning of AlSi10–20 wt.% SiC. The turning conditions were: v = 100 $m.min^{-1}$, f = 0.1 $mm.rev^{-1}$ and DOC = 0.5 mm. The coating thickness of DLC, amorphous hard carbon and CVD diamond were: 1.4, 1.6 and 6–20 μm; respectively. Uncoated WC–6 wt.% Co, DLC and amorphous hard carbon exhibited short tool life (less than 2 min) and 20 μm CVD diamond showed tool life of 30 min compared to 12 min for 6 μm CVD diamond coating. For comparison, the PCD tool did not reach the end of its lifetime after 17 min of turning of AlSi10–20 wt.% SiC, and did not exhibit abrasive wear. Moreover, for turning of AlZnMnCu0.5, a 9 μm CVD diamond coated WC–6 wt.% Co cutting tool, showed higher tool life than un–coated and DLC–coated WC–6 wt.% Co cutting tool.

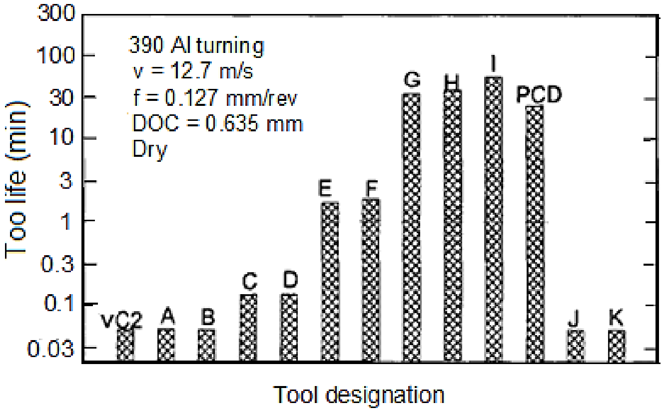

Figure 14. Performance comparison between a PCD, an uncoated carbide (VC2), and CVD diamond coated inserts (A–K) from various sources [96].

Moreover, concerning CVD diamond coated cutting tools as an alternative for PCD cutting tools, Polini et al. [98] investigated dry turning of alumina/aluminum composites with HFCVD diamond coated Co–cemented tungsten carbide tools. W6A.10A.T6 (Al6061–10 vol.% Al_2O_3) from Duraclan was used as the workpiece material in turning conditions of v = 480 m.min^{-1}, f = 0.4 mm.rev^{-1} and DOC = 1.5 mm. HFCVD diamond coatings with thicknesses of 11, 23 and 24 μm were deposited on WC–6 wt.% Co cutting tools with 1 μm of grain size, while HFCVD diamond coatings with thicknesses of 23, 24, 28, 23 and 26 μm were grown on WC–6 wt.% Co cutting tools with 3 μm of grain size. For comparison, PCD inserts with the same geometry were also examined. The results indicated that a 23 μm HFCVD diamond coated 1 μm WC–6 wt.% Co cutting tools illustrated low flank wear after both 10 and 15 min of turning the Al6061–10 vol.% Al_2O_3 which could compete with flank wear created on PCD tools.

Similar studies have been accomplished by Kanda [99] and Oles [100] for diamond–coated cemented carbide cutting tools for turning of Al–Si alloys. Their results indicated that diamond–coated carbide tools showed higher cutting performance than uncoated carbide tools and it can be an alternative for PCD cutting tools. Kremer et al. [101] carried out the turning of Al–5 vol.% SiC and Al–15 vol.% SiC MMC materials using three diamond morphologies coatings on hardmetal tools: a 6 μm monolayer rough diamond, a 6 μm monolayer smooth diamond and a 6 μm bi–layer rough/smooth diamond coating at v = 400–900 m.min^{-1} and f = 0.1, 0.3 mm.rev^{-1} in dry conditions. The rough monolayer coating demonstrated lowest flank wear compared to the smooth monolayer coating and bi–layer rough/smooth diamond coating. Regarding to surface roughness, Qin et al. [59] achieved to contrary findings compared to Kremer [101] when the turning of Al–20 vol.% SiC composite was evaluated at v = 4, 8 m.min^{-1}, f = 0.15, 0.3 mm.rev^{-1} and DOC = 1 mm using 25–30 μm nanocrystalline diamond coated WC–6 wt.% Co and conventional microcrystalline diamond (MCD) coated tools. The smoother diamond coatings demonstrated better cutting performance than microcrystalline diamond (MCD). The same behavior was observed for turning of an Al–SiC MMC using un–coated and DLC, HFCVD MCD and micro/nanocrystalline multilayered ultra–smooth diamond (USCD) coated WC–6 wt. % Co in which USCD exhibited 5 times tool life more than that of un–coated hardmetal tool and more than DLC and MCD coated WC–6Co [102].

In the present work, multilayer micro/nanocrystalline diamond (MCD/NCD) are deposited on cutting tools made of Si_3N_4 to machine Al–based metal matrix composite (Al–MMC) workpiece material. Cutting performance of the multilayer micro/nanocrystalline diamond (MCD/NCD) coated Si_3N_4 ceramic cutting tools in different conditions of cutting speed (v), feed rate (f) and depth of cut (DOC) is evaluated.

1.4. Mechanical seals

Figure 15 illustrates the revenue trend for mechanical seals market in USA, Canada and Mexico during 2005–2015 provided by Frost and Sullivan [103]. Frost and Sullivan is a global growth consulting company which provides market analysis; estimated the total mechanical seals market revenues in USA, Canada and Mexico reached to $992.4.0 million in 2008. The lowest revenues belong to 2009–2010 due to the financial crisis, but is expected that the mechanical seals market reaches to $1287.2 million revenues by 2015.

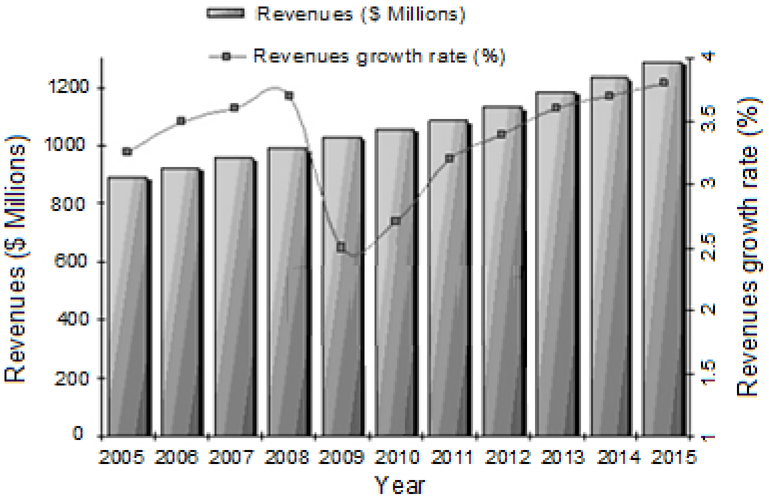

Figure 15. Seals market trend: revenue variation of mechanical seals in USA, Canada and Mexico during 2005–2015 [103].

Mechanical seals which for the first time were produced in 1940 are used in industrial pumps, compressors, mixers and other applications to provide a leak–prevented seal during liquids and gases motion between component parts. Regardless of the specific design of mechanical seals, three basic parts of mechanical seals involve seal faces, secondary sealing elements (O–rings, rubber boots, bellows) and metal parts (springs, retaining rings, drive pins, set screws, compression rings). Figure 16 shows a schematic representation of main parts of a typical mechanical seal. The seal performance is mostly defined by the sealing interface and interface materials design used [104].

Failure modes of mechanical seals can be categorized in three main categories: pressure, temperature, velocity and the combination of these factors. For instance, fluid pressure can cause extra heat at the seal face and consequently can increase the wear rate and maybe finally fracture and failure of material face and leakage of fluids. A very important parameter in mechanical seals design is the pressure–velocity (PV) coefficient. The PV coefficient is known as seal face product or system pressure and the seal linear velocity. This parameter is useful for estimation of seal reliability when it compared with manufacturer's limits. If the PV limit is exceeded, face seal may wear at a rate more than expected. Moreover, mechanical face materials design has the great of importance.

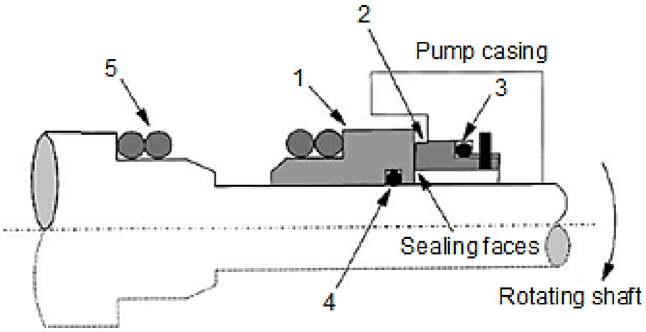

Figure 16. Schematic representation of a simple five–component mechanical seal: (1) rotary seal ring; (2) stationary seal ring; (3) stationary seal ring packing; (4) rotary seal ring packing; (5) spring [104].

The mated surface must have proper contact in order to prevent the dynamic motion of seal faces and creation of excessive heat which would conduct to failure of face seals and consequently increment of leakage rate. Also improper material face seal can cause the wear rate increment and face seal life decrement. Some examples of mechanical seal rings represented in Figure 17.

Figure 17. Some examples of mechanical seal rings.

Carbon has been used as a first material for one of the rubbing pairs in mechanical seals; however, Mechanical seal materials were developed in 1980s and a number of second generation alternatives have been created afterwards. These include the addition of some dopants to silicon carbide, such as TiB_2 and graphite, and the fabrication of distribution of pores in silicon carbide ceramic matrix; however, although those seals had successfully used, but they do not provide the obvious change in seal performance technology [104].

As mentioned above, face seal materials are one of the three main parts of a conventional mechanical seals. Face seal materials must have some physical and mechanical properties for good efficiency in mechanical seals like heat conductivity, wear resistant, stability, inertness and moreover face materials should be produced in easy and economical way. For the early usage of mechanical seals, some seal faces fabricated from metals like copper, bronze and Cr, Cr–Ni, and Cr–Ni–Mo hardened steels. Materials face seals have changed during time and some new materials face seals have been used such as SiC (reaction–bonded, pressure less sintered, silicon carbide/graphite composites), WC, Al_2O_3 ceramics and various types of carbon face seals because of high hardness and wear resistance, high stiffness and low thermal expansion [105–107].

Regarding to mechanical seal materials, Carrapichano et al. [108] accomplished the sealing performance of Si_3N_4 and Si_3N_4/SiC composite rings for dynamic sealing of circulating fluids. Si_3N_4 and Si_3N_4/30 wt.% SiC seal rings were tested as self–mated pairs and dissimilar sealing systems against grey cast iron i.e. Si_3N_4/Si_3N_4, Si_3N_4/GCI, and Si_3N_4/30 wt.% SiC/GCI. The tribological experiments were conducted in a ring–on–ring tribometer at $V = 4\ ms^{-1}$ of linear speed, in the range of 0.3–1 kN of applied load, under a pressure of 2×10^5 Pa of a mixture of 20 vol.% of hydrogen peroxide in deionized water, which gives an effective pressure (P) between 0.2 and 1.3 MPa. Their results showed that the system with better performance is the dissimilar pair Si_3N_4/grey cast iron, that presented wear coefficient values of $k = 4.2 \times 10^{-8}\ mm^3\ N^{-1}\ m^{-1}$ for the ceramic ring and $k = 1.3 \times 10^{-7}\ mm^3\ N^{-1}\ m^{-1}$ for the metallic ring, in tests performed for about 60 h and 890 km, with full sealing. This system presented an excellent combination $k \times PV \sim 0.1$ $\mu m.h^{-1}$, this product being a measure of the surface loss of a machine component for a given time of service.

Using carbon–base materials for sealing purposes, Wang and coworkers [109] carried out the experimental study on friction and wear behavior of amorphous carbon coatings for mechanical seals in cryogenic environment. Amorphous carbon (a–C) coatings were deposited on 9Cr18 alloy steel seals with $D_i = 45.5$ mm and $D_o = 55.5$ mm using pulsed DC magnetron sputtering and the seal tests were performed in liquid N_2 at 3000 rpm, 1 MPa during 400 seconds. Before deposition of a–C coatings, the wear rate of the 9Cr18 alloy steel seal was $3.5\times10^{-4}\ mm^3N^{-1}m^{-1}$. By a–C deposition, the wear rate decreased significantly to $6.7\times10^{-7}\ mm^3N^{-1}m^{-1}$.

Carrapichano and coworkers [110] studied the functionality diagrams for hybrid mechanical seals with silicon nitride rings. Ring–on–ring tribological tests were carried out by hybrid mechanical seals with silicon nitride (Si_3N_4) rings. The k × PV product, where k is the wear coefficient, P the sealing pressure, and V the linear speed, is proposed as a parameter to characterize the total working range of a mechanical seal system. The rotary Si_3N_4 rings exhibit the better sealing performance of $k \times PV = 0.05$ μm.h^{-1} against WC–Co mating faces.

One of the first works on deposition of diamond films on mechanical seal faces returns to 1990, in which an effort made to coat microcrystalline diamond films on SiC face seals. It has been proposed that diamond films can be worked with good efficiency for mechanical seal applications [111]. Owing to superior physical and mechanical properties of diamond like extreme hardness, low friction coefficient, high thermal conductivity, excellent chemical inertness, high abrasion and wear resistance diamond can be an ideal candidate coating material for usage in seal interfaces. Crystalline diamond films with different morphologies from large microcrystalline to ultra–nanocrystalline (UNCD) can be grown on different metallic and ceramic substrates via CVD processes. By having an extreme hardness and low coefficient of friction; diamond films have the ability to enhance the tribological properties of the seal faces [102].

Hollman and coworkers [112] examined the hot flame microcrystalline diamond coated WC–6Ni seal faces with the diamond thickness of 3.5–4 μm and compared with the commercially available seal materials in the self–mated tribosystem. The tests were performed with a nominal contact pressure of 0.5 MPa and a rotational speed of 3000 rpm which corresponds to a sliding speed of 3.5 ms^{-1}. In the steady state conditions, very low coefficient of friction (< 0.1) for diamond–diamond was obtained in water lubrication. Their work indicated that diamond as seal face coating has some advantage such as energy saving and longer seal life due to very low coefficient of frictions and very low wear rates.

Using diamond–coated mechanical seal faces, Tomé and coworkers [113] investigated the sealing performance of CVD diamond self–mated Si_3N_4 rings. Si_3N_4 seal faces were coated by microwave plasma chemical vapor deposition (MPCVD) technique during 2 h and 6 h, resulting in diamond coating thickness of 8 μm and 25 μm. The MPCVD diamond self–mated sealing systems were tested in ring–on–ring configuration varying the internal water pressure, the rotating speed and the applied load, leading to PV conditions in the range of 0.1–5.7 MPa.ms^{-1}. Their work showed that the finer grain sized diamond tribosystem could guarantee full sealing at PV∼ 0.8

$MPa.ms^{-1}$, by keeping a low friction coefficient of 0.05, for very long running time of 430 h (5730 km) without measurable wear.

Using nanocrystalline CVD diamond, Mubarok et al. [114] evaluated the enhanced sealing performance with CVD nanocrystalline diamond films in the self–mated mechanical seals. Nanocrystalline diamond (NCD) films were grown on Si_3N_4 mechanical seal faces. The nanocrystalline diamond coatings were grown through microwave plasma–assisted chemical vapor deposition (MPCVD) using $CH_4/H_2/N_2$ gas mixture with the diamond coating thickness of about 2 μm. The sealing performance and friction behavior of self–mated nanocrystalline diamond coatings were studied using the ring–on–ring configuration in which the rotating speed and the applied load was varied. Water sealing conditions were obtained in the PV (P, the effective pressure and V, the linear speed) range of 0.5–4.8 $MPa.ms^{-1}$. Their study indicated that the high hardness and smoothness of the nanocrystalline diamond coatings resulted in a very low and stable friction coefficient value of 0.01, without any measurable wear.

Sumant and coworkers [115] tested the ultra–nanocrystalline diamond (UNCD) film as a wear resistant and protective coating for mechanical seal applications. MPCVD ultra–nanocrystalline diamond with R_a = 20–30 nm and grain size 2–5 nm were coated reaction–bonded silicon carbide (SiC) seals (92% SiC and 8% Si). In addition, un–coated SiC seals have been tested under sealing conditions. Sealing tests were carried out in water with the rotational speed of 3000 rpm and 0.7 MPa pressure during 21 days (504 h). The results demonstrated that UNCD coated SiC seals compared to carbon counterbodies showed significantly higher performance than the uncoated SiC seals against carbon counterbodies or UNCD coated SiC seals against SiC counterbodies. They found that UNCD is an excellent material for application as a low friction and low wear rate coating for rotating shaft seals. In addition, UNCD coatings reduced the consumed energy, increased the seal life and decreased the maintenance cost.

Jones [116] studied the tribological behavior of carbon mechanical seal face materials in dry line contact. Different grades of carbon (composed of carbon, carbon/graphite and graphite), α–SiC and reaction–bonded SiC were used as mechanical seal materials. Initial seal tests were performed for measuring PV capability with the 0.5 ms^{-1} speed for 24 km in relative humidity around 55%. More tests were carried out using different grades of carbon and SiC mechanical seals for 25 km to evaluate potential for the transition from stable to unstable operating conditions. Carbon seals were as rotating cylinder and SiC seals were as stationary pad. The friction coefficient, frictional heat generated, the wear rate and surface roughness before and after the seal tests were measured. The PV values for carbon mechanical seals against α–SiC and reaction–bonded SiC were between 55–75 depends on the type of carbon mechanical seal. COF values at steady state were between 0.2–0.3 and the wear rates between 10^{-11}–10^{-12} $m^3.m^{-1}$ for carbon mechanical seals against α–SiC. Moreover, they found that these contact coating breakdown is by a seizure mechanism in which the breakdown of the contact coating caused a transition from a very low wear regime to a severe wear regime.

Using different seal materials, Jones [117] accomplished the tribological behavior of mechanical seal face materials in dry line contact using bulk ceramics, CVD diamond and diamond–like carbon (DLC) films. The tested seal materials were sintered α–SiC and reaction–bonded SiC, sintered α–SiC and reaction–bonded SiC+ graphite, WC–Co, different grades of mechanical carbon grades (carbon and carbon/graphite), diamond like carbon (DLC) film coated by unbalanced magnetron sputtering plus PACVD with 3.5–4.5 μm thickness and MPCVD grown coatings with 5–6 μm in thickness. Different combinations from seal materials were examined. Initial seal tests were performed for measuring PV capability with the 0.5 ms^{-1} speed for in relative humidity around 55% in pad and cylinder geometry. The friction coefficient, frictional heat generated, the wear rate and surface roughness before and after the seal tests were measured. Using bulk ceramic, the combinations of reaction bonded SiC with WC–Co and sintered sintered α–SiC were tested, also reaction bonded SiC + 30% graphite with α–SiC were examined. In addition, using hard coating, different combinations of reaction bonded SiC, sintered α–SiC with DLC and CVD diamond were tested. The results indicated that under dry moderate contact conditions mild deformation controlled wear occurred with contact surface polishing. Coating one of the contact surfaces with a CVD diamond or DLC film modified the contact dynamics which produced low friction coefficients. Also, the CVD coating increased the PV capability.

In the present work, Si_3N_4 ceramic face seal surfaces were coated by HFCVD with multilayered diamond and studied in a self–mated mechanical face seal tribometer.

Chapter 2

Experimental procedure

This chapter includes the details about fabrication, surface pre–treatments of Si_3N_4 ceramic substrates and multi–layered micro/nanocrystalline diamond films deposition in a semi–industrial hot–filament CVD (HFCVD) reactor. The as–grown diamond–coated Si_3N_4 ceramic samples are analysed using several characterization techniques. The experimental procedures concerning the tribological tests of diamond–coated Si_3N_4 discs and balls in lubricated and non–lubricated conditions are also included in this chapter. In addition, the experimental details of diamond–coated Si_3N_4 mechanical seal ring fabrication and sealing tests are a part of this chapter. Finally, the Si_3N_4 cutting inserts fabrication, CVD coating with diamond multilayers and turning conditions of an Al–based metal matrix composite (Al–MMC) workpiece material are given.

2.1. Silicon nitride (Si_3N_4) substrate fabrication

The first step of the present work was the fabrication of dense silicon nitride ceramic as a substrate for diamond deposition. The powder mixture was prepared using commercial powders: α–Si_3N_4 (Starck Gr. C), Y_2O_3 (Starck Gr. M11), and Al_2O_3 (Alcoa CT–3000SG) in 89.3/7.0/3.7 % weight proportion, respectively. At the next step, the mixed powders were milled by silicon nitride balls (200 g) in an attrition mill (Retsch PM 400) for 8 h in isopropyl alcohol (90 ml) media. The mill with the homogeneous suspension was placed in an oven at 75˚C for drying the homogeneous suspension and then milled for a few seconds to de–agglomerate the dried powder. After initial compaction of the powders by uniaxial compressive stress (30 MPa), the substrates were cold isostatically pressed (CIP) at 200 MPa and afterwards placed in a graphite crucible covered by a powder bed of Si_3N_4/BN (1:1).

The pressureless sintering process was performed in a graphite furnace (Thermal Technologies Inc.) at 1750˚C during 2 h under 0.1 MPa nitrogen atmosphere to prevent decomposition of silicon nitride at these temperatures. Pressureless sintering process of silicon nitride ceramic substrate followed the thermal cycle: heating up at 10˚C/min up to 1750˚C, 2 h stage at 1750˚C and cooling down at 10˚C/min stage. The density of the sintered specimens was determined by immersion using the Archimedes method (theoretical density of the powder mixture α–Si_3N_4, Y_2O_3 and Al_2O_3 by considering the weight proportions equals 3.254 g.cm^{-3}). The samples were weighted in a digital balance with 0.0001g accuracy and the relative density of the substrates was more than 99%. Figure 18 shows the graphite furnace for sintering of Si_3N_4 ceramic substrates in N_2 atmosphere used in the work.

Figure 18. Graphite furnace for sintering of Si_3N_4 ceramic substrates in N_2 atmosphere used in the work.

2.2. Fracture toughness of sintered Si_3N_4 ceramic substrates

Hardness is a property of a material that allows it to resist plastic deformation in the subsurface region of the material, which normally is caused by penetration into the surface of material. In this work, Vickers hardness test (Zwick/Roell ZHU, type 8187.5 LKV) with the load of 10 kgf (HV 10) was used to measure the hardness of sintered Si_3N_4 ceramic samples according to ASTM E92 and/or ISO 6507 (Figure 19). The full load was applied for 15 seconds. The indentations were repeated five times to minimize errors. Afterwards, the indentation marks were observed in optical microscopy and the average length of diagonal left by indenter calculated by IJ software and finally Vickers hardness values were calculated using following equation:

$$HV= 0.1891\times F/d^2 \qquad (2)$$

where d is the average length (mm) of the diagonals left by indenter and F is the indentation load (N).

Figure 19. Apparatus for hardness and fracture toughness of sintered Si_3N_4 ceramic substrates.

Fracture toughness (K_{1c}) is a measure of the resistance to catastrophic mechanical failure that bulk materials or thin films have in the presence of cracks. Common determination methods include single edge pre–cracked beam (SEPB), single edge notch beam (SENB), chevron notched beam, dual cantilever beam, dual torsion and surface crack in flexure methods. An alternative method is indentation fracture (IF) which has been widely used for determining fracture resistance of ceramics since it was initially proposed by Lawn et al. [118]. This method is particularly useful for samples of limited size. In this work, indentation test used to measure the fracture toughness of pressure less sintered Si_3N_4 ceramic specimens. There are some equations such as Niihara [119], Anstis [120], Evans [121], Shetty [122], and based on radial (median) and Palmqvist for mechanical properties measurement of ceramic substrates e.g. fracture toughness, hardness and Young´s modulus. In this work, the indentation fracture resistance, K_{1C}, was determined from the as indented crack lengths by the Niihara's equation for median crack system as follows [119].

$$K_{1C} = 0.0309\ (E/H)^{2/5} P C^{-3/2} \tag{3}$$

where E and H are Young's modulus and the Vickers hardness, respectively, P is the indentation force, and c is the half–length of the as–indented surface crack length.

2.3. Surface preparation of disc and ball Si_3N_4 ceramic substrates

Disc–shaped silicon nitride based ceramic samples were subjected to the following surface pre–treatment: 46 µm grit size diamond wheel grinding to obtain the final dimension (10 mm diameter and 3 mm thickness), 15 µm diamond polishing on a metallic plate, and CF_4 plasma etching for 10 min using a RF generator (13.56 MHz, EMITECK K1050X). Subsequently, Si_3N_4 discs were rinsed in an ethanol bath in ultrasound bath for 10 min. Diamond nucleation on non–diamond surfaces is usually very slow. Unlike diamond substrates, a non–diamond substrate often needs a pre–treatment prior to diamond deposition. Several different pre–treatment methods have been developed, such as manual scratching, ultrasonic abrasion, and bias enhanced nucleation. These are very useful methods for achieving a high nucleation density and uniform grain size. In this work, diamond seeding of the substrates was done by abrasion in an ultrasonic bath by the diamond powder and ethanol. Diamond seeding of disc–shaped Si_3N_4 substrates was done by ultrasonic agitation with nano–diamond powder suspension for 1 h in ethanol to promote diamond nucleation. After diamond seeding, disc samples were rinsed in ethanol bath by ultrasonic agitation for 5 min and then dried. Concerning the Si_3N_4 balls, part of the surface was flattened by diamond coated metallic wheel. Then they were polished with 15 µm sized diamond powder suspension for 3 h in order to obtain a rougher surface and seeded by ultrasonication with nano–diamond suspension for 1 h. After diamond seeding, Si_3N_4 balls were rinsed in ethanol bath by ultrasonic agitation for 5 min and then dried.

2.4. Hot–Filament CVD (HFCVD) reactor system

A home–made HFCVD system with 50 cm diameter made of stainless steel coupled with a 400 A DC power supply, a vacuum rotary pump and gas feed connectors, uses tungsten wire (ϕ = 0.3 mm) as a filament for the production of CVD diamond coatings on flat and ball Si_3N_4 ceramic specimens. In this semi–industrial apparatus (Figure 20) the deposition area may be as large as 20x30 cm^2.

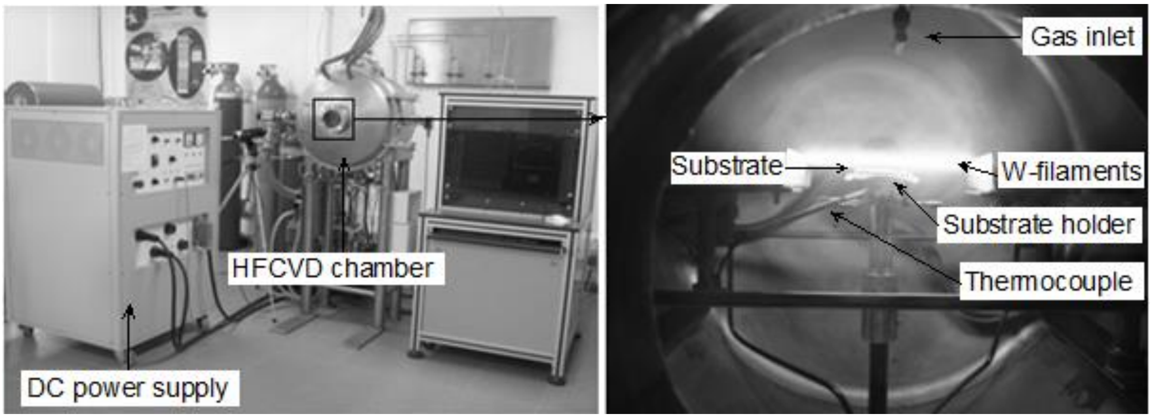

(a) (b)

Figure 20. Home–made hot–filament CVD (HFCVD) reactor present in this work.

For diamond deposition, the gas phase reactants mostly used were hydrogen and a carbonaceous precursor such as methane. Before deposition, the chamber is evacuated to remove all oxygen. Figure 21 shows the vacuum level versus time for HFCVD reactor which used in this study, in a procedure done to ensure that there are no major leaks before each run.

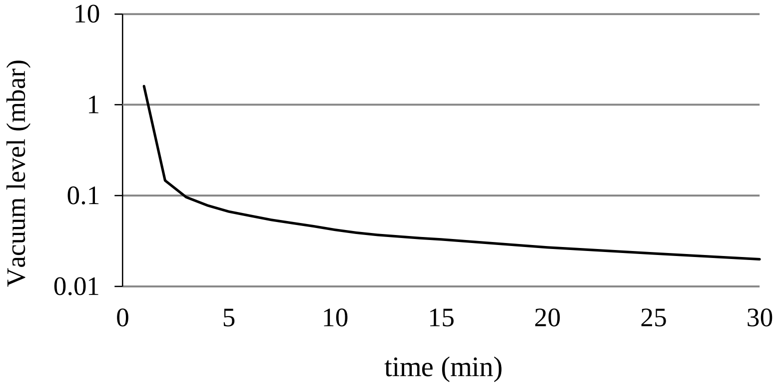

Figure 21. Vacuum level versus time for HFCVD reactor in the present work.

Generally, refractory metals such as W, Ta and Re are used to make the filaments for HFCVD reactors. It is important that the filament material or their carbides (WC, W_2C or TaC, Ta_2C) have a very high melting point. In this work W filaments were used for the activation of the gas mixture. Tungsten wires 300 µm in diameter were unwound from the roll in lengths of 15 cm to make a horizontal arrangement over the Si_3N_4 ceramic substrates. The distance between each W–filament was 5 mm. The DC power supply in current control mode was used to heat the filament to about 2250–2300˚C and the required current is typically in the range 10–11 A/filament during deposition. The temperature of the filaments was measured using a two colour pyrometer (Raytek). For the carburization of W filaments, done before the deposition, they were heated up to 2400˚C in the reactor chamber under methane (CH_4) and hydrogen (H_2) gas mixture with methane to hydrogen ratio of 4 and a total flow of 1000 ml.min^{-1}. Because of the carburization process of W filaments and the resulting resistivity increment, the filament temperature is drastically increased for the imposed current that is then reduced to the deposition conditions using the current controller. During carburization of W, the filaments are kept away from the substrate to prevent the deposition of amorphous or undesired components. The resulting carburized filaments are more stable than the metallic ones under the diamond deposition conditions. However, a disadvantage of the carburization process is that carburized filaments lose their ductility and become very brittle, which make their lifetime short. After carburization of the W filaments, the reactant gases were removed from the reactor chamber and the deposition conditions were then imposed according to the scheduled experiment.

Figure 22(a) & (b) shows typical filament and substrate temperature versus time curves during carburization of W filaments which are repeatable for the given carburization conditions ($CH_4/H_2 = 0.04$, total flow = 1000 ml.min^{-1}, 6 filaments and vacuum level= 0.02 mbar). Substrates were kept 15 cm away from the W filament to prevent formation of metallic W carbides on the ceramic substrates.

A 5 mm diameter metallic tube was used as a gas inlet to feed the gas mixture consisting of methane and hydrogen into the reaction chamber. Mass flow controllers were used to regulate the methane and hydrogen gas flow, keeping constant the flow rate of the reactant gasses during the diamond deposition process using HFCVD reactor. The pressure inside the chamber of the HFCVD reactor was measured using an accurate pressure gauge. A substrate holder made of silicon nitride ceramic was positioned right beneath the W filaments. The substrate temperature was measured using a thermocouple mounted just below the substrate holder. The substrate temperature, one of the most important parameters in HFCVD process of diamond coating, can affect the morphology of the coated diamond. It strongly depends on the filament temperature. Substrate–filament distance during HFCVD process of diamond coating is another important factor, which should be less than 10 mm (about 5–7 mm). Due to the difference in the coefficients of thermal expansion (CTE) between the film and the substrate the cooling step after diamond deposition using HFCVD reactor was done slowly (10–15˚C/min) to prevent crack propagation and spall off of diamond film from the substrate.

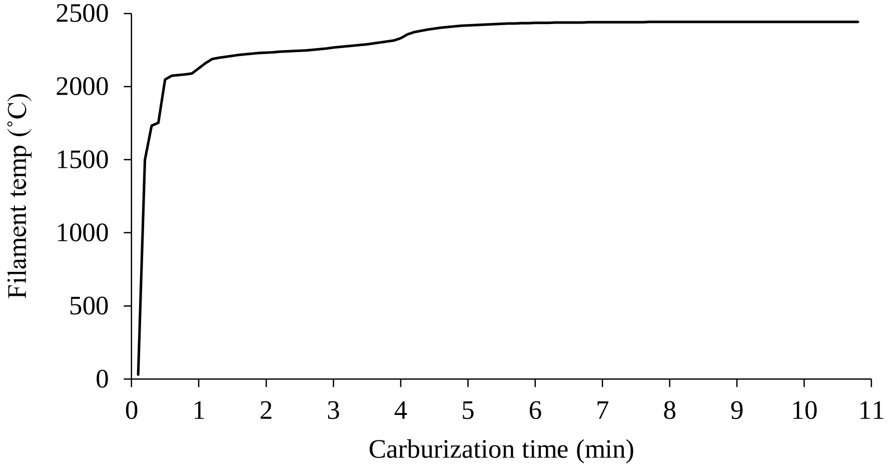

(a)

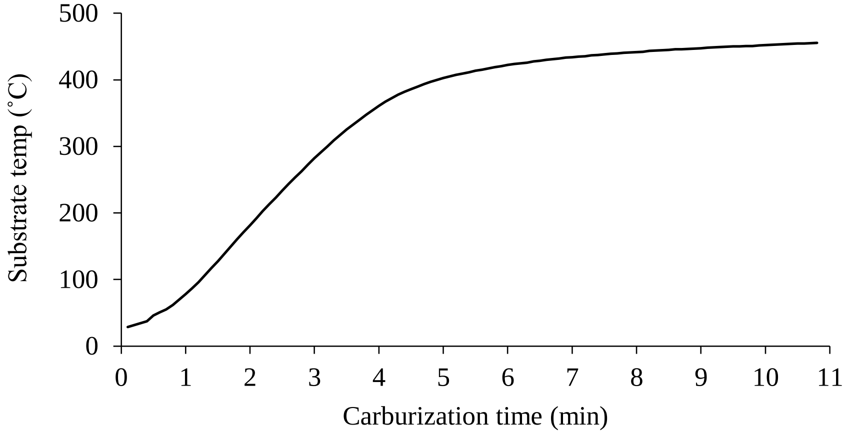

(b)

Figure 22. Typical (a) filament and (b) substrate temperature vs time curve during carburization of W filaments in the HFCVD reactor present in this work ($CH_4/H_2 = 0.04$, total flow = 1000 $ml.min^{-1}$, 6 filaments and vacuum level= 0.02 mbar).

In summary, there are many parameters such as filament ($T_{fil.}$) and substrate temperature ($T_{sub.}$), total flow (F) of reactant gases, chamber pressure (P), and methane to hydrogen ratio, affecting the CVD process. Many experiments were performed in order to optimise the conditions of the experiment for the desired morphology of the coated diamond on substrate.

2.5. Characterization of diamond–coated Si_3N_4 ceramic samples

Field emission scanning electron microscopy (FE–SEM) was carried out using a Hitachi SU–70 or a Hitachi S–4100 system for surface morphology characterization of top view and cross section of the diamond–coated Si_3N_4 ceramic substrates. UV μ–Raman spectroscopy (Horiba Jobin Yvon HR 800UV), using the line 532 nm from a He–Cd laser (Kimmnik series) permits the identification of the carbon phases i.e. diamond, DLC and graphitic phases. Linear profilometry (Mahr, Perthometer M1) and AFM scans (Nanoscope IIIa, Digital Instruments) were employed to determine the surface roughness of uncoated and diamond–coated Si_3N_4 ceramic substrates. Crystalline structure of the diamond coatings and ceramic substrates was determined using X–ray diffraction analysis (XRD) carried out by a Philips X'Pert MPD equipment with Cu K_α, λ =1.5406 Å (40 kV; 50 mA).

Adhesion strength is a very important parameter to evaluate the mechanical properties of coated surfaces in order to optimize the coating process. Adhesion strength can be determined by the application of a force to the coating–substrate system. This force may be applied in normal or parallel directions to the surface by performing scratch or indentation tests. In the evaluation of diamond adhesion, the simpler method of Brale indentation is usually performed. The Brale indenter tip is the same used in Rockwell hardness tests (diamond, cone angle of 120˚ and tip radius of 0.2 mm) but it was coupled to a universal mechanical testing machine for applying increasing force values. Figure 23 presents the apparatus (Zwick/Roell type Z 020) for adhesion strength determination of diamond coated Si_3N_4 ceramic substrates in the present work. After indentation, adhesion strength is determined by measuring the induced radial and lateral cracks in the film.

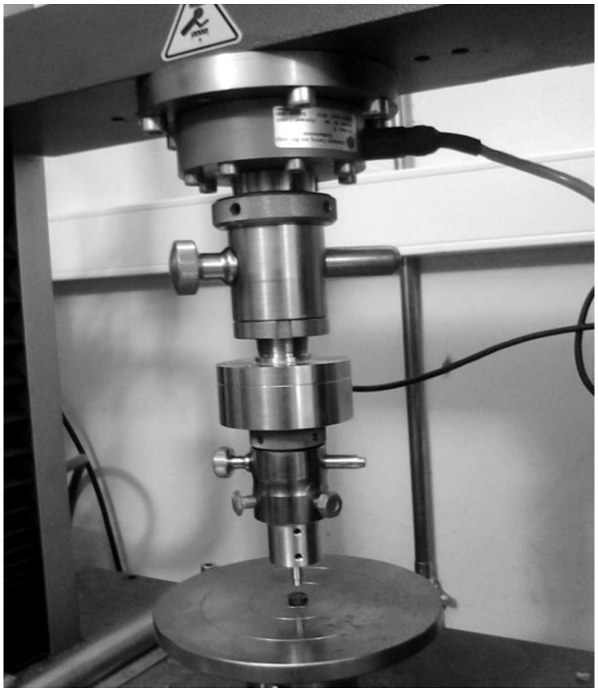

Figure 23. Apparatus for adhesion strength evaluation of diamond–coated Si_3N_4 ceramic substrates.

2.6. HFCVD diamond coated large Si_3N_4 discs and balls and their tribological testing

Large disc–shaped silicon nitride based ceramic substrates (ϕ45 mm × 9 mm) were subjected to the following surface pre–treatment: 15 μm diamond polishing on a metallic plate, and CF_4 plasma etching for 10 min in a RF generator (13.56 MHz, EMITECH K1050X). Subsequently, Si_3N_4 discs were rinsed in an ethanol bath for 10 min. In this work, commercial Si_3N_4 ceramic balls (KemaNord) with a 5 mm diameter were used as counterface in the self–mated tribological tests. The Si_3N_4 ceramic balls were roughened by 15 μm diamond suspension for 3 h. Diamond nucleation on non–diamond surfaces is very slow. Unlike diamond substrates, a non–diamond substrate often requires a pretreatment before diamond coating. Substrate scratching by diamond particles was found to be the simplest, very useful way to achieve a high nucleation density and uniform grain size. Diamond seeding of the substrates was performed through scratching in an ultrasonic bath by the nano–diamond powder and ethanol. Diamond seeding of disc–shaped Si_3N_4 substrates and Si_3N_4 balls was done by ultrasonic agitation with nano–diamond suspension for 1h in ethanol to provoke diamond nucleation. After diamond seeding, large Si_3N_4 disc and ball substrates rinsed in ethanol bath by ultrasonic agitation for 5 min and then dried.

Table 1 represents HFCVD optimized conditions for diamond deposition onto Si_3N_4 large disc and ball ceramic substrates.

Table 1. HFCVD conditions for multilayer diamond deposition on Si_3N_4 large disc and ball ceramic substrates.

	Monolayer MCD	Monolayer NCD
$T_{fil.}$(˚C)	2260	2330
T_{sub}.(˚C)	850	750
CH_4/H_2 (%)	2	4
F (ml.min^{-1})	1800	900
P (mbar)	75	25
t (min)/layer	60	84
t (h)/total	5	7

Sliding wear tests of self–mated diamond coated large discs and balls tribosystem were performed in a ball–on–flat (BOF) adapted tribometer (Plint 67/R) using an unlubricated reciprocating sliding configuration with constant frequency (1 Hz) and stroke length (8 mm). In this configuration, normal applied loads varied in the 40–190 N range and relative humidity changed from 10–90%. The effect of temperature was studied in this configuration in the 25°C–100°C range. Above 100°C ball–on–disc (BOD) circular sliding tests were conducted.

Table 2 illustrates wear test conditions of multilayer micro/nanocrystalline diamond (MCD/NCD) coated large Si_3N_4 discs in the present work: load (F), time (t), sliding distance (X), relative humidity (RH), temperature (T) and linear velocity (v).

Table 2. Wear test conditions of multilayer micro/nanocrystalline diamond coated large Si_3N_4 discs.

Configuration	F (N)	t (h)	X (m)	RH (%)	T (°C)	v (mm.s^{-1})
Ball–on–flat (reciprocating)	40–190	1	14.4–57.6	10–90	25–100	16
Ball–on–disc (circular)	40–80	1	260–340	ambient	100–250	94.2*

*Linear velocity for r= 15 mm, depends on the r, the linear velocity changes in circular wear tests.

Figure 24 illustrates the wear test configuration used in the present work for tribological investigation of self–mated multilayer micro/nanocrystalline diamond (MCD/NCD) HFCVD coated Si_3N_4 discs and Si_3N_4 ball counterfaces.

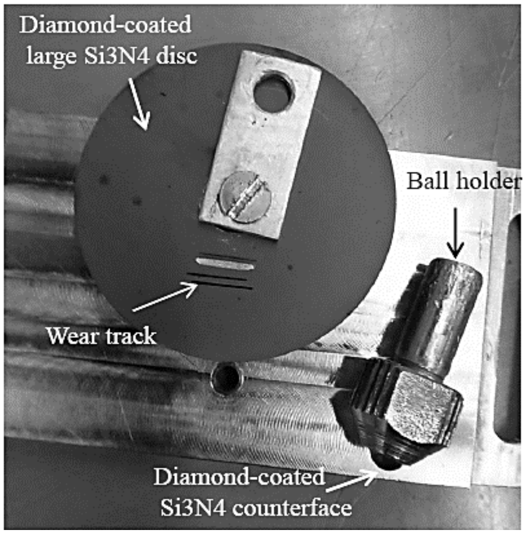

Figure 24. Ball–on–flat reciprocating sliding wear test configuration used in the present work.

The friction force was measured by a load cell, its signal amplified and processed by a personal computer. Prior to testing, the load cell was calibrated by applying two to three known dead–weights in the range of the measured loads. The friction coefficient is given by the ratio of the friction force and the normal load. The wear coefficient (*k*) of the ball specimens was estimated from the wear volume (*V*), obtained from near–circular wear scars of diameter (*d*) measured by optical/electron microscopy micrographs and the ball radius (*r*), divided by the applied normal load (*W*) and the sliding distance (*L*), following Archard's equation of wear:

$$k = \frac{V}{W \times L} = \frac{\pi \times d^4}{64 \times r \times W \times L} \qquad (4)$$

In the case of the discs, a 3D optical profilometer (Sensofar, S–neox) was used to acquire topographic images and data of the volume (V) of the wear tracks was calculated using SensoMap software. After the sliding tests, the surface morphology of the bare SN, the as–deposited diamond films and the wear tracks were observed by optical microscopy (OM) and scanning electron microscopy (SEM).

2.7. HFCVD diamond coated small Si_3N_4 discs and balls and their tribological testing

Small pressureless sintered Si_3N_4 discs (10 mm diameter per 3 mm thickness) and commercial balls (5 mm diameter) were tested in bare state and also used as substrate materials for the deposition of CVD diamond films. Prior to the diamond deposition, the discs were lapped with 15 µm diamond suspension followed by diamond seeding with 1 µm powder suspension in ultrasonic bath for 1 hour. Similarly, the balls were pre–treated with a 15 µm diamond suspension in ethanol in a rotary container for 1 hour and then seeded with the 1 µm powder suspension for more 30 min. The diamond coatings were grown by HFCVD. Two types of coatings were performed: i) a single layer (SL) of microcrystalline diamond (MCD); ii) three bilayers of microcrystalline /nanocrystalline diamond (ML samples). The respective growth conditions are presented in Table 3.

Table 3. Growth conditions of the single layer (SL) and multilayer (ML) diamond coatings and their respective root–mean–square (RMS) surface roughness values of the as–deposited end surfaces.

	MCD	NCD
T_{fil} (ºC)	2225	2275
T_{Sub} (ºC)	900	800
CH_4/H_2 (%)	1.5	3
F ($ml.min^{-1}$)	900	900
P (mbar)	175	25
RMS (nm)	340 ± 40	120 ± 25

The characterization of the coatings was performed by scanning electron microscopy (SEM, FEI Magellan and Hitachi SU–70) and atomic force microscopy (AFM, Digital Instruments Model NanoScope IIIa) operated in tapping mode with a scan size of 15×15 μm^2.

For comparison, self–mated steel tribopairs were made of AISI 52100 hardened chrome alloy steel. The plate was the flat surface of a disc machined by a local supplier, with a hardness value around 64 HRC, obtained by oil quenching from 850 ºC, followed by tempering at 150 ºC. The discs, of 70 mm in diameter and 5 mm in thickness, were ground finished, having a measured hardness value of 800 HV10 (62.5 HRC) and mirror–polished to a R_a ~ 2 nm, having a final hardness value of 700 HV10 (58.5 HRC). The ball counterparts were supplied by PCS Instruments, having 6.35 mm in diameter, hardness value specified to 58–66 HRC and a mirror–polished surface with R_a ~ 20 nm.

The tested fuel is a commercial soybean oil derived biodiesel (Shell), with a kinematic viscosity of 4.2 mm^2/s at 40 ºC. It has an ester content of 98.4 wt% and the main fatty acid methyl esters (FAMEs) constituents are: C16:0 – methyl palmitate – 14.0 wt%; C18:0 – methyl stearate – 4.2 wt%; C18:1 – methyl oleate – 25.5 wt%; C18:2 – methyl linoleate – 47.5 wt%; C18:3 – methyl linolenate – 5.4 wt%. The other contaminants, which can influence the tribological behaviour, are: monoglycerides (0.5 wt%), diglycerides (0.16 wt%); triglycerides (0.1 wt%) and water content (870 ppm).

The self–mated tribological tests of the four types of tribopairs (bare Si_3N_4 ceramic disc – SN, SL, ML and steel) were conducted in a CETR UMT3 tribometer, with a reciprocating ball–on–flat configuration under 6 mm stroke and 1 Hz frequency (average linear velocity of 12 $mm.s^{-1}$) in a bath lubricated with biodiesel. Tests under applied loads ranging from 20 to 100 N (corresponding to 2.5 to 4.5 GPa of initial maximum Hertzian contact pressures) were run for 2 hours of test time (~ 86 m of sliding distance, named short–term tests). Additional tests were performed at a chosen Hertzian contact pressure of ~ 3 GPa (40 N for the SN, SL and ML systems, and 145 N for the steel one), lasting 18 h of test time (~ 780 m of sliding distance, named endurance tests).

The friction coefficient is given by the ratio of the tangential contact force, measured by a load cell attached to the upper ball sample holder, and the normal load, measured by the same load cell. The wear coefficient (k) of the ball specimens using Archard's equation of wear (Eq. 4). In the case of the discs, a 3D surface profiler (Taylor Hobson PGI 830) with dedicated software (TalyMap) was used to process the images and get data of the volume (V) of the wear tracks for the Archard's equation.

2.8. Testing of HFVCD diamond coatings on Si_3N_4 mechanical seal rings

For the tribological testing of mechanical seals, pressureless sintered Si_3N_4 rings were fabricated and coated with multilayered CVD diamond, according to Table 4. The dimensions of the rings are the following: (external diameter × internal diameter × thickness): 43 mm × 33 mm × 8.5 mm (upper rings) and 46 mm × 31 mm × 7.5 mm (lower rings). After flat lapping with 15 µm diamond suspension, they were dry etched with CF_4 plasma for 10min. Seeding was done by nano–diamond slurry in ultrasound agitation for 1 h.

Table 4. HFCVD diamond growth conditions of monolayer microcrystalline diamond (MCD) and multilayer micro/nanocrystalline diamond (MCD/NCD) diamond coatings on Si_3N_4 mechanical seal faces.

	Monolayer MCD	Multilayer MCD/NCD
$T_{fil.}$ (˚C)	2255	2255; 2325
T_{sub} (˚C)	850	850; 750
CH_4/H_2 (%)	2	2; 4
F(ml.min^{-1})	1800	1800; 900
P (mbar)	75	75; 25
t(min)/layer	–	60; 84
t (h)/total	10	12 (5; 7)

Figure 25 shows the rotary tribometer (TE–92 Plint) used for the sealing tests of HFCVD diamond–coated Si_3N_4 mechanical seal faces which were carried out in biodiesel and pressurized water (2 bars) conditions. The tribological behaviour was investigated in ring–on–ring self–mated planar contact configuration according to ASTM D3702 standard. The friction coefficient (µ) is the average value for each working regime taken from the instantaneous torque appraised from a load cell in steady–state condition.

Figure 25. TE–92 Plint tribometer for the sealing tests of HFCVD diamond–coated Si_3N_4 mechanical seal faces.

Figure 26 is a sketch of the geometry of the ring–on–ring self–mated diamond–coated Si_3N_4 mechanical seal faces in the present work. Tables 5 and 6 compile the testing conditions of monolayer microcrystalline diamond (MCD) and multilayer micro/nanocrystalline diamond (MCD/NCD) coated Si_3N_4 mechanical seal ring faces in biodiesel lubrication.

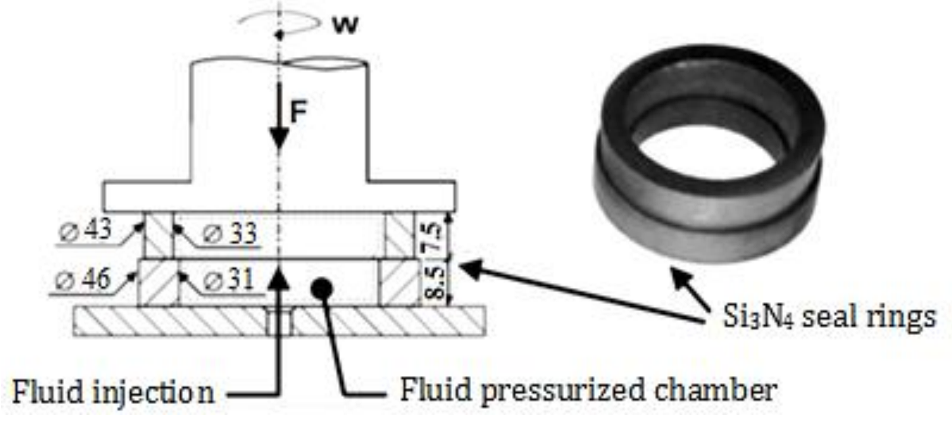

Figure 26. Sketch of the geometry of the ring–on–ring tribological test under internal fluid pressure (ω–angular speed of the upper ring; F–normal applied load). Rotating sample–upper ring; fixed sample–lower ring [108].

Table 5. Sequential runs of testing of single layer (SL) microcrystalline diamond (MCD) coated Si_3N_4 mechanical seal ring faces under biodiesel lubrication. ω─angular speed of the upper ring; F─normal applied load; V– linear velocity; P – contact pressure; t– duration of run; L – sliding distance.

ω (rpm)	V (ms^{-1})	F (N)	P (MPa)	t (s)	L (m)
250	0.5	150	0.24	3600	1800
250	0.5	250	0.40	3600	1800
250	0.5	350	0.56	1800	900
250	0.5	450	0.72	10800	5400
250	0.5	550	0.88	1800	900
250	0.5	650	1.04	1800	900
250	0.5	750	1.20	1800	900
250	0.5	850	1.36	1800	900
250	0.5	900	1.44	1800	900
250	0.5	500	0.80	14400	7200
250	0.5	500	0.80	14400	7200
250	0.5	500	0.80	14400	7200
250	0.5	500	0.80	14400	7200
250	0.5	350	0.56	18000	9000
250	0.5	350	0.56	18000	9000
250	0.5	350	0.56	10800	5400
250	0.5	350	0.56	28000	14000
250	0.5	350	0.56	3600	1800
250	0.5	350	0.56	14400	7200
250	0.5	350	0.56	28800	14400
350	0.7	350	0.56	3600	2520
350	0.7	350	0.56	14400	10080
400	0.8	350	0.56	3600	2880
450	0.9	350	0.56	3600	3240
500	1	350	0.56	3600	3600
600	1.2	350	0.56	3600	4320
600	1.2	350	0.56	3600	4320
600	1.2	350	0.56	3600	4320
600	1.2	250	0.40	10800	12960
			Total	71.7 h	152.2 km

Table 6. Sequential runs of testing of multilayered (ML) micro/nanocrystalline diamond (MCD/NCD) coated Si_3N_4 mechanical seal ring faces under biodiesel lubrication. ω–angular speed of the upper ring; F–normal applied load; V– linear velocity; P – contact pressure; t– duration of run; L – sliding distance.

ω (rpm)	V (ms^{-1})	F (N)	P (MPa)	t (s)	L (m)
250	0.5	350	0.56	14400	7056
250	0.5	350	0.56	3600	1764
250	0.5	350	0.56	10800	5292
250	0.5	350	0.56	10800	7056
250	0.5	350	0.56	10800	7056
250	0.5	350	0.56	14400	7056
250	0.5	350	0.56	14400	7056
250	0.5	350	0.56	14400	7056
250	0.5	350	0.56	14400	8820
250	0.5	350	0.56	14400	14112
250	0.5	350	0.56	18000	14112
250	0.5	350	0.56	28800	14112
250	0.5	350	0.56	22800	14112
250	0.5	350	0.56	28800	14112
250	0.5	350	0.56	28800	14112
250	0.5	350	0.56	28800	14112
250	0.5	350	0.56	28800	14112
250	0.5	350	0.56	28800	14112
250	0.5	350	0.56	28800	14112
250	0.5	350	0.56	28800	14112
250	0.5	350	0.56	28800	14112
250	0.5	350	0.56	28800	14112
250	0.5	350	0.56	28800	14112
250	0.5	350	0.56	28800	14112
250	0.5	350	0.56	28800	14112
250	0.5	350	0.56	28800	14112
350	0.7	350	0.56	10800	7452
450	0.9	350	0.56	3600	3204
250	0.5	350	0.56	28800	14112
250	0.5	350	0.56	28800	14112
250	0.5	350	0.56	28800	14112
250	0.5	350	0.56	28800	14112
250	0.5	350	0.56	28800	14112
250	0.5	350	0.56	7200	5688
600	1.1	350	0.56	7200	5688
250	0.5	350; 900	0.56; 1.44	7200	3528
			Total	220 h	394 km

Moreover, after this series of tests, longer single run ring–on–ring tests under biodiesel lubrication were performed for self–mated SL and ML mechanical seal ring pairs, Table 7. These tests were performed in stable conditions regarding vibrations and temperature evolution.

Table 7. Long tests of multilayered (ML) micro/nanocrystalline diamond (MCD/NCD) coated Si_3N_4 mechanical seal ring faces under biodiesel lubrication. ω─angular speed of the upper ring; F─normal applied load; V– linear velocity; P – contact pressure; t– duration of run; L – sliding distance.

	ω (rpm)	V(ms^{-1})	F (N)	P (MPa)	t (h)	L (km)
SL	250	0.5	350	0.56	16	28.8
ML	250	0.5	350	0.56	16	28.8

The sealing tests of SL and ML pairs were done with pressurized water (P_{H2O}= 2 bar) and not with biodiesel due to safety issues related to excessive heating. Test conditions until sealing P.V conditions were reached are given in Table 8 and Table 9, for SL and ML rings, respectively.

Table 8. Water sealing testing conditions of single layer (SL) microcrystalline diamond (MCD) coated Si_3N_4 mechanical seal ring pairs. ω─angular speed of the upper ring; F─normal applied load; V– linear velocity; P – contact pressure; t– duration of run; L – sliding distance.

ω (rpm)	V (ms^{-1})	F (N)	P (MPa)	t (s)	L (m)
250	0.5	350*	0.56	1800	882
250	0.5	500*	0.8	1800	882
250	0.5	650**	1.04	–	–
250	0.5	800**	1.28	–	–
250	0.5	900**	1.44	–	–
250	0.5	1000	1.6	1800	882
			Total	1.5 h	2.6 km

* Leakage observed

** Still high leakage (which requires the increase of load) – Immediate stop

Table 9. Water sealing testing conditions of multilayer layer (ML) MCD/NCD coated Si_3N_4 mechanical seal ring pairs. ω─angular speed of the upper ring; F─normal applied load; V– linear velocity; P – contact pressure; t– duration of run; L – sliding distance.

ω (rpm)	V (ms^{-1})	F (N)	P (MPa)	t (s)	L (m)
250	0.5	900	1.44	1800	882
250	0.5	900	1.44	1800	882
250	0.5	900	1.44	14400	7056
			Total	5 h	8.8 km

Moreover, long tests with ML rings were carried out in water lubrication conditions at a much higher angular velocity of ω= 2000 rpm in load range of F= 350–900 N as presented in Table 10. These tests were performed in order to determine the P.V limit of the ML seal rings.

Table 10. Long seal tests of multilayer layer (ML) MCD/NCD coated Si_3N_4 mechanical seal ring faces under water. ω─angular speed of the upper ring; F─normal applied load; V– linear velocity; P – contact pressure; t– duration of run; L – sliding distance.

ω (rpm)	V (ms^{-1})	F (N)	P (MPa)	t (s)	L (m)
2000	3.9	350	0.56	3600	14040
2000	3.9	500	0.8	3600	14040
2000	3.9	650	1.04	3600	14040
2000	3.9	650	1.04	3600	14040
2000	3.9	650	1.04	3600	14040
2000	3.9	650	1.04	7200	28080
2000	3.9	650	1.04	7200	28080
2000	3.9	650	1.04	7200	28080
2000	3.9	800	1.28	7200	28080
2000	3.9	900	1.44	7200	28080
2000	3.9	900	1.44	7200	28080
2000	3.9	850	1.36	7200	28080
2000	3.9	850	1.36	7200	28080
			Total	21 h	293 km

2.9. Fabrication of silicon nitride (Si_3N_4) ceramic inserts, HFCVD diamond growth and turning tests of Al–MMC workpiece material

Production of the ceramic cutting inserts followed the powder route using the HC Starck StarCeram grade P ready–to–press spray dried powder. This is a mixture of Si_3N_4, sintering aids (Al_2O_3 and Y_2O_3) and a polymeric binder. After uniaxial pressing in an insert die, the triangularly shaped inserts with a central hole were debound under air at 400 °C during 4 h and then fully densified by pressureless sintering at 1750 °C for 2 h, in an atmosphere of 0.1 MPa N_2. The sintered ceramic parts were ground to standard normalized triangle geometry (TNMA160408F) shaped inserts. The tool face was lapped with 15 μm diamond slurry in an iron/polymer plate. Prior to diamond coating, all inserts were dry etched in a CF_4 plasma treatment that has proved to largely increase the adhesion of diamond. A controlled micro–roughness is obtained by etching of the Si_3N_4 grains, thus increasing the mechanical interlocking of diamond at the surface of the substrate. Finally, they were ultrasonically seeded in an ethanol suspension of nanodiamond powder (4–6 nm) for 1 h.

Ten–fold multilayer micro–/nanocrystalline (MCD/NCD) diamond coatings were grown by HFCVD on one of the faces of the inserts, thus yielding three cutting tips per tool. The total of ten layers is made of five MCD and five NCD alternating layers with deposition conditions in Table 11, always starting with MCD. Two types of inserts were produced: ML10x1 with 12–14 µm of total thickness; and ML10x2 where the thickness of each layer was doubled resulting in 21–24 µm of total thickness.

Table 11. HFCVD conditions of multilayer micro/nanocrystalline diamond growth on Si_3N_4 cutting inserts.

	10L(MCD/NCD)/12μm	10L(MCD/NCD)/24μm
$T_{fil.}$ (˚C)	2255; 2325	2255; 2325
T_{sub} (˚C)	850; 750	850; 750
CH_4/H_2 (%)	2; 4	2; 4
F (ml.min^{-1})	1800; 900	1800; 900
P (mbar)	75; 25	75; 25
t (min)/layer	48; 96	96; 192
t (h)/total	4; 8	8; 16

An Al–based metal matrix composite (Al–MMC) was used as the workpiece material in the present work. Light metal matrix composite materials reinforced with ceramic particles have received wide attention during past decades due to their superior mechanical properties. Al_2O_3 reinforced Al–MMCs have been mostly used in automotive, aircraft industry and aerospace because of casting productivity, high strength to weight ratio, and proper tribological properties compared to the unreinforced alloys. A billet–shaped Al–MMC (∅20cm x L40cm cylinder) from Leichtmetall Kompetenzzentrum Ranshofen (LKR, Austria) of the type W6A.15A (aluminium wrought alloy 6061 reinforced with 15 vol.% Al_2O_3 particles) was used as the workpiece material. Density measurements on the workpiece materials using Archimedes principle returned a density of 2.83 $g.cm^{-3}$, while the bulk Vickers hardness measured using a 10kgf load is HV_{10} = 113 kgf/mm^2.

The Si_3N_4 cutting inserts used to machine this MMC are shown in Figure 27a shows, while the SEM micrograph in Figure 27b shows the microstructure of this Al_2O_3–Al composite, evidencing irregularly shaped alumina particles (5–15 µm) evenly distributed in the aluminium matrix, inside the grains and across grain boundaries. It can also be seen that the microstructure is generally free of pores.

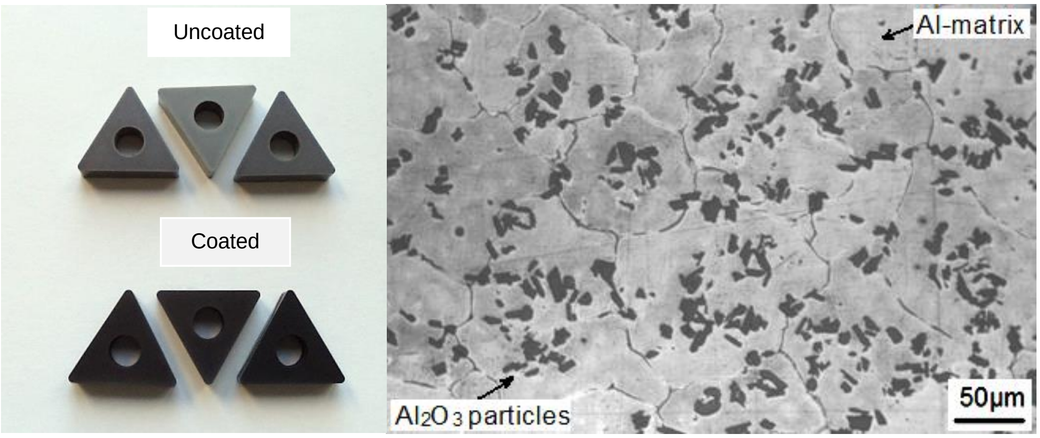

(a) (b)

Figure 27. a) Si_3N_4 cutting inserts before and after diamond coating using a home–made HFCVD reactor; b) SEM micrograph of the Al–MMC workpiece material etched by Keller´s reagent.

The turning tests of Al–MMC workpiece material were performed in DURIT Company using a CNC lathe (Mori Seiki) with a maximum spindle speed of 3500 rpm. A three–axis dynamometer platform (Kistler type 9129AA) was coupled into the lathe, where the tool holder (Walter MTJNR2020 K 16) is fixed. The tool angles of the turning tests are presented in Table 12.

Table 12. Major cutting edge tool angles according to the tool–in–hand system and corner radius [123].

Tool angles and corner radius	Value
γ_n, tool normal rake	–6°
α_n, tool normal clearance	6°
ψ_r, tool lead angle	–3°
κ_r, tool cutting edge angle	93°
λ_s, tool cutting edge inclination	–6°
ε_r, tool included angle	60°
β_n, normal wedge angle	90°
r_ε, corner radius (mm)	0.8

A schematic view of the insert during turning of Al–MMCs workpiece material is shown in Figure 28. The signals from the three components of the cutting force (main component, F_c, measured in the direction of primary motion; feed force, F_f, measured in the direction of feed motion, and depth–of–cut force, F_{DOC}, perpendicular to F_c and F_f, in the radial direction of the workpiece) up to a maximum allowed value of 10 kN were amplified in a multichannel charge amplifier (Kistler 5070A). A PC with an analogic–to–digital data acquisition board (PCMCIA, Keithley) recorded the information in real time for the duration of each test (single pass and multi–pass).

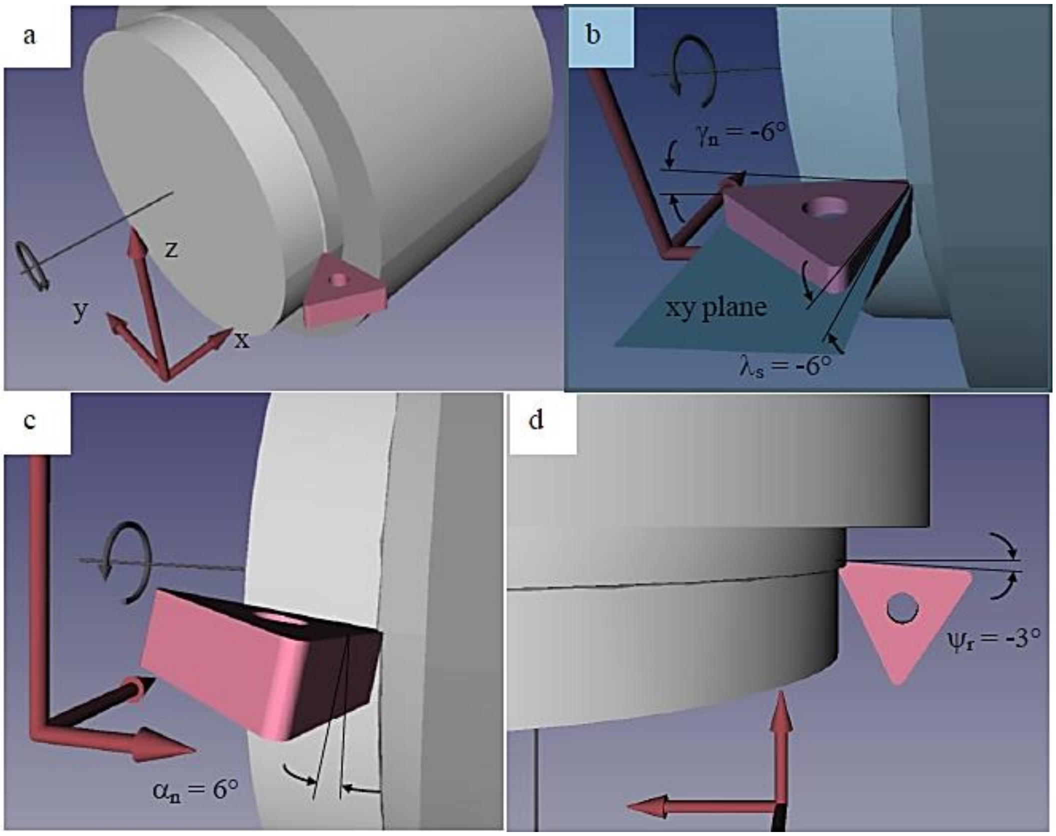

Figure 28. a) Schematic view of a TNMA160408F insert and the turning geometry resulting from the use of a MTJNL2020 K 16 tool holder. b) Detail of the insert showing that the tool normal rake and tool cutting edge inclination are negative; c) insert with a 6° tool normal clearance and d) tool lead angle of –3°. Axis: x– feed direction (F_{feed}); y– DOC direction (F_{DOC}); z– primary motion direction = direction of the main component of cutting force (F_c).

Figure 29 presents the experimental set up in a turning operation. The cutting parameters used in the testing of the two types of cutting inserts are in the following range: cutting speed (v) of 250 to 1000 m.min^{-1}; depth of cut (DOC) from 0.5 to 3 mm and feed (f) between 0.1 and 0.4 mm.rev^{-1}. The full set of tests given in Table 13 intended to determine the effects of cutting speed and feed on the behaviour of the inserts with the thinner coating while the effect of the DOC was studied solely for the thicker coating. Some longer tests were done using four consecutive passes under selected conditions. All the tools were analysed using Hitachi S 4100 and SU–70 scanning electron microscopes (SEM) for evaluation of tool damage and wear of the tips. Analysis of the inserts was performed before and after the cleaning of the cutting tools. Si_3N_4 cutting inserts were ultrasonically cleaned in 10% NaOH and then thoroughly in acetone to remove the Al alloy built up at the cutting edge.

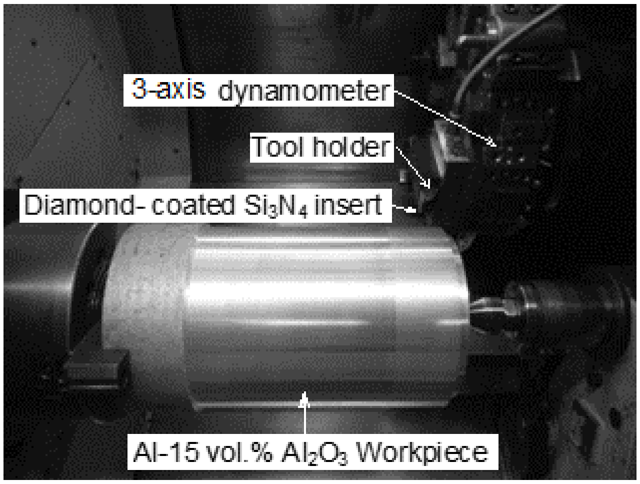

Figure 29. Experimental set up for turning tests of Al–MMC workpiece material.

Table 13. Turning conditions of Al–MMC workpiece material in this work.

Insert	v ($m.min^{-1}$)	f ($mm.rev^{-1}$)	DOC(mm)	L (m)	t (s)	n (rpm)
ML10x1	250	0.1	1	1812	435	391
	250	0.4	1	460	110	387
	500	0.1	1	2021	243	705
	500	0.2	1	993	119	717
	500	0.3	1	653	78	732
	500	0.4	1	485	58	735
	750	0.1	1	1879	150	1133
	750	0.4	1	479	38	1113
	1000	0.1	1	2001	120	1424
	1000	0.4	1	474	28	1497
ML10x2	500	0.1	1	1708	205	819
	500	0.3*	1	1975	237	938
	500	0.3**	1	1878	225	985
	500	0.4	0.5	411	49	849
	500	0.4	1	422	51	828
	500	0.4	1.5	404	48	862
	500	0.4	2.0	388	47	896
	500	0.4	3.0	375	45	927
	750	0.4	1	413	33	1267
	1000	0.4	1	418	25	1672

* Values corresponding to the 4 passes dry cutting tests. ** 4 passes, lubricated. n – spindle speed is that of the last pass; t– machining time; L– machining length.

Chapter 3

CVD growth and characterization of multilayered diamond coatings on Si_3N_4 ceramic substrates

This chapter discusses the morphological, structural and mechanical features of multilayered micro/nanocrystalline diamond–coated silicon nitride substrates. The studies were supported by scanning electron microscopy (SEM), Raman spectroscopy, X–ray diffraction (XRD), atomic force microscopy (AFM) and adhesion assessment by Brale indentation testing.

3.1. Sintered silicon nitride (Si_3N_4) ceramic substrates

Figure 30 shows the SEM micrograph of CF_4 dry–etched of sintered Si_3N_4 ceramic substrate with 7 wt.% Y_2O_3 and 3.7 wt.% Al_2O_3 as sintering additives after 10 min.

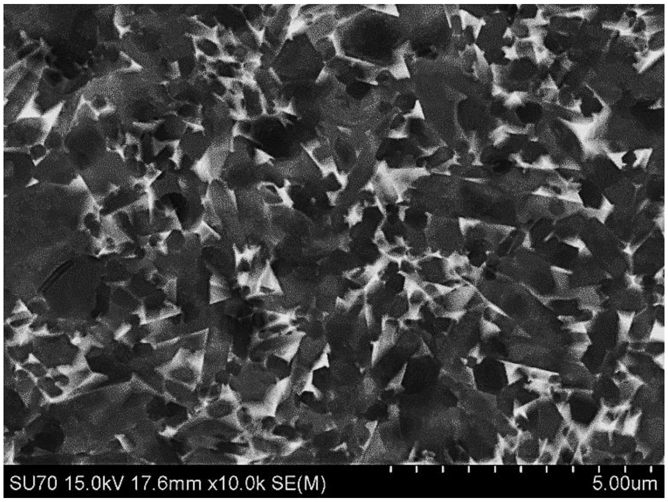

Figure 30. SEM micrograph of CF_4 dry–etched (10 min) of sintered 89.3 wt.% Si_3N_4 ceramic substrate with 7 wt.% Y_2O_3 and 3.7 wt.% Al_2O_3 as sintering additives.

The microstructure of silicon nitride ceramics in Figure 30 depicts dark contrast β–Si_3N_4 grains (elongated and in cross section) surrounded by a white intergranular phase, according to the following reaction:

$$\alpha\text{–}Si_3N_4 + Y_2O_3 + Al_2O_3 \rightarrow \beta\text{–}Si_3N_4 + \text{Si–Y–Al–O–N (intergranular phase)} \qquad (6)$$

The intergranular phase is formed from the sintering additives Y_2O_3 or Al_2O_3 that are added to initial powders in order to densify silicon nitride ceramics. Honma et al. [124] proposed that the relationship between behaviour of sintering aids and the microstructure formation during sintering can be divided into three temperature regions: (i) in the first stage (below 1500°C) the sintering additives react among them and with SiO_2, which exists on the Si_3N_4 powder surface, and the densification proceeds in a non–uniform way; (ii) in the second step (1500–1700°C), the densification carries on rapidly because of the formation of a homogeneous glassy phase at grain boundaries, and transformation of α–Si_3N_4 to β–Si_3N_4 starts; (iii) finally, in the third stage (above 1700°C) final densification takes place and transformation of α–Si_3N_4 to β–Si_3N_4 is completed with the growth of prismatic grains. Densification of Si_3N_4 ceramics is controlled mainly by particle rearrangement and solution–reprecipitation, both of which are increased by liquid–phase formation at the grain boundary. Particle rearrangement contributes to densification at low temperatures, at which the viscosity of the glass phase is high, and solution–reprecipitation is dominant at high temperatures, where phase transformation also becomes active [124,125].

Figure 31 shows a typical X–ray diffraction (XRD) pattern of sintered Si_3N_4 ceramic substrate. Most of the peaks correspond to the crystalline phase of β–Si_3N_4 but it can be seen that the intergranular phase partially recrystallized as yttrium–silicon oxynitride compound upon cooling [126–130].

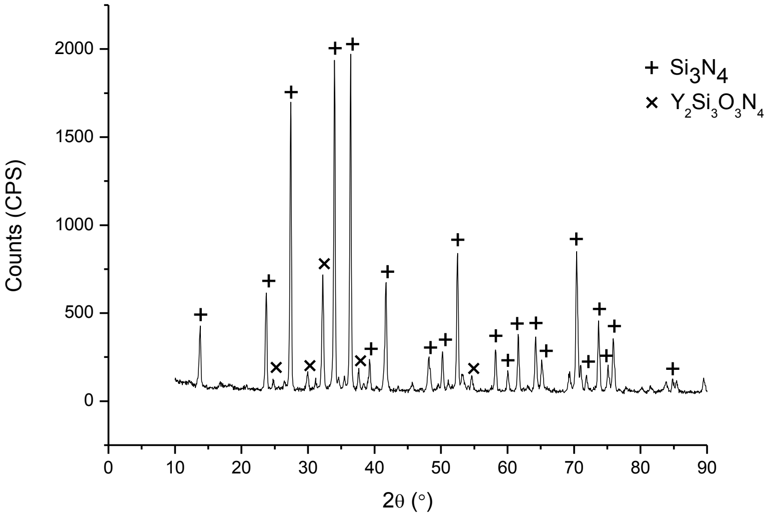

Figure 31. XRD of sintered Si_3N_4 ceramic substrate with 7 wt.% Y_2O_3 and 3.7 wt.% Al_2O_3 sintering additives.

The Vickers hardness of the Si_3N_4 ceramic substrates was measured as HV= 14±0.5 GPa. Taking into account this value and a Young´s modulus of 300 GPa [131], the average indentation fracture toughness value according to Niihara’s equation, is K_{1C}=6.5 MPa.m$^{1/2}$. Moreover, the microstructure of sintered Si_3N_4 has the important effect on mechanical properties of silicon nitride like fracture toughness and hardness. Sun and co–workers [126] investigated the effect of Y_2O_3/Al_2O_3 ratio on fracture toughness of sintered silicon nitride ceramics and they found that toughening of silicon nitrides is primarily due to bridging and pull out of their rod–shaped β–grains. In conventional silicon nitride ceramics, the rod–shaped grains are randomly oriented, resulting in isotropic microstructures. The amount of over–extended β–Si_3N_4 grain increased with the additive content. That can be explained by the increasing of transformation velocity at higher additive contents. With the increasing of the additive amount the ratio of a binding phase at the grain boundary increased [125–128]. Those authors obtained fracture toughness values in the range of 4.6–5.9 MPa $m^{1/2}$ [131], comparable to the value obtained in the present work.

3.2. Morphology and surface roughness of the diamond films

SEM micrographs of top views and cross sections of monolayered MCD and NCD coatings are shown in Figure 32(a,c) and Figure 32(b,d), respectively. The HFCVD deposition conditions used for micro– and nanocrystalline HFCVD diamond film are those mentioned in Table 3.

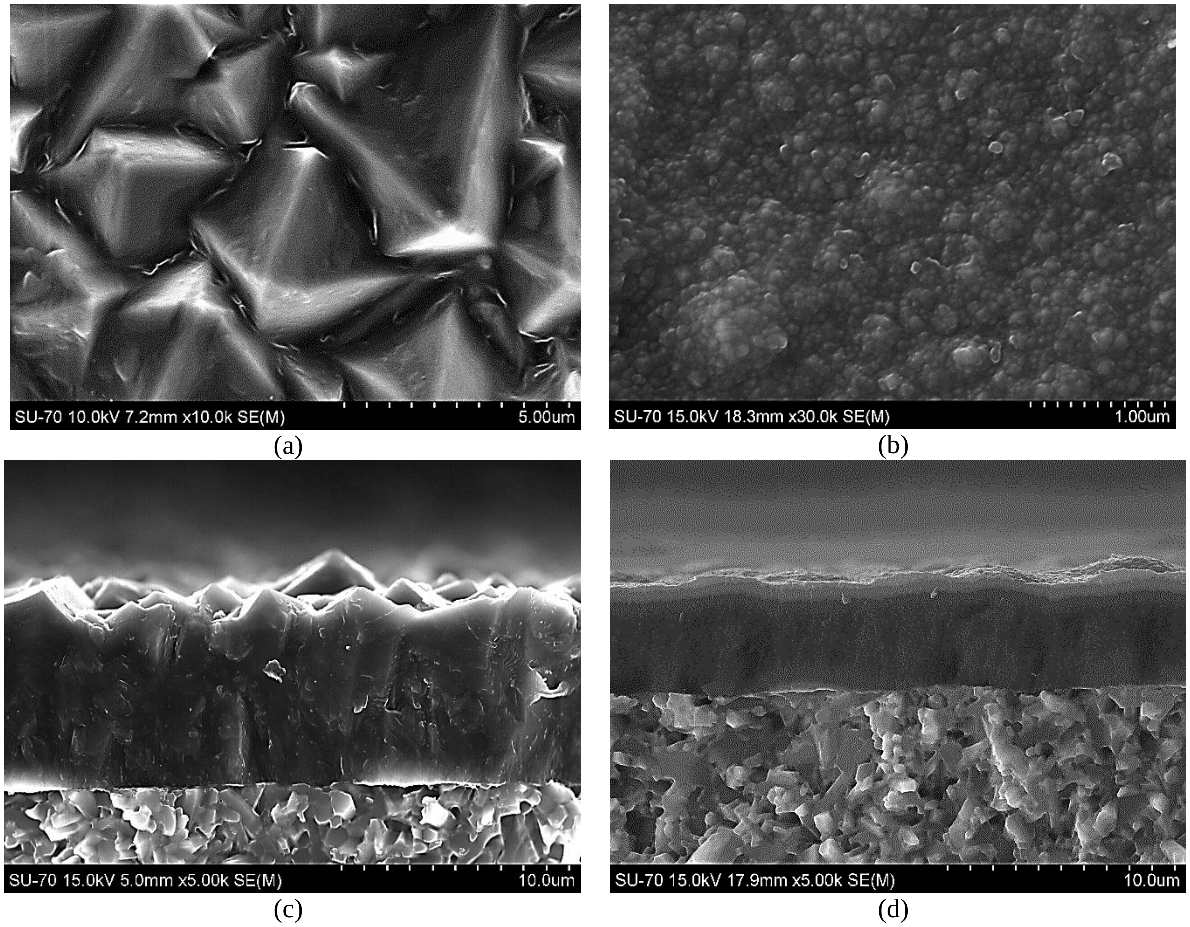

(a) (b)

(c) (d)

Figure 32. SEM micrographs of top view: (a) MCD grown for 10 h, (b) NCD grown for 6 h; and cross section: (c) MCD, (d) NCD coatings on Si_3N_4.

Highly faceted, large pyramid–like, diamond grains typical of conventional microcrystalline diamond can be seen in Figure 32(a) for the MCD samples. On the contrary, the NCD grade obtained by increasing the methane concentration to 3vol. % and decreasing the substrate temperature and pressure, has a much smaller diamond grain size as can be seen in Figure 32(b). By comparing Figure 32(a) and (b), it can be seen that MCD is rougher than NCD. Concerning the growth mechanism of diamond thin films, microcrystalline diamond thin film has columnar growth, Figure 32(c) while the nanocrystalline diamond thin film has equiaxed growth, as shown in Figure 32(d). From the SEM micrographs in Figures 32(c) and (d) the growth rate of MCD and NCD coatings are almost similar, around 0.8 $\mu m.h^{-1}$.

Microcrystalline diamond, despite having a rough surface it is known to be more adherent to silicon nitride substrates than NCD [24,25], but for tribological applications such as cutting tools it is very important to have diamond layers with a smooth surface. Nanocrystalline diamond films have a smooth and uniform surface morphology. The combination of micro– and nanocrystalline diamond film and production of films in the form of multilayer is therefore used in order to simultaneously provide high adhesion, low surface roughness but also high fracture toughness compared to the single micro– and nanocrystalline diamond films [52,53].

SEM micrographs of top view and cross sections of multilayer MCD/NCD diamond film (5 layers of each) on Si_3N_4 are shown in Figure 33(a) and 33(b,c). The first layer over the substrate is MCD while the free surface of the coating ends with NCD. HFCVD conditions for each micro– and nanocrystalline HFCVD diamond layer are given in Table 3.

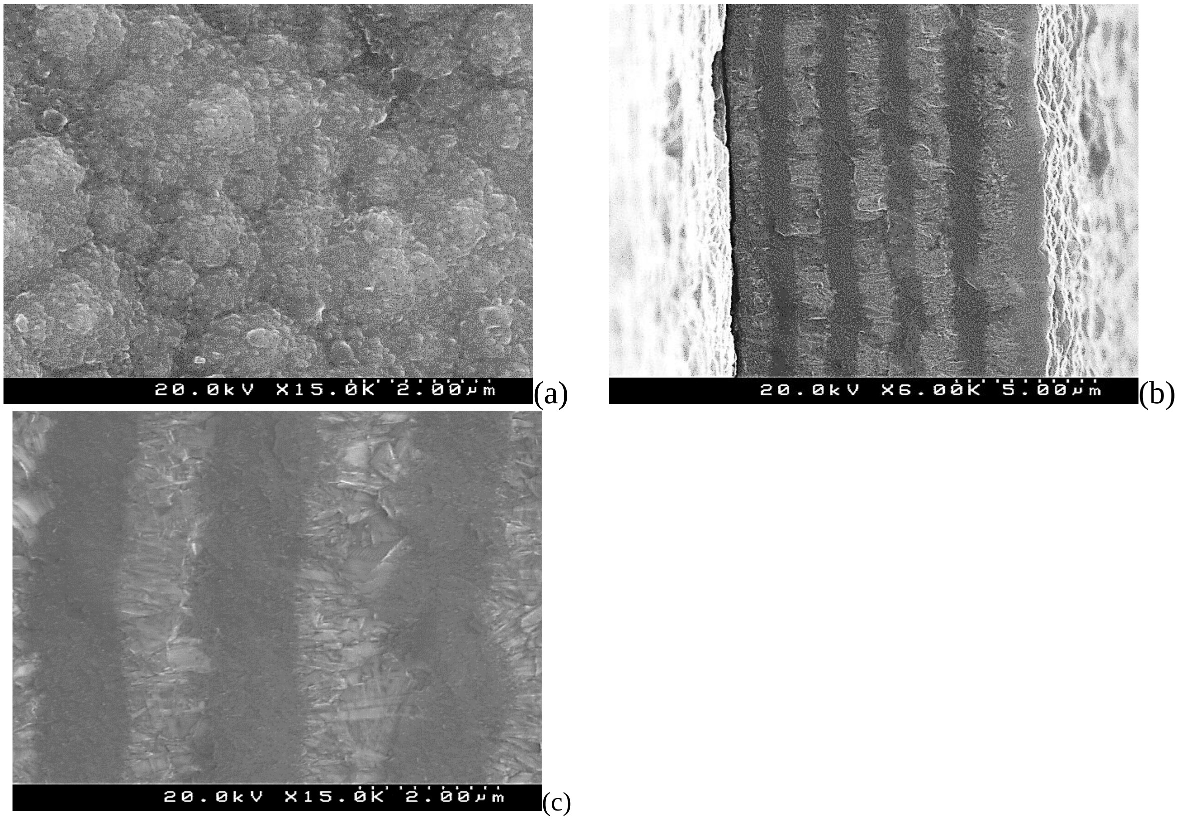

Figure 33. SEM micrographs of (a) top view and (b, c) cross sections of multilayer (10 layers) micro– and nanocrystalline diamond. MCD growth time: 72 min; NCD growth time: 72 min (growth rate ~ 0.8 $\mu m.h^{-1}$ for each MCD and NCD layer).

Surface roughness data after diamond deposition are shown in Table 14. Surface roughness of diamond films was measured using atomic force microscopy (AFM) in a 15 μm×15 μm scan area in tapping mode, Figure 34.

Table 14. Surface roughness parameters after diamond deposition.

Surface roughness	MCD	NCD	Multilayer
RMS (μm)	0.35	0.09	0.11
R_a (μm)	0.28	0.06	0.08

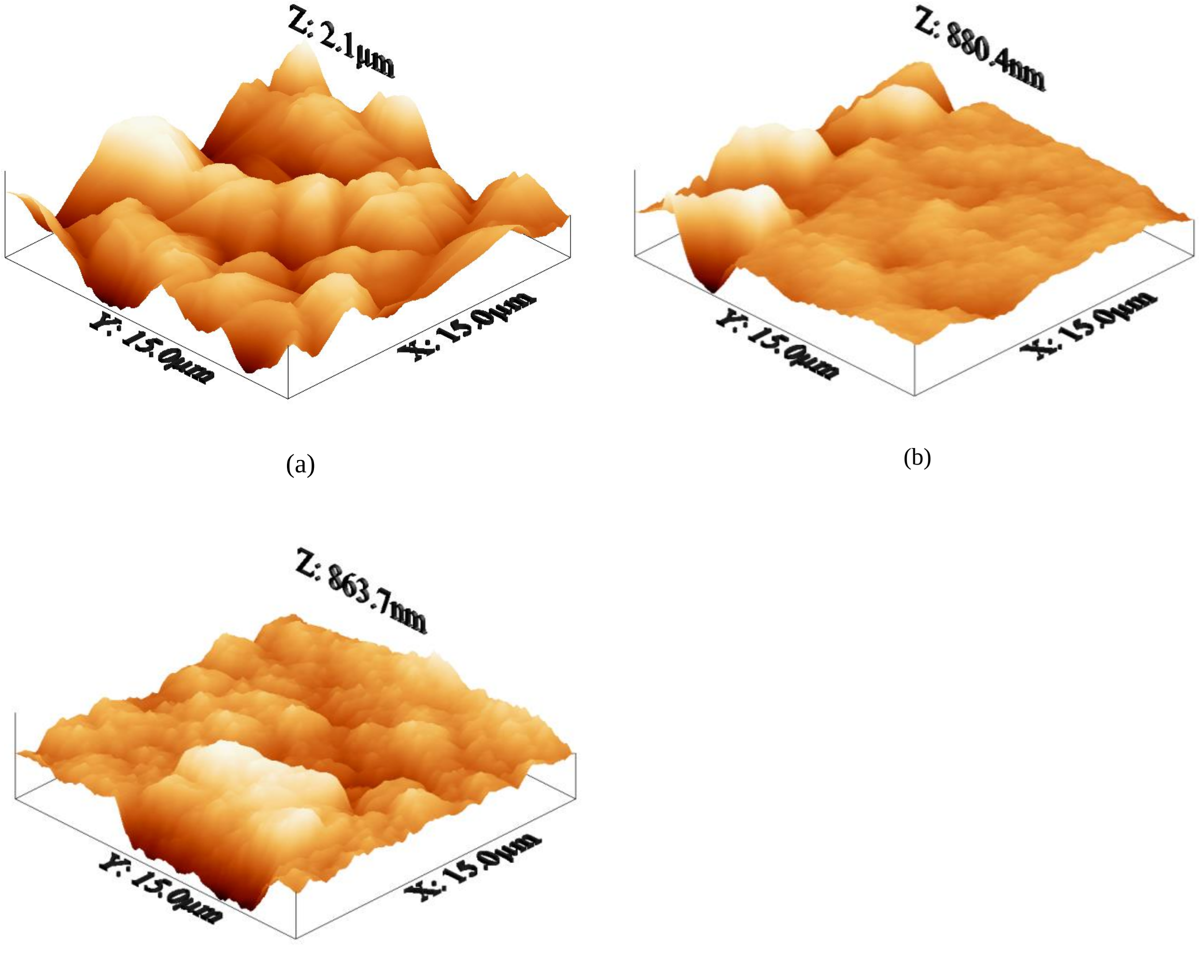

(a)

(b)

(c)

Figure 34. AFM scan micrographs of monolayer (a) micro, (b) nanocrystalline and (c) multilayer micro and nanocrystalline diamond coated Si_3N_4 substrates.

As shown in Figure 34(a) and (b), microcrystalline film has higher surface roughness than the nanocrystalline one, which can be attributed to the columnar growth morphology of MCD. The much lower surface roughness of NCD, Figure 34(b) can be related to the equiaxed growth morphology of nanocrystalline diamond films [87]. For multilayer MCD/NCD coatings, despite the top layer being NCD, the surface roughness values are between those of monolayer MCD and NCD, Figure 34(c). Thus, the multilayer strategy does reduce the surface roughness relatively to a single MCD layer.

3.3. Characterization by Raman spectroscopy and X–ray diffraction

Figure 35 compares Raman spectra for monolayer MCD, NCD and multilayer MCD/NCD films. One important aspect is the decreasing of the diamond peak (1332 cm^{-1}) and raising of the graphitic D–band (~ 1360 cm^{-1}), as the diamond crystallite size decreases (NCD). Also, the intensity of the G–band of graphite (~ 1560 cm^{-1}) particularly increases for NCD films. The increase in the sp^2 character of the films can be explained by high hydrocarbon super saturation and decrease of atomic H density in MCD and NCD specimens, which is responsible for etching the non–diamond carbon phases. Moreover, Raman spectra show the presence of peaks near 1140 and 1480 cm^{-1}, related to C–H chain structures as trans–polyacetylene and are accepted as the typical of NCD [132–135]. As it can be seen, the most important Raman peaks for diamond which are relevant for micro and nanocrystalline type, also can be found for the multilayer diamond one. Also the intensity of the main Raman peaks for multilayer diamond film is located between micro and nanocrystalline ones.

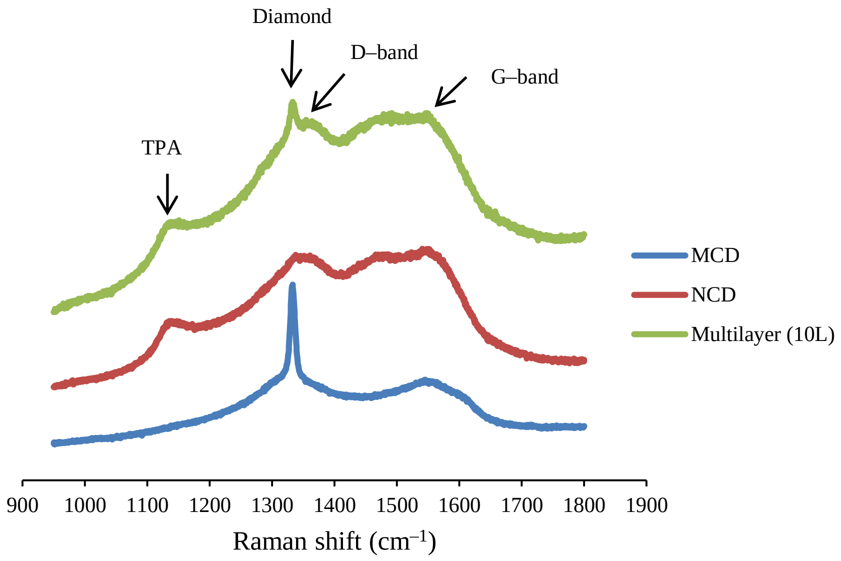

Figure 35. Raman spectra of monolayer micro, nanocrystalline and multilayer diamond coated Si_3N_4 ceramic substrate by HFCVD process.

Figure 36 shows the XRD pattern of monolayer microcrystalline (CH_4/H_2=0.02), nanocrystalline (CH_4/H_2=0.04), and multilayer (CH_4/H_2=0.02, CH_4/H_2=0.04) micro/nanocrystalline HFCVD diamond–coated Si_3N_4 substrates in the present work.

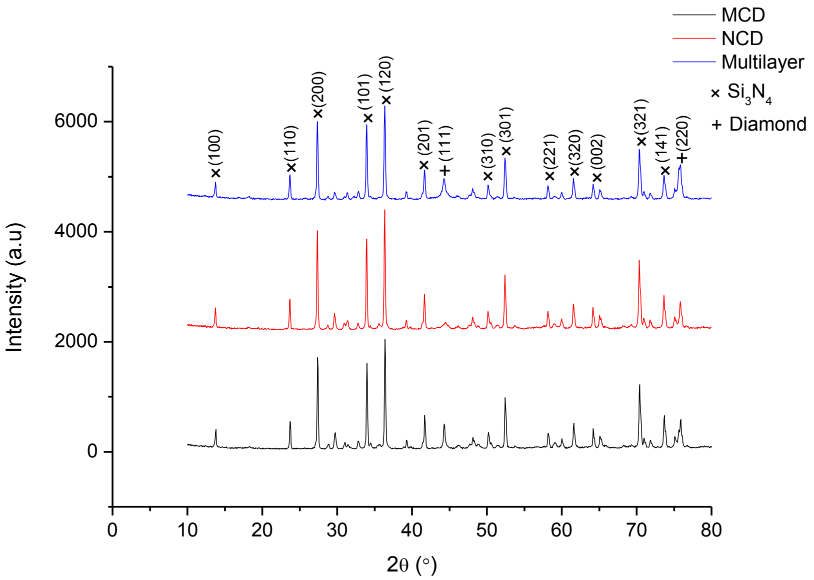

Figure 36. XRD pattern of monolayer micro (CH_4/H_2=0.02), nanocrystalline (CH_4/H_2=0.04), and multilayer (CH_4/H_2=0.02, CH_4/H_2=0.04) micro/nanocrystalline diamond.

The characteristic (1 1 1) and (2 2 0) diamond peaks are clearly observed for all the as–grown diamond coatings. But there is a large difference in the maximum height of their (1 1 1) diamond peaks. The XRD pattern indicates that the monolayer microcrystalline diamond (MCD) coating has larger diamond crystals, because its (1 1 1) diamond peak and has the smallest full width at half maximum (FWHM) when compared with the monolayer nanocrystalline diamond (NCD) and multilayer micro/nanocrystalline (MCD/NCD) diamond coatings. Also, the higher intensity of the (1 1 1) diamond peak of the MCD coating reflects its higher purity, as observed in the Raman spectrum, and the preferential growth direction of the crystals.

3.4. Adhesion strength of the diamond coatings on silicon nitride substrates

SEM micrographs in Figure 37 illustrate the differences in the adhesion strength of nanocrystalline diamond on Si_3N_4 substrate using different surface finishing: (a–c) 15 µm diamond powder flat lapping; and (d–f) polishing by 50 nm silica suspension.

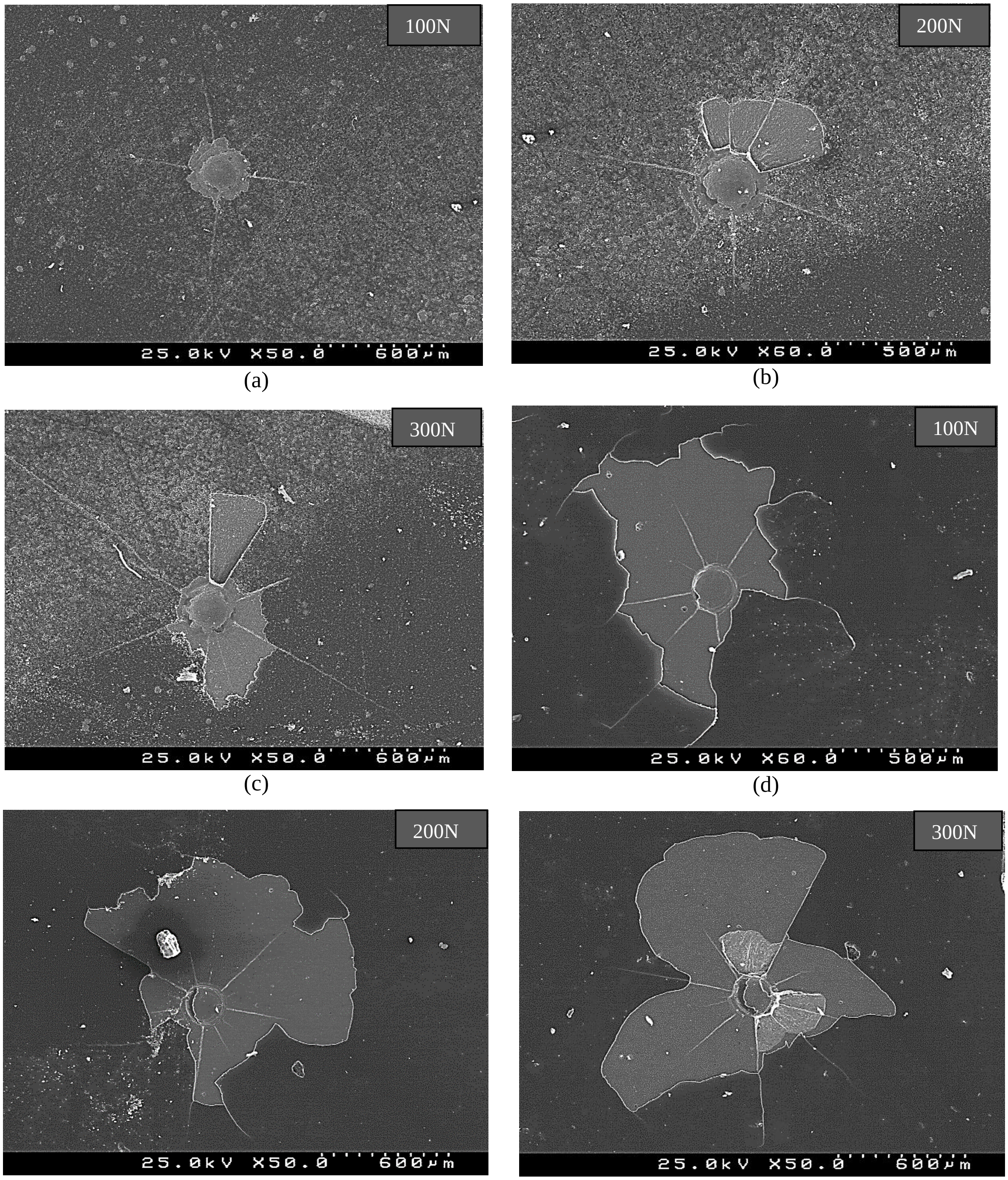

(a) (b) (c) (d) (e) (f)

Figure 37. SEM micrographs of Brale tip indentation marks on NCD over Si_3N_4 substrate with different surface finishing (a–c) 15 µm flat lapping and (d–f) polishing with silica suspension.

The loads applied to the Brale indenter were in the range 100–300 N. Because of the brittle nature of the silicon nitride substrate, the indentation cracks initiate in the silicon nitride ceramic bulk substrate [24,53]. Film detachment occurs when radial and circumferential cracks meet, leading to lift–off of substrate material and placing a large stress at the coating/substrate interface, figure 37(b,c). When adhesion is insufficient, the formation of cracks in the substrate may be sufficient to provoke extensive film delamination, as occurs for the silica polished substrates, Figure 37(d–f).

One of the important factors which can affect coating–substrate adhesion is surface roughness. Surface with higher roughness values can have higher adhesion strength to coatings [136]. This explains why the rougher substrates, flat lapped and with R_a ~ 0.055 µm, withstand higher loads with less delamination (Figure 37(a–c)). The polished substrates, with R_a~ 0.030 µm have much worse adhesion strength, as expected, Figure 37(d–f).

All the Si_3N_4 ceramic substrates were thus ground and flat lapped by 15 µm diamond suspension and subsequently dry etched by a CF_4 plasma for 10 min in order to improve adhesion. Finally, they were seeded by nano–diamond slurry in an ultrasound bath, before diamond deposition. The optical micrographs of Brale indentations in Figure 38 correspond to MCD, NCD and MCD/NCD multilayer coated Si_3N_4 ceramic substrates that suffered these pretreatment steps. In order to allow a direct comparison of the adhesion behaviour of the different diamond films, the diamond film thickness was adjusted to about 8 µm for the tested types of coatings by varying the deposition time. On the left hand side column, the micrographs show the threshold load just before delamination, while on the right hand side, the micrographs were taken at the load where the first delamination event takes place.

Monolayer microcrystalline diamond coating (Figure 38(a,b)) showed higher adhesion failure load (800 N), when compared to monolayer nanocrystalline monolayer film (Figure 38(c,d)) that failed under a load of 600 N. This behaviour is the result of the very high crystallinity degree of the microcrystalline diamond coating compared to the nanocrystalline film, as shown by Raman spectroscopy (Figure 35), which promotes adhesion in two ways: direct bonding by epitaxial growth of the film on the substrate [137] and the coating hardness is increased and thus the substrate plastic deformation is reduced [138].

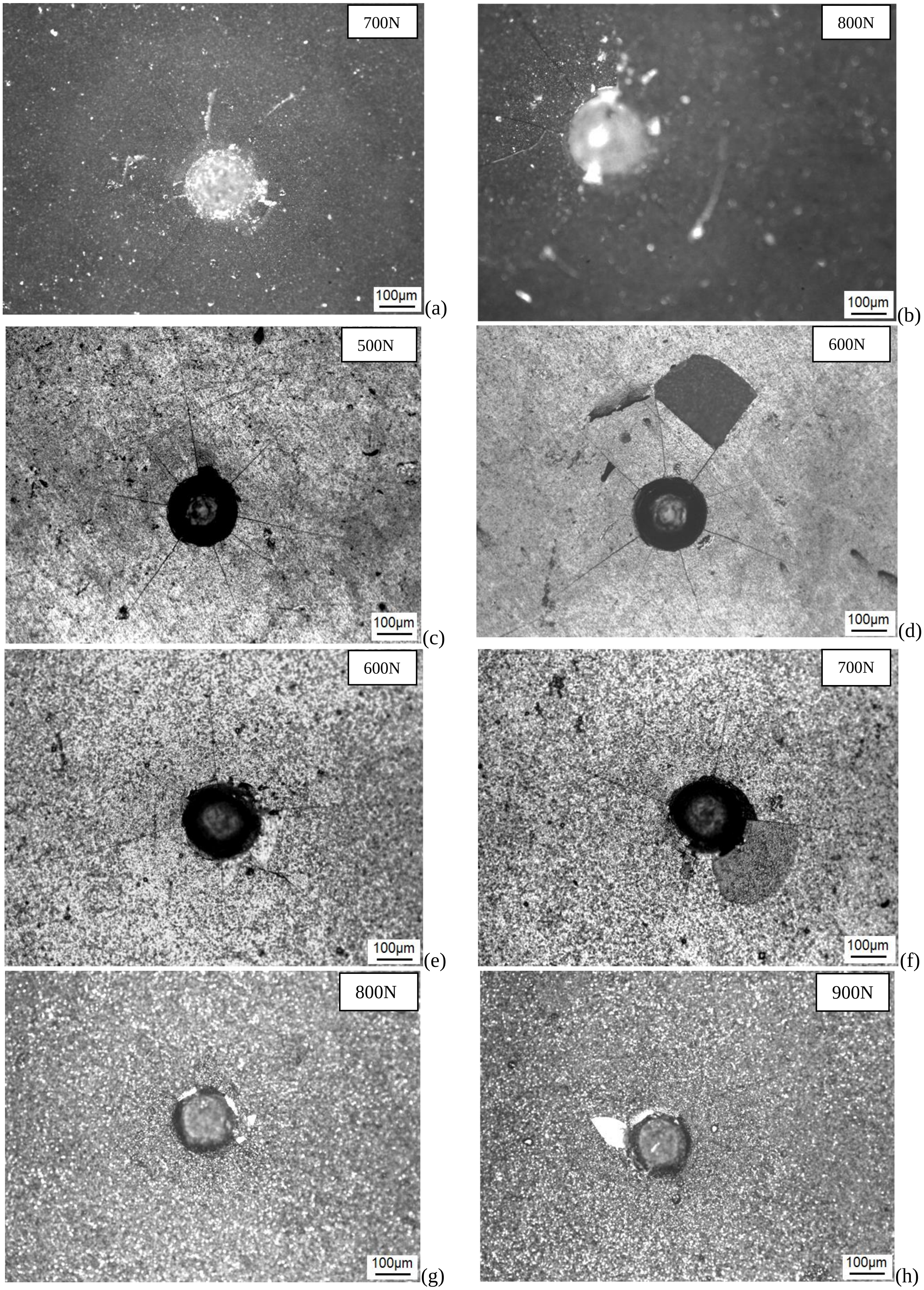

Figure 38. Optical micrographs of Brale indentations of diamond–coated Si_3N_4 substrate: (a,b) monolayer MCD, (c,d) monolayer NCD, (e,f) bilayer MCD/NCD and (g,h) ten layers MCD/NCD.

The higher graphite content of nanocrystalline diamond (sp^2) (Figure 35) resulted in lower adhesion strength to the substrate [139]. The finer grain size of nanocrystalline diamond increases the grain boundary area where non–diamond phases and higher degree of sp^2 content are present [25,140]. Adhesion failure values of 700 N were found for the bilayer coating (Figure 38(f)), close to that of the MCD monolayer (800 N, Figure 38(b)). The indentation adhesion of the bilayer coating is determined by the adhesion strength of the first layer of microcrystalline diamond to the silicon nitride substrate. For the multilayer diamond–coated silicon nitride substrate, the film detachment (900 N, Figure 37(h)) is higher than the monolayer microcrystalline indentation load (800 N, Figure 38(b)).

These results are in the line of those observed in four layers MCD/NCD coatings [53]. Multilayered diamond films were achieved by the deposition of alternate rough microcrystalline diamond and smooth fine–grained diamond layers, allowing simultaneously a smoother surface and an enhancement of the adhesion strength, as shown by the data in Figure 38.

3.5. Characterization of multilayered diamond films for tribological assessment

Multilayered micro/nanocrystalline diamond films have been coated in silicon nitride large discs and 5 mm diameter balls for tribological testing. The HFCVD conditions for the production of the multilayered films are those mentioned in Table 1. The morphology of the diamond surfaces on the discs and balls is somewhat different. While the former (Figure 39a) is similar to that of the small discs (Figure 33a), the diamond growth on the balls led to a top NCD layer with a marked cauliflower morphology (Figure 39b) that arises due to high local concentrations of methane [101]. The cross–section of a multi–layered film grown in a large disc is shown in Figure 39c.

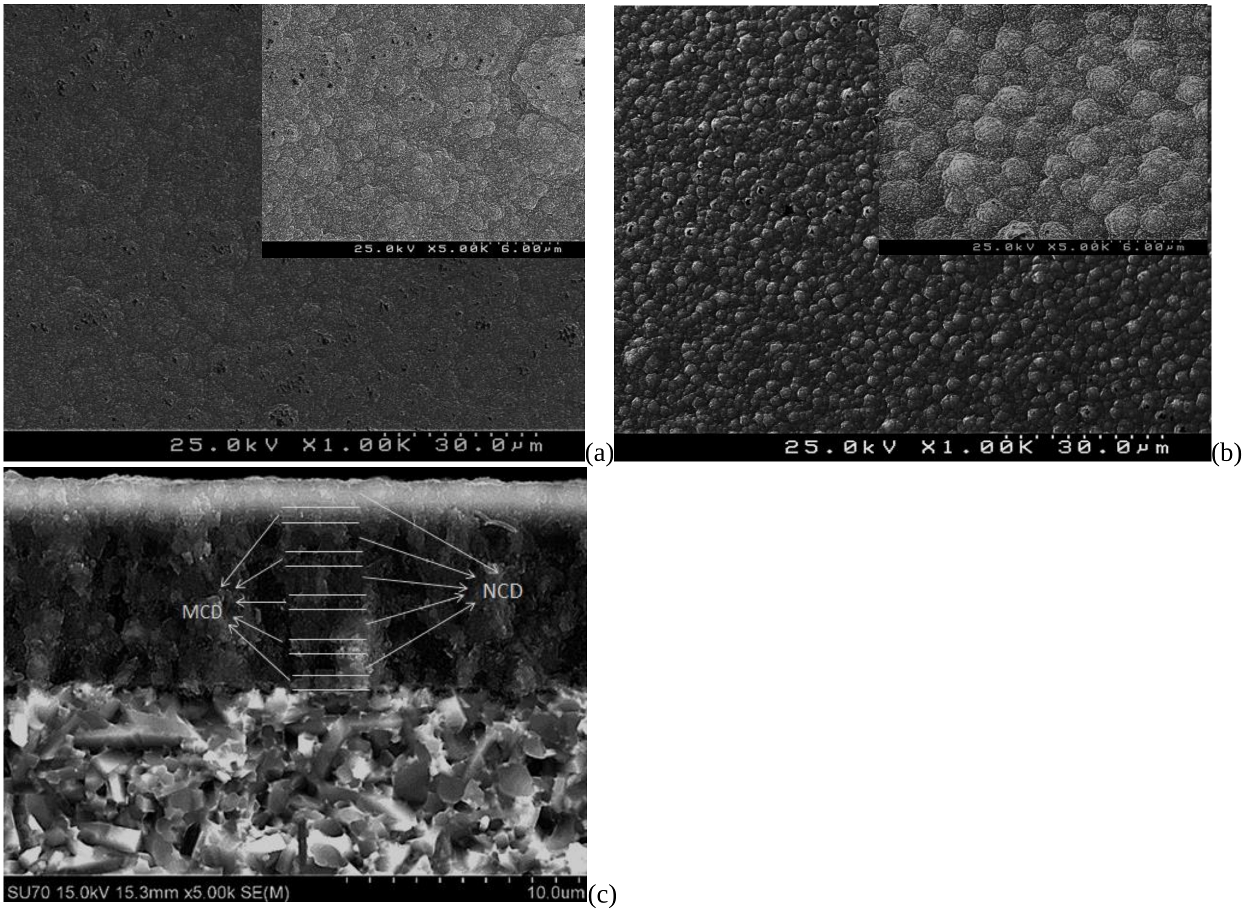

Figure 39. SEM micrographs of multilayer micro/nanocrystalline diamond–coated: (a) Si_3N_4 large disc and (b) Si_3N_4 ball, and (c) cross section of multilayer micro/nanocrystalline diamond–coated Si_3N_4 large disc (total thickness ~8.8 µm).

Figure 40 shows the Raman spectra of the multilayered micro/nanocrystalline diamond–coating on the large Si_3N_4 discs, showing the same spectrum features as the same type of coating on small discs, Figure 35.

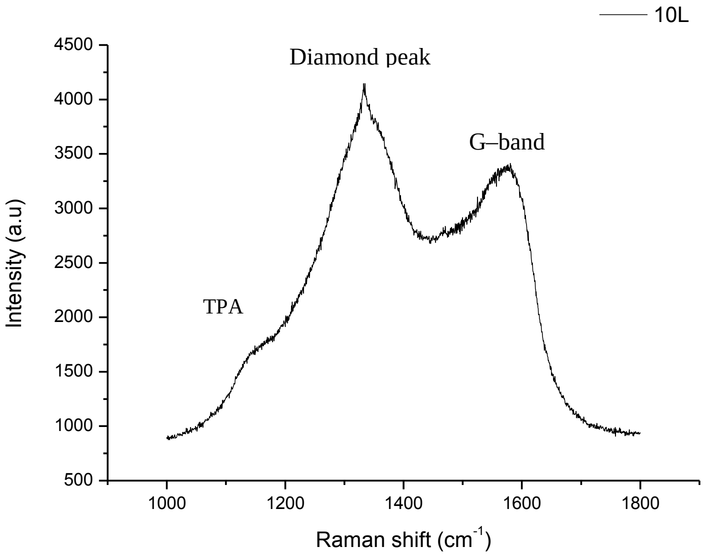

Figure 40. Raman spectra of multilayer micro/nanocrystalline diamond–coated large Si_3N_4 ceramic substrate.

An AFM micrograph of multilayer CVD micro and nanocrystalline diamond coated Si_3N_4 large disc substrate is shown in Figure 41. Surface roughness of micro, nanocrystalline and multilayered diamond films was measured using AFM microscopy in a scan area of 100 μm × 100 μm, larger than for the small discs which was 15 μm × 15 μm (Figure 34c) although giving similar RMS and Ra values.

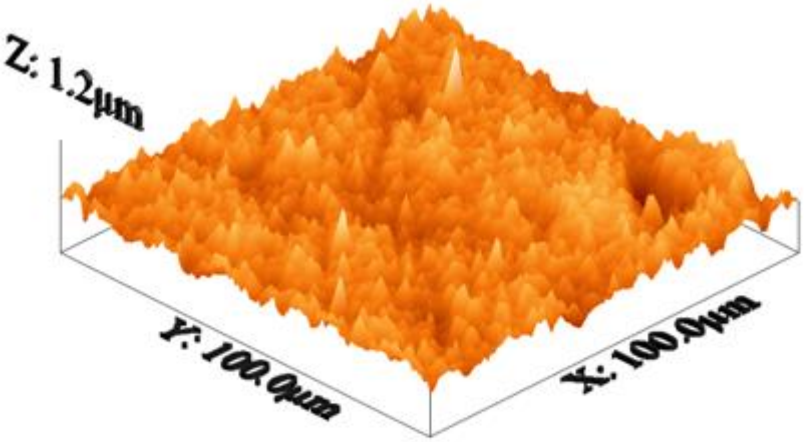

RMS (R_q) = 97 nm, R_a = 75 nm

Figure 41. AFM micrograph of multilayered micro/nanocrystalline diamond–coated Si_3N_4 large disc substrate.

The surface roughness values of the three types of coatings, mono– and multilayered are given in Table 15.

Table 15. Surface roughness of monolayer micro, nano and multilayer micro/nanocrystalline diamond coated Si_3N_4 disc substrates.

	Monolayer MCD	Monolayer NCD	Multilayer (10L)
RMS (nm)	348.5	33	75
R_a (nm)	279	22.5	97

Chapter 4

Tribology of CVD multilayered diamond coatings

This chapter includes the experimental results and discussion about the tribological behaviour of self–mated single layer MCD and MCD/NCD multilayered diamond coatings using reciprocating ball–on–flat and circular ball–on–disc configurations. The effects of relative humidity and temperature were studied as also was the effect of biodiesel lubrication.

4.1. Tribological behaviour of self–mated multilayered diamond coatings under different RH conditions

Figure 42(a) shows a representative curve of the evolution of the coefficient of friction (COF) versus sliding distance (X) of self–mated multilayered diamond sliding at loads below the threshold load, obtained at the sliding wear conditions of RH= 20% and W= 50 N (this normal load enforces a maximum Hertzian stress of P_{max} ~ 4.3 GPa) and Figure 42(b) presents the details of the first 2.5 m of the sliding.

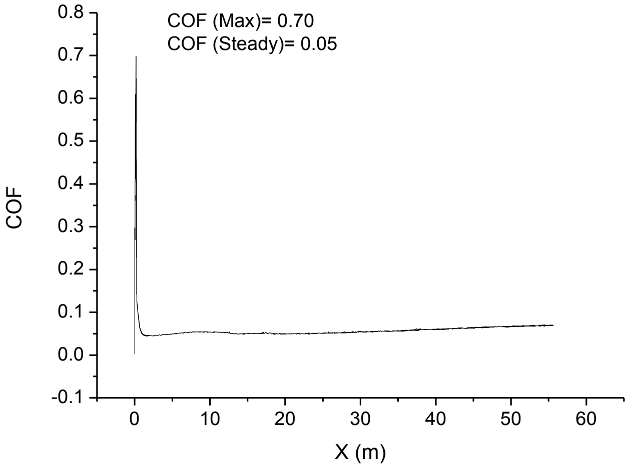

(a)

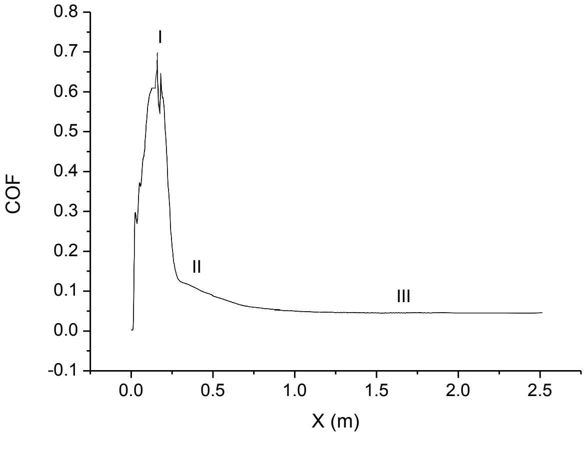

(b)

Figure 42. (a) Coefficient of friction (COF) curve variation as a function of the sliding distance (X) for self–mated sliding tests at the sliding wear conditions at room temperature, of RH= 20% and W= 50 N in the reciprocating configuration and (b) details of first 2.5 m sliding.

As shown, it has three main distinguished stages which are marked as I, II, and III in. The friction peak (I) occurs in the first cycles (in this test after about 15 cycles of the sliding) and for a typical sliding wear test it corresponds to the maximum value of COF. This maximum friction value is generated through the strong effect of mechanical interlocking of the self–mated cauliflower–like nanocrystalline diamond–coated Si_3N_4 ball and counterface disc asperities in the initial cycles of the sliding which is followed by breaking and smoothening of the trapped asperities in the contact area during sliding. The height of the primary friction peak is dependent to the surface roughness of the diamond coatings [20,40–43].

After the first sharp friction stage, in the second stage the COF drops within a short period (Figure 42b). This step corresponds to the running–in stage (II) and contributes to the rapid smoothening of asperities and filling up the valleys between nanocrystalline diamond clusters with broken wear debris [20,40–43], and it is achieved in less than 1 m of sliding distance. As the sliding wear test continues, a steady–state stage (III) is reached after about 2 m of sliding distance. The steady–state stage (III) is attributed to the smoothening of the nanocrystalline diamond plateaus. Since the diamond coated self–mated contact areas are not delaminated, the coefficient of friction during this stage (III), is almost constant until the end of the sliding test regardless the initial surface roughness or applied load [20,40–43]. This representative friction coefficient evolution also was observed in other self–mated diamond–on–diamond sliding wear tribotests [20,23,28,40–43,52]. This self–mated diamond–on–diamond tribosystem showed μ_{Max}= 0.69 and μ_{Steady}= 0.05 during the sliding test.

Figure 43(a) exhibits the evolution curve of the coefficient of friction (COF) versus sliding distance (X) of self–mated diamond–on–diamond sliding at the sliding wear conditions of RH= 10% and W= 40 N, and Figure 43(b) presents the details of the first 2.5 m of the sliding.

This coefficient of friction variation curve versus sliding distance does not display the typical curve for diamond–on–diamond sliding and it is quite different due to the high number of maximum friction peaks. This behavior may be attributed to the contacting of the alternating morphology of diamond–coated Si_3N_4 disc and ball i.e. sliding of the nanocrystalline diamond–coated disc against microcrystalline diamond–coated ball and vice versa, since the coating architecture is multilayer in the present work and interlayer delamination may happen during the sliding period and/or degradation of the micro and nanocrystalline diamond layers [52]. Another reason for this behavior can be attributed to the very low humidity conditions of this sliding wear test, because the water molecules in the vapor phase can be adsorbed by the surface and passivate the surface through the formation of C–H dangling bonds and/or by formation a layer between the self–mated diamond–coated disc and ball from the water vapor species which resulted in the reducing the contact area [26,36,141–148]. Figure 43(b) displays the first 2.5 m of the sliding test. The regions of I and II are referred to the primary friction peak and running–in stage; respectively. This self–mated diamond–on–diamond tribosystem showed $\mu_{Max} = 0.23$ and $\mu_{Steady} = 0.09$ during the sliding test.

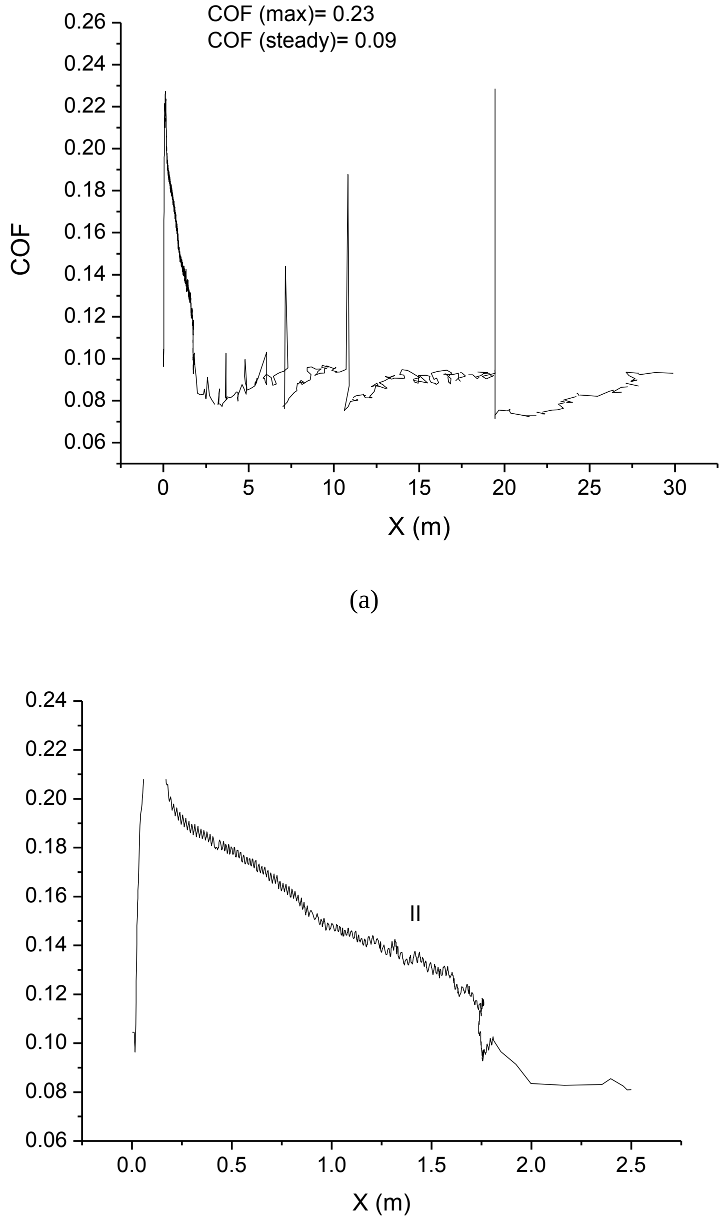

(a)

(b)

Figure 43. (a) Coefficient of friction (COF) curve variation as a function of the sliding distance (X) for self–mated sliding tests at the sliding wear conditions of RH= 10% and W= 40 N in the reciprocating configuration and (b) details of first 2.5 m sliding.

SEM micrographs of the worn surfaces of this test (RH= 10% and W= 40 N) are presented in Figure 44(a) and (b). Both diamond–coated Si_3N_4 disc and ball could withstand the sliding and no signs of complete diamond coating delamination were observed. The smoothing of the nanocrystalline top layer and microcracking events can be observed in the wear scar of the ball (inset of Figure 44a) and in the wear track on the disc (Figure 44b), where there is a large fraction of polished areas. Since the tribosystem is diamond–on–diamond (self–mated), the main wear mode is abrasive, caused by the sliding action between asperities (two–body abrasive wear) and from debris action on the surfaces (three–body abrasive wear). This behaviour also was observed in other self–mated microcrystalline, nanocrystalline and micro/nanocrystalline diamond tribosystems in different wear conditions of load, dry and water–lubricated medium [20,23,28,39–43,52,149–153].

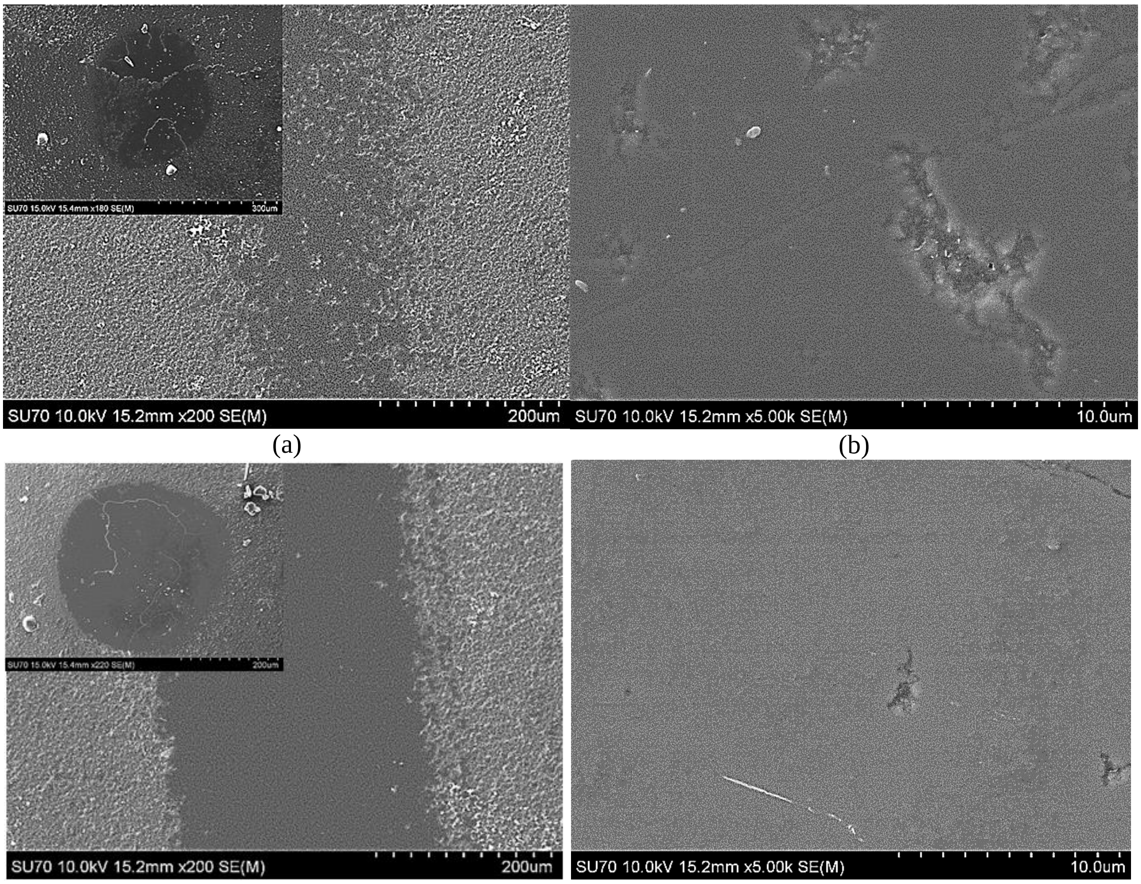

(a) (b)

(c) (d)

Figure 44. SEM micrographs of the worn surfaces of diamond–coated: (a), (c) disc and ball (insets); and (b), (d) wear track magnifications at RH=10%, W=40N (P_{max}~ 4.0 GPa) and RH= 90%, W= 120 N (P_{max}~ 5.8 GPa).

Figures 44(c,d) present the SEM micrographs of the worn surfaces of multilayered diamond–coated discs and balls at sliding conditions of RH= 90% and W= 120 N (P_{max}~ 5.8 GPa). Due to higher applied normal load of W= 120 N, the width of wear track is higher than for W = 40 N, as it can be observed in Figures 44(a) and (c). Observation of the worn surface of the wear track shows an almost complete polishing of the coating, without delamination (Figure 44d). Only some cracks are found on the surface of the ball (inset of Figure 44c).

Figure 45(a) shows SEM images of wear tracks of disc and ball tested with a higher load (150 N) at the same RH = 90%. The respective evolution of the COF as a function of sliding distance is shown in Figure 45(b). As seen in Figure 45(a), the diamond–coated Si_3N_4 ball did not delaminate, while the diamond–coated Si_3N_4 disc failed, exposing the substrate surface. The light–contrast region in the center corresponds to the worn ceramic substrate, with two lateral dark contrast stripes where the film delaminated exposing the substrate but without contact with the sliding ball. Beyond those stripes the pristine multilayered diamond coating can be seen. The COF curve, Figure 45(b) starts with a maximum initial peak of 0.22 and after a short term of running–in period, it drops and increases alternatingly, without ever reaching a steady state regime. This behavior is probably due to fracture and delamination events between layers until substrate exposure.

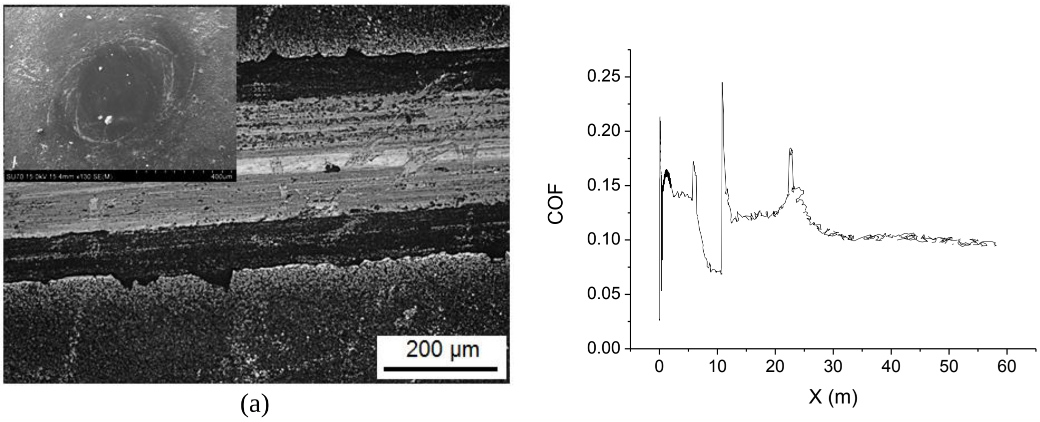

(a)

(b)

Figure 45. Worn surface images of the diamond–coated: (a) Si_3N_4 disc and ball and (b), COF versus X at RH= 90%, W= 150 N.

Table 16 summarizes the values of the maximum friction coefficient (μ_{Max}), steady state friction coefficient (μ_{Steady}), wear coefficient of disc (k_{Disc}) and ball (k_{Ball}) samples obtained in the reciprocating self–mated sliding tests of multilayered diamond coatings.

The highest value of the coefficient of friction was generated in the sliding conditions of RH= 20%, W= 50 N, while the lowest value appeared in RH= 90%, W= 100 N. However, there is no obvious trend in the μ_{Max} value with the RH In addition, the sliding test of RH= 25%, W= 40 N exhibited the highest steady state coefficient of friction, while the sliding test of RH= 80%, W= 60 N showed the lowest steady state coefficient of friction, but again without any discernible trend. The only clear difference is between the average values of the maximum friction coefficient ($\bar{\mu}_{Max}$ = 0.32) and the average of the steady state ones ($\bar{\mu}_{Steady}$ = 0.09).

Table 16. Test conditions, maximum (μ_{Max}) and steady state (μ_{Steady}) friction coefficients, wear coefficients of disc and ball measured in reciprocating sliding tests at room temperature.

RH (%)	W (N)	μ_{Max}	μ_{Steady}	k_{Disc} ($mm^3N^{-1}m^{-1}$)	k_{Ball} ($mm^3N^{-1}m^{-1}$)
10	40	0.23	0.09	4.1×10^{-7}	2.1×10^{-7}
20	50	0.70	0.05	1.7×10^{-7}	1.3×10^{-7}
25	40	0.23	0.14	1.8×10^{-7}	6.7×10^{-8}
80	60	0.26	0.02	5.2×10^{-8}	4.6×10^{-8}
80	80	0.33	0.13	4.0×10^{-7}	9.9×10^{-8}
90	100	0.20	0.11	9.3×10^{-7}	1.3×10^{-7}
90	120	0.31	0.07	4.4×10^{-7}	9.5×10^{-8}
		$\bar{\mu}_{Max}$:0.32	$\bar{\mu}_{Steady}$:0.09		

The effect of relative humidity (RH) on the critical load (W_c, the maximum load allowed before of the either the ball or the disc coating), is presented in Figure 46. As illustrated, the critical load increases with RH. The most significant result is that at RH=90% the system withstands a load that is thrice that of the one achieved at RH=10% due to the load bearing effect afforded by the presence of water molecules on the diamond surfaces [43]. Moreover, increasing the relative humidity, increases the water molecules trapped between the two sliding surfaces, which resulted in decreasing the temperature of the contact area between diamond–coated disc and ball.

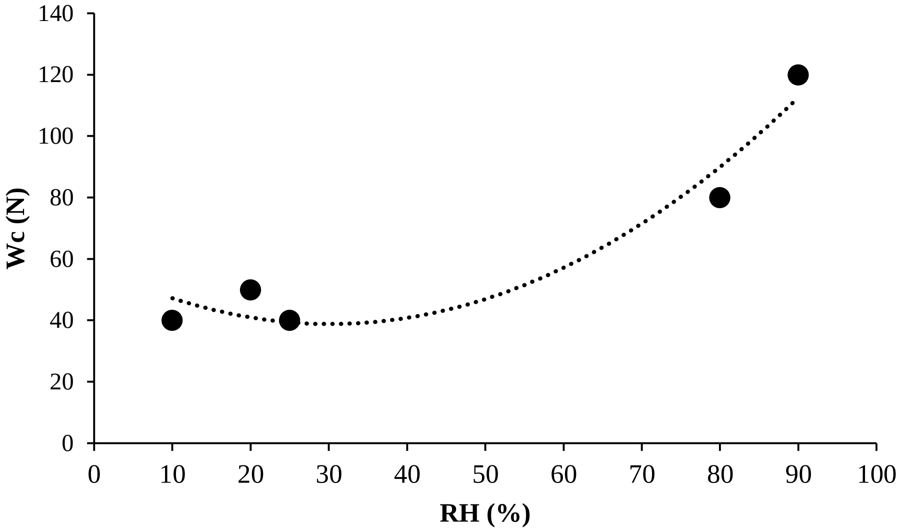

Figure 46. Effect of relative humidity on the critical load of the tribosystems based on multilayered self–mated diamond coatings.

With respect to the wear coefficients of the discs, values in the vicinity of ~10^{-7} mm^3/Nm indicate a mild wear regime while the balls are in the mild to very mild wear regime (~10^{-7}–10^{-8} mm^3/Nm). The lower wear resistance of the discs is a result of fatigue effects induced by the intermittent contact during the reciprocating sliding [43,52]. Figure 47 shows the dependence of the wear coefficient (k) as a function of RH for the tests conducted under the critical load.

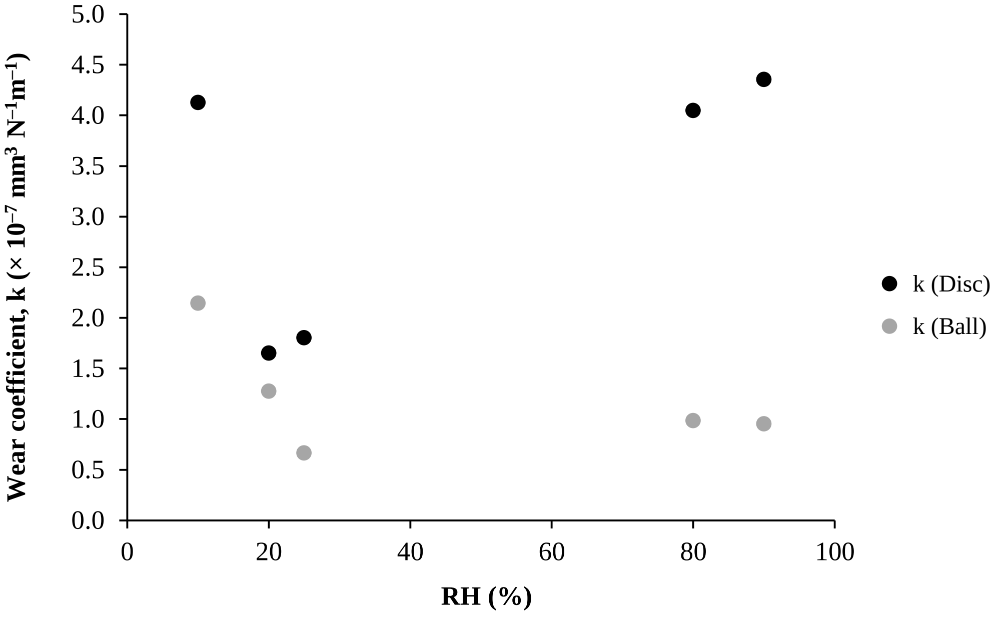

Figure 47. Wear coefficient values (k), estimated at the critical loads, as a function of relative humidity on self–mated diamond coated Si_3N_4 disc and ball tribosystem.

The wear coefficient has a valley–shaped evolution for the disc in the 10% to 90% RH range while for the balls there is an increase of k for low humidity conditions. The increment of the wear coefficient for high RH can be attributed to fatigue enhancement by the increased critical loads, while the absence of adsorbed water, and thus reduced lubrication, at low RH accounts for the high k values on the left hand side.

4.2. Temperature effect on friction and wear coefficients

Table 17 shows the maximum COF (μ_{Max}), steady state COF (μ_{Steady}), wear coefficient of flat and sphere specimens for non–delaminated self–mated sliding wear tests diamond–coated Si_3N_4 discs and counterbodies in the reciprocating configuration.

Table 17. Maximum COF (μ_{Max}) and steady COF (μ_{Steady}) for self–mated sliding tests in the reciprocating configuration (ambient RH).

T (°C)	W (N)	μ_{Max}	μ_{Steady}	k_{Disc} ($mm^3N^{-1}m^{-1}$)	k_{Ball} ($mm^3N^{-1}m^{-1}$)
50	40	0.64	0.01	1.5×10^{-7}	6.9×10^{-8}
50	50	0.81	0.12	1.6×10^{-7}	1.1×10^{-7}
50	55	0.73	0.05	2.2×10^{-7}	1.3×10^{-7}
75	40	0.33	0.06	1.9×10^{-7}	8.9×10^{-8}
100	50	0.71	0.09	2.4×10^{-7}	1.7×10^{-7}
		$\bar{\mu}_{Max}$: 0.64	$\bar{\mu}_{Steady}$: 0.07		

Comparing with the friction coefficient values from the room temperature testing (Table 16), it is clear that at higher temperatures the maximum COF peaks are larger ($\bar{\mu}_{Max}$ = 0.64) while the steady state ones are similar ($\bar{\mu}_{Steady}$ = 0.07).

The clearest difference between the two sets of experiments is observed for the critical loads. The values achieved in the tests with temperature are limited to the range 40–55 N, while at room temperature a value of 120 N was reached (Figure 46). Interestingly, the latter was obtained at high relative humidity while the critical loads under dry conditions (≤ 25% RH) are similar to those attained at high temperature. Likewise, the wear coefficients of the discs are also of the same order of magnitude of those measured under low RH conditions.

Regarding the sliding wear tests performed in circular configuration at 150°C–250°C due to the temperature limitations of the reciprocating system, delamination occurred in all the tested tribopairs. By increasing the sliding wear temperature, there is a decrease in the amount of surface groups such as hydrogen terminations, or hydroxyl from vapor or liquid, and of the water molecules trapped between the two sliding surfaces. These occurrences result in the absence of surface passivation during sliding and in a very low humid environment during which lead to higher wear and friction with respect to the lower sliding temperature [26,141–147].

SEM micrographs of the worn surfaces of diamond–coated Si_3N_4 disc and ball (inset) and magnified views of the wear track center and border at sliding reciprocating conditions of T= 100 °C, W= 50 N, are shown in Figure 48. The worn morphology is representative of the high temperature experiments. The surface condition shown in

Figure 48(b) indicates that self–polishing is the dominant wear mechanism similarly to the observed for the RH tests, at low humidity conditions (Figure 44b). The net difference between unworn and worn surface morphologies is evidenced in the transition at the border of the wear track, Figure 48(c).

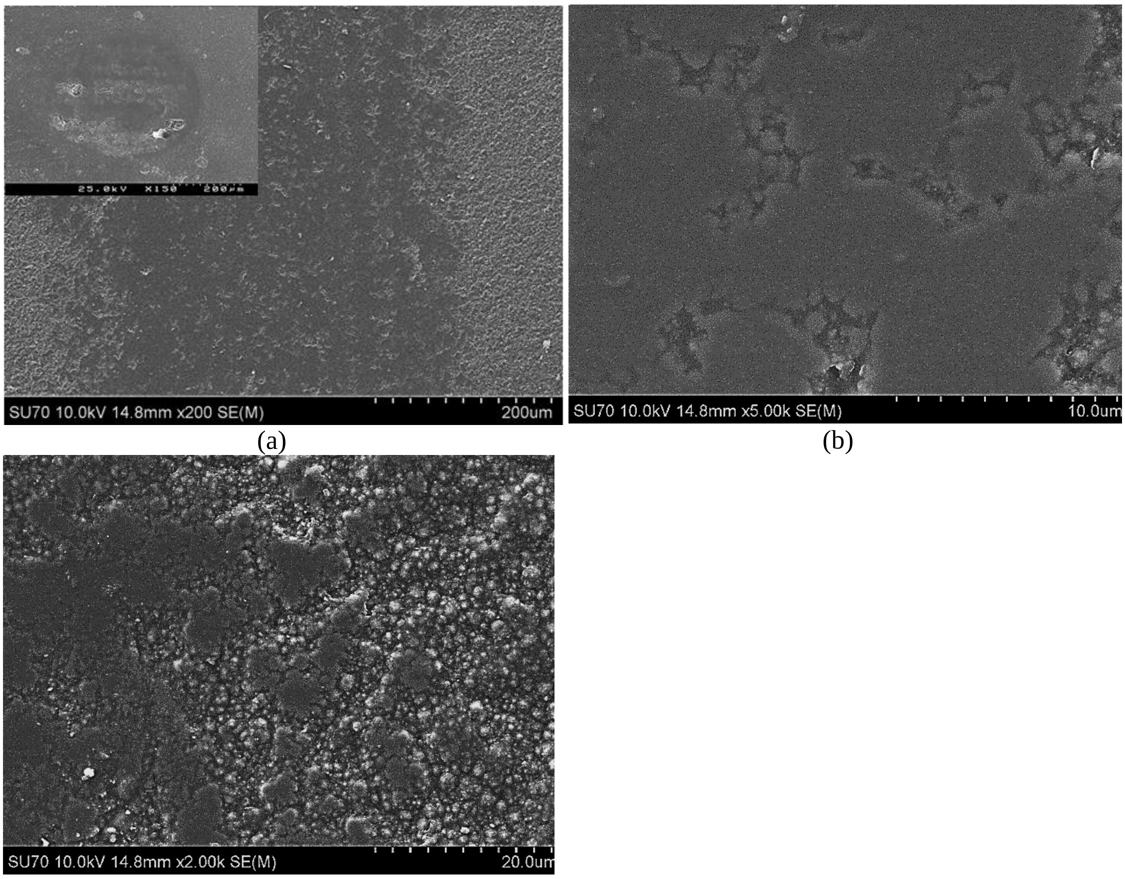

(a) (b)

(c)

Figure 48. SEM micrographs of: (a) worn surfaces of diamond–coated Si_3N_4 disc and ball and (b) magnified wear track and (c) track border at reciprocating sliding conditions of T= 100 °C, W= 50 N.

Optical profilometry (Sensofar Sneox) was used to study the worn track surfaces of the diamond–coated Si_3N_4 flat samples. The obtained images were used to determine the volume loss of the wear tracks in all the above reciprocating tribological experiments. Figure 49 illustrates the optical profilometry images of a wear track taking as an example the wear conditions of T= 100 °C, W= 50 N.

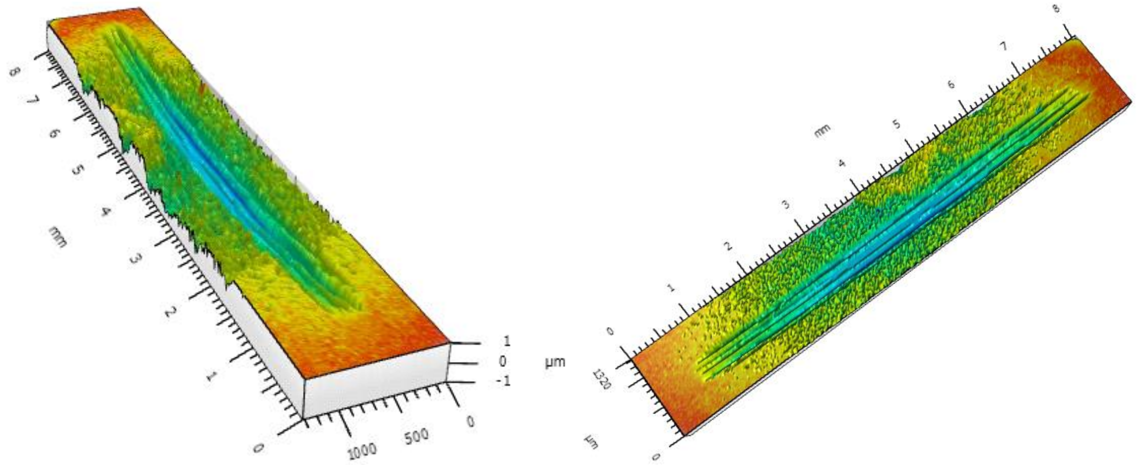

(a) 3D image of the wear track.

(b) 2D image of the wear track.

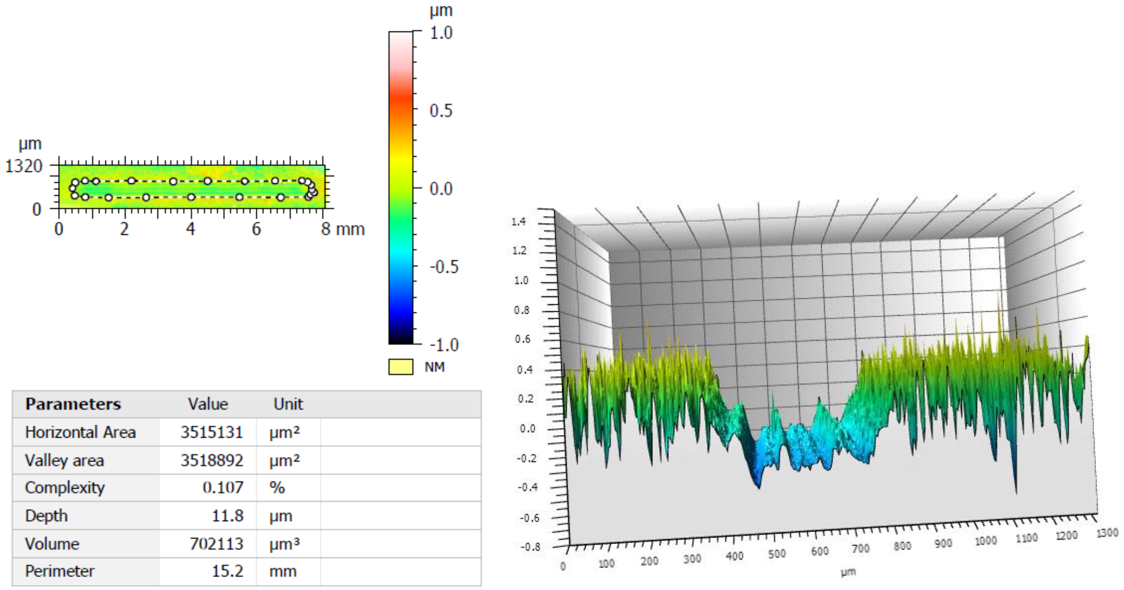

Parameters	Value	Unit
Horizontal Area	3515131	µm²
Valley area	3518892	µm²
Complexity	0.107	%
Depth	11.8	µm
Volume	702113	µm³
Perimeter	15.2	mm

(c) Volume loss of the wear track.

(d) 3D profile of un–worn and worn surface roughness.

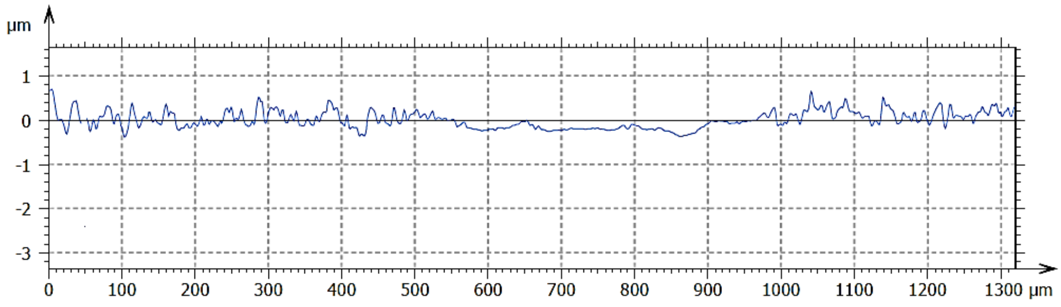

(e) 2D profile of surface roughness of the non–worn surface and worn track.

Figure 49. Optical profilometry images of the reciprocated wear tracks of the diamond–coated Si_3N_4 discs at the wear conditions of T= 100 °C, W= 50 N.

Figure 50 shows a 3D optical profilometry image of a delaminated region of a wear track. This served to measure the actual multilayered diamond coating thickness and that is 8.5 µm, in line with the findings reported in Chapter 3 (Figure 39c).

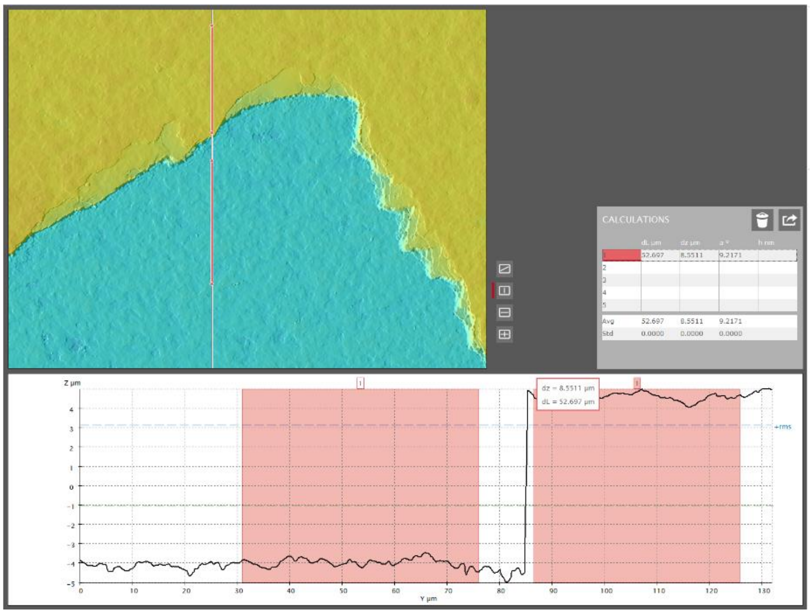

CALCULATIONS

	dL µm	dz µm	a °	h nm
1	52.697	8.5511	9.2171	
2				
3				
4				
5				
Avg	52.697	8.5511	9.2171	
Std	0.0000	0.0000	0.0000	

Figure 50. Optical profilometry image of a delaminated region of a wear track of the multilayered diamond–coated Si_3N_4 discs.

4.3. Tribological behaviour of self–mated CVD diamond coatings under biodiesel lubrication

This section contains the results of the tribological behaviour of CVD diamond–coated Si_3N_4 ceramic substrates under biodiesel lubrication. The balls and discs used in these tests have a different number of MCD and NCD layers, so details of these particular samples are given in the following.

The morphologic features of the surfaces of the distinct triboelements coated with diamond, prior to the tribological tests, are presented in Figure 51. Top view SEM images of the diamond coated samples are presented in Figures 51(b) and 51(c) for the single layer MCD coating (SL) and the six layered MCD/NCD (ML) coating, respectively.

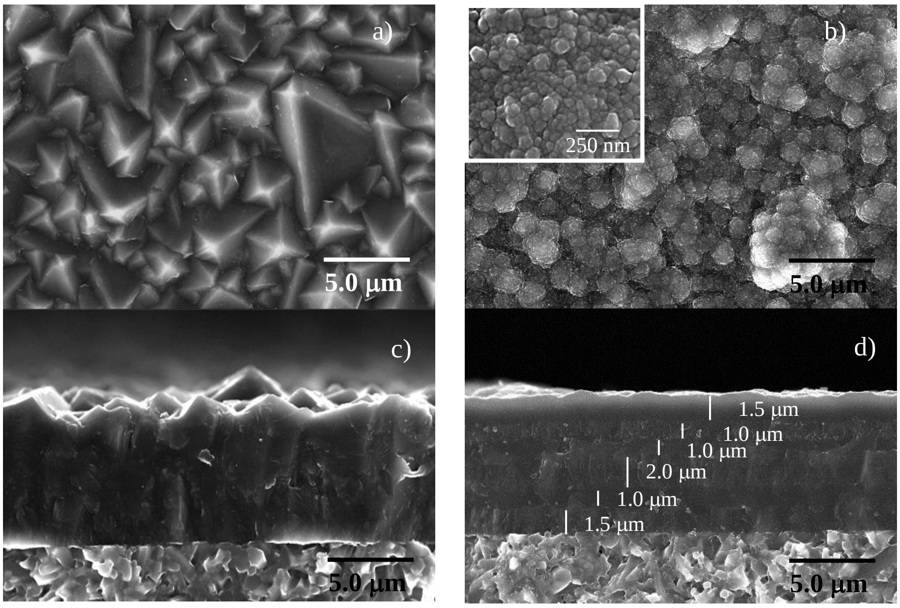

Figure 51. SEM top–view images of the: (a) as–deposited monolayered MCD – SL coating and (b) the multilayered diamond (ML) coated samples. SEM cross–section images of the: (c) SL and (d) the ML coating.

The diamond morphology of the SL coating (Figure 51a) reveals a pyramidal habit typical of a preferential <100> growth direction [154]. The SEM cross–section images reveal the columnar growth of the MCD coating (Figure 51c), resulting in the large diamond grains at the surface. On the contrary, the top layer of the ML coating is of nanocrystalline nature (Figure 51b and the respective inset in high magnification), similar to the nucleation stage of the microcrystalline diamond where a preferential orientation is still undefined. The nanometric size and the hindering of crystal growth in this ML system help on lowering the surface roughness. In the case of the ML coating, which starts by an adherent MCD layer on the SN substrate, the surface roughness is reduced by successively alternating the growth conditions with those of NCD (Table 3 in Chapter 2: HFCVD film growth) until a total thickness of 8 μm, the same as for the single layer MCD samples. The stacked structure of the ML composite diamond film is presented in the cross–section image of Figure 51(d).

Representative SEM micrographs of the wear tracks on the SN and the diamond coated disc samples after the short tests (86 m) are presented in Figure 52 and Figure 53.

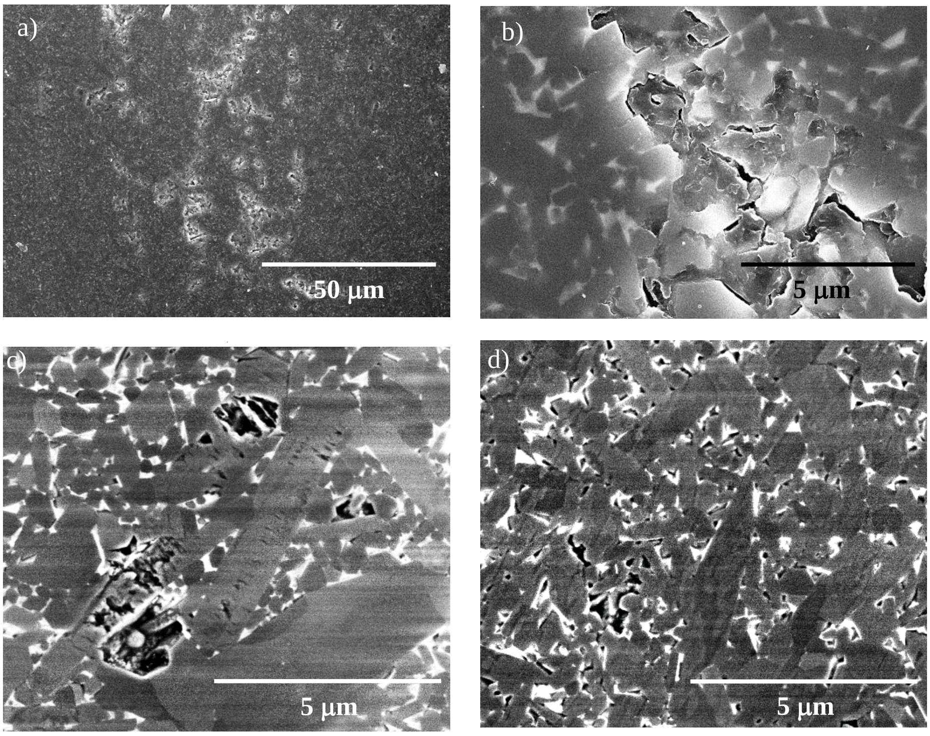

Figure 52. SEM micrographs of a SN disc after sliding 86 m under 100 N of applied load in biodiesel fluid. (a) broad view; (b) inter-granular cracking; (c) trans-granular fracture; (d) tribo-layer formation.

Figure 52(a) shows a broad view of the centre of the wear track of a SN sample tested with the maximum applied load of 100 N. Cracks along the grain boundaries are observed (Figure 52b), while some grains present transgranular micro–fracture that leads to material chipping (Figure 52c). In some regions, as the one of Figure 52(d), the presence of a thin adhered layer is found. EDS analysis only detected the presence of elements that constitutes the ceramic material. This layer is thus probably formed by wear debris, which are plastically deformed by the tribological action.

The SEM micrographs of Figures 53(a) and 53(b) are low magnifications of the border of the wear tracks of the SL and the ML samples, respectively, after sliding 86 m under 40 N load. The smoother worn areas (left–hand side in each micrograph) can be clearly recognized by their dark and low contrast aspect in SEM observation and further evidenced by their respective insets of AFM scans. At the end of the tests, the intrinsic surface roughness of the SL and the ML coatings decreased by about 60% and 85% that of the un–worn areas, respectively: R_q reached values of about 130±25 nm for the SL and 17±8 nm for the ML samples.

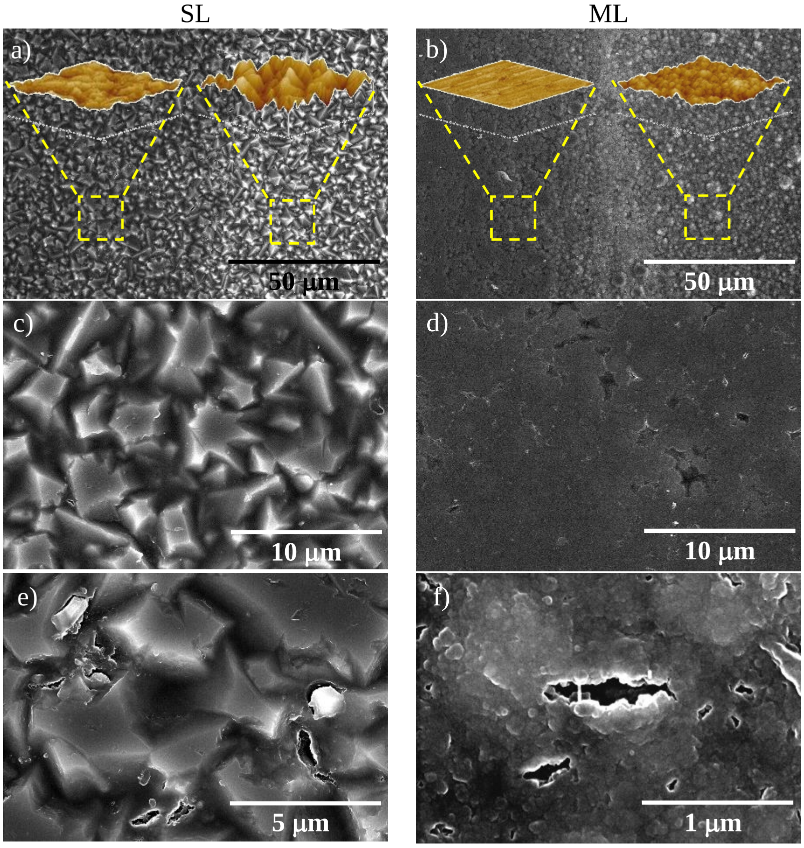

Figure 53. SEM micrographs of the wear tracks of the SL coated samples (left–hand side) and the ML coatings (right–hand side) after sliding 86 m under 40 N of applied load with biodiesel lubrication: a) and b) low magnifications of the border of the wear tracks of the SL and ML diamond coated samples, respectively; c) and e) high magnifications of the wear tracks of the SL coated samples and micro–cracks development, respectively; d) and f) the same for the ML diamond coated samples.

Figures 53(c) and 53(e) present higher magnifications of the worn area of the SL sample, showing polished plateaus originated by the truncation of the tips of the micro–pyramidal diamond crystals and the chipping formation by the development of micro–cracks. The same, polished plateaus of the top NCD diamond conglomerates can be seen on the Figure 53(d) for the ML sample, the depressions between the plateaus corresponding to undamaged NCD regions. Micro–cracks occurring along the nanometric crystals are well visualized in Figure 53(f). These observations reveal that wear takes place by an abrasive self–polishing mechanism in both the SL and the ML coatings.

The influence of the applied load on the wear behaviour is further discussed. For the bare SN tribosystem, both the ball and the disc wear coefficients undergo a net increase with the applied load above 40 N (Figure 54). At 100 N, there is a significant number of fractured regions on the wear tracks (Figure 52) that intensify the wear phenomenon. The trend for the SL diamond coatings is the opposite, as the wear coefficient diminishes with load (Figure 54). At lower load solicitations, high initial local pressures are generated due to a limited number of diamond asperities bearing most of the applied load [155]. After the running–in period, a polished area is formed and the contact pressure drastically decreases, thus decreasing the wear evolution. At loads around 60 N, the fraction of polished area is more significant and wear coefficients approach that of the ML diamond coatings, which have already lower levels of surface asperities and load effect. Comparing the k values of the balls and plates for the SL coatings, it is possible to see that the wear in the plates is about 3 times higher than in the balls (Figure 54b and 54a, respectively). This fact evidences that surface fatigue caused by the intermittent contact [155] in the plate specimens is controlling the wear loss in the case of the SL coated surfaces. The larger surface flaws are stress concentrators for the nucleation and growth of fatigue cracks. Regarding this, a more even performance was obtained by the ML tribosystem, the wear rates being similar for the balls and plates (Figures 54a and 54b). In this case, an average k value of 5×10^{-8} $mm^{3}\cdot N^{-1}\cdot m^{-1}$ was obtained. As expected, the lower surface roughness and finer grains of the top NCD layer contribute to the near load and fatigue insensitivity recorded in the graphics of Figure 54.

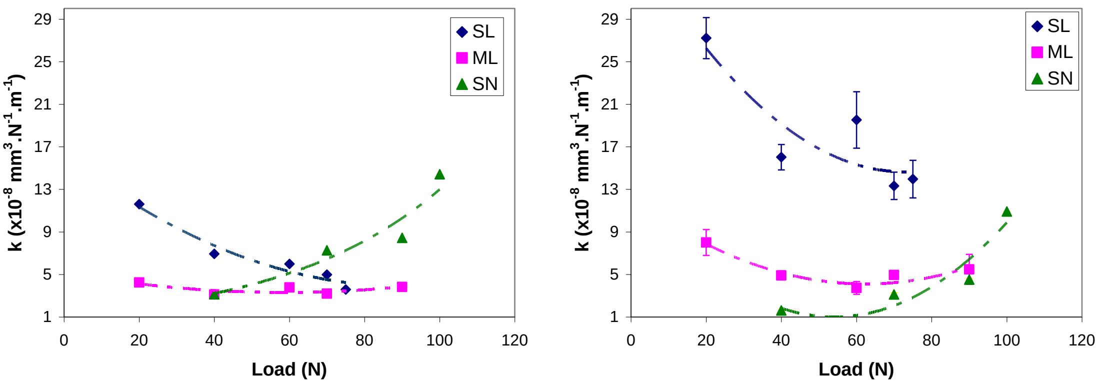

(a) Ball (b) Plate

Figure 54. Wear coefficient (*k*) values as a function of the applied load under biodiesel lubrication for: a) ball; and b) plate specimens.

Figure 55 presents the COF values of the experiments as a function of the sliding distance. There is an initial friction coefficient peak, strongly influenced by the intrinsic surface roughness of the diamond coatings [27,156]. Higher initial friction levels (COF~ 0.35) happens for the SL coatings (Figure 55), as more energy is spent in the sliding of the rough MCD starting surfaces, due to the fact that the asperities have to fracture or to overcome each other [27]. The fragmentation and deformation of contacting asperities of the diamond crystals at this stage is responsible for most part of the wear. After that, there is a running–in step, characterized by a self–polishing mechanism, reaching low COF values of 0.08 at the stationary regime, which takes place after only a few meters of sliding distance (Figure 55b). On the other hand, the smoother starting topography of the top NCD layer of the ML coating results in much lower initial COF values of about 0.15 (Figure 55b), decreasing to 0.09 in the stationary regime, after blunting of the diamond nanoclusters.

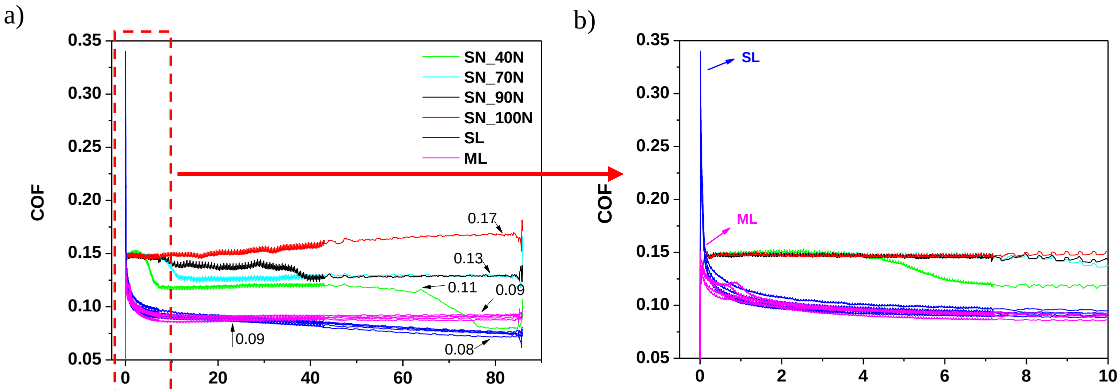

Figure 55. Friction coefficient of self–mated SN and diamond films under biodiesel lubrication: a) evolution under different applied loads (MCD and Multi coatings had the same COF evolution with load, which varied from 20 to 90N); b) Details of the first 10 m of the tests.

Regarding the steady–state COF values, only the bare SN experiments a load effect, increasing with the applied load (Figure 55). The described mechanism of chipping causing wear is responsible for surface roughening that contributes to increased friction. Contrarily, for the SL and ML diamond coated systems there is no load effect on friction (Figure 55). The slight differences among the steady–state COF of these diamond coated systems might be related to the better ability of the MCD surface of the SL sample in retaining the lubricant in the valleys between the polished plateaus (Figure 53c).

All samples were compared to 52100 steel, in short–term (86 m) and in endurance tribotests (780 m), under initial hertzian pressures of 3 GPa (40 N for the SN and the SL and ML diamond coated samples, and 145 N for the steel ones). The results of the endurance tests showed that steel presented the highest COF values at the stationary regime, 0.12, a lower value than those of the SL and ML coated tribosystems (0.08 and 0.09 in Figure 55a).

Figures 56(a) and 56(b) compare the wear coefficient values of the different tribosystems. As the Y–axis scale in Figure 56(b) is four times enlarged comparatively to Figure 55(a), it is evident that most part of the wear takes place at the beginning of the tribotests, at the running–in period, the k values decreasing up to one order of magnitude in the case of the SL sample endurance tests. Similar k values of about 3×10^{-8} mm^3·N^{-1}·m^{-1} for the SN, ML and steel balls were found in the short time tests, but they behave differently when increasing the sliding distance, as it can be seen in the results of the Figure 56(b) for the endurance tests. Here, a decrease in the k values in more than 80% is reached for the SN and ML samples, decreasing their values to about 5×10^{-9} mm^{3}N^{-1}m^{-1}. On the other hand, the k values of the steel samples did not decrease as significantly as in the case of the others tribosystems, reaching 1.5×10^{-8} mm^{3}N^{-1}m^{-1} for the endurance tests, indicating a more progressive wear of the surfaces. The data in Figure 56(b) indicating “plate*” (yellow coloured bar) is the calculated k value of the plate when not considering the volume of wear in the running–in period. It can be seen that an even better behaviour of the diamond coated samples could be reached if the starting surfaces were pre–polished, the k values of the SL plates, for instance, decreases in about 50%, from 3.2×10^{-8} mm^{3}N^{-1}m^{-1} to 1.6×10^{-8} mm^{3}N^{-1}m^{-1} if the volume of wear of the running–in period is not considered. In the case of the ML samples, a reduction of about 65% is reached, from 8.1×10^{-9} mm^{3}N^{-1}m^{-1} to 2.9×10^{-9} mm^{3}N^{-1}m^{-1}. The SN samples experienced the highest reduction in wear, decreasing the k value from 0.2 to 0.02×10^{-8} mm^{3}N^{-1}m^{-1}. Steel samples had the less significant change in their k values, showing that they did not experience the running–in regime in the same order as the other tribosystems.

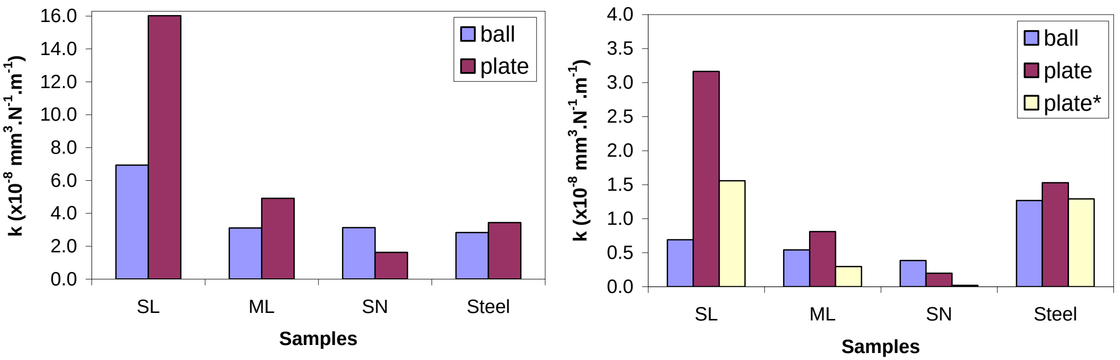

(a) L= 86 m

(b) L= 780 m

Figure 56. Wear coefficient values of the: a) short; and b) endurance tribotests.

In summary, a first net advantage of bare and diamond coated ceramics is the lower friction coefficient under biodiesel lubrication than that of the steel tribopair, which presents a COF above 0.10, which can limit engineering applications. Another disadvantage of steel is that, in case of fuel failure, this material is more susceptible to scuffing [157] due to the increase of friction coefficient. For instance, tribological data of steel–on–steel 52100 pairs shows that this material presents a very high friction coefficient of 0.60 and a calculated k value of ~ 2×10^{-5} $mm^3N^{-1}m^{-1}$, taken from wear data on the ASTM G99 standard, when in unlubricated condition [158].

Moreover, ceramics are lighter, harder, more temperature resistant, and less susceptible to corrosion. Regarding the wear behaviour under biodiesel lubrication, all the tested materials have shown similar mild wear coefficients. The SL tribopair presented a high initial friction peak associated to the highest wear during running–in, which may be critical if cracks nucleate and develop to fracture. However, if the system survives this initial event, or the surfaces are pre–polished, the system is the best one regarding friction. It is worth noting that ML coatings do not possess such drawback due to their much smoother surfaces. SN samples behaved similarly to the ML coated materials, but both friction and wear increase considerably with the increasing of the applied load. Moreover, homologous pairs of SN ceramics can experience very high wear levels if the lubrication fails, as their k values in unlubricated conditions reach the order of 10^{-5} $mm^3N^{-1}m^{-1}$ [159], contrarily to what happens in unlubricated diamond tribosystems (relative humidity – RH: 50–60%) where mild to very mild regime is attained k~ 10^{-7}–10^{-8} $mm^3N^{-1}m^{-1}$ [26,40]. The RH condition (2–100%) was studied for diamond/steel sliding contacts showing that it only influences the steel counterbody wear that increases with decreasing RH [160]. In the case of self–mated diamond tribosystems in various atmospheres as humid air (RH 40%), dry nitrogen (RH < 1%), ultra–high vacuum, and distilled water, only in ultra–high vacuum conditions the diamond films showed limitations due to inappropriate friction coefficients (about 0.30) and severe wear rates (order of 10^{-4} $mm^3N^{-1}m^{-1}$) [33]. Another conclusion of the later study was that polished coarse–grain CVD diamond films sliding in distilled water exhibited the lowest assessed wear rates, with extremely low values (less than 10^{-10} $mm^3N^{-1}m^{-1}$), characteristic of ultra–mild wear regimes. This is important information, since biofuels have residual water in their constitution, which can be problematic for other tribosystems.

Chapter 5

Applications of multilayered diamond as cutting inserts and mechanical seal rings

In this chapter the application of multilayered diamond coatings (ML) as cutting tools and seal rings are presented and discussed. The first part of this chapter covers the machining performance of ML coated inserts in the turning of an Al–15%Al_2O_3 metal matrix composite (MMC). The evolution of forces is related to cutting conditions and wear of the tools and the performance of the inserts is evaluated and critically assessed. In the second part, the tribological behavior of mechanical seal rings under biodiesel lubrication and the full sealing conditions of pressurized water are described.

5.1. Multilayered diamond coated inserts in the machining of Al–15%Al_2O_3 MMC

Representative top and cross–sectional SEM images of the two types of coatings used for machining of the MMC workpiece, ML10x1 and ML10x2, are given in Figure 57. The free surfaces of the coatings (Figure 57a and 57b) present clusters of nanosized diamond particles without any crystalline facets as described for similar diamond multi–layered coatings [52]. The cross sections obtained by fracture (Figure 57c and 57d) depict the multi–layered structure of the coatings, the MCD layers being much thinner than NCD. This coating architecture relies on the strong adhesion of a first layer of MCD to the plasma etched Si_3N_4 ceramic substrate [84] and on the insertion of intermediate MCD layers creating MCD/NCD interfaces that act as energy sinks to crack propagation. The top layer is of NCD to ensure a smooth surface, Ra_{ML10x1}= 79 ± 7 nm and Ra_{ML10x2}= 145 ± 6 nm, relatively to uncoated, etched substrates or to substrates coated solely with MCD [52]. Thick NCD layers combined with thin MCD layers act in a way that further contributes to reduce the surface roughness of the tools. The larger surface roughness of the thicker coating (ML10x2) is merely a consequence of the larger thickness of the MCD layers in the ML10x2 inserts.

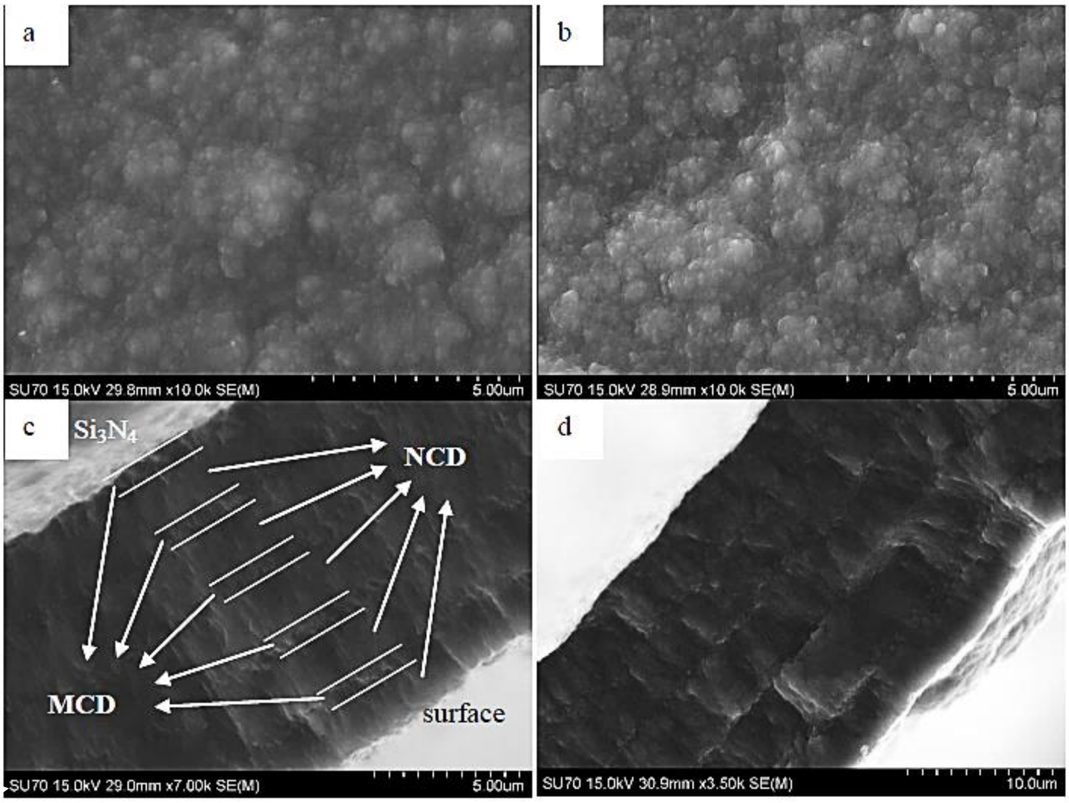

Figure 57. Representative SEM micrographs of the surfaces of a) ML10x1 and b) ML10x2 inserts and respective cross sections in c) and d) (notice the scale difference in the bottom pictures). Ra_{ML10x1}= 79 ± 7 nm and Ra_{ML10x2}= 145 ± 6 nm.

The real time evolution of the cutting forces for the ML10x1 inserts, showed a visible increase in all orthogonal components of the cutting force with machining time, Figure 58. The main component (F_c) is always larger at the beginning but the depth of cut (F_{DOC}) and feed (F_{feed}) components generally show steeper increases during turning. An example of this evolution for two different machining conditions is given in the graphs of Figures 58a and 58b and is usually related to wear of the cutting tip [64]. The inset SEM micrographs of the cutting tip show that there was delamination at the flank (major and minor) and tool face, resulting in a strong flank and also crater wear of the base substrate material, the Si_3N_4 ceramic, with VB values exceeding 500 µm after 1812 m and 476 m of turning at 250 $m \cdot min^{-1}$/0.1 $mm.rev^{-1}$ and 500 $m.min^{-1}$/0.4 $mm.rev^{-1}$, respectively. The SEM micrographs and charts in Figure 58 also show that the force increase was lesser for the tip where the diamond coating did not delaminate completely, Figure 58b. This somewhat improved wear resistance was due to the presence of the diamond coating on part of the tool face, next to the cutting edge at the corner of the insert. Data also show that, while for the 250 $m.min^{-1}$ and 0.1 $mm.rev^{-1}$ feed test it was possible to clearly detect the onset of film delamination (at about 30 s machining time), Figure 58a, the absence of an abrupt transition in the curves of Figure 58b indicates that at those turning conditions, delamination might have occurred at the first moments of contact between the tool and the workpiece material. This was the case for all the other tests conducted with the thinner coating, ML10x1 that could not withstand the stresses at the cutting tip. This level of detail in the way forces change when diamond coated tools fail is hard to find in the literature, but comments by some authors [59,97] indicate that this is a common occurrence whenever there is delamination of the film from the tool substrate. PCD tools, on the contrary, never show this steep increase of the cutting force in the machining of MMCs. Rather, wear of the cutting edge is continuous as is the increase of the cutting force and lathe power consumption with time, as was found by Ramesh et al. [161].

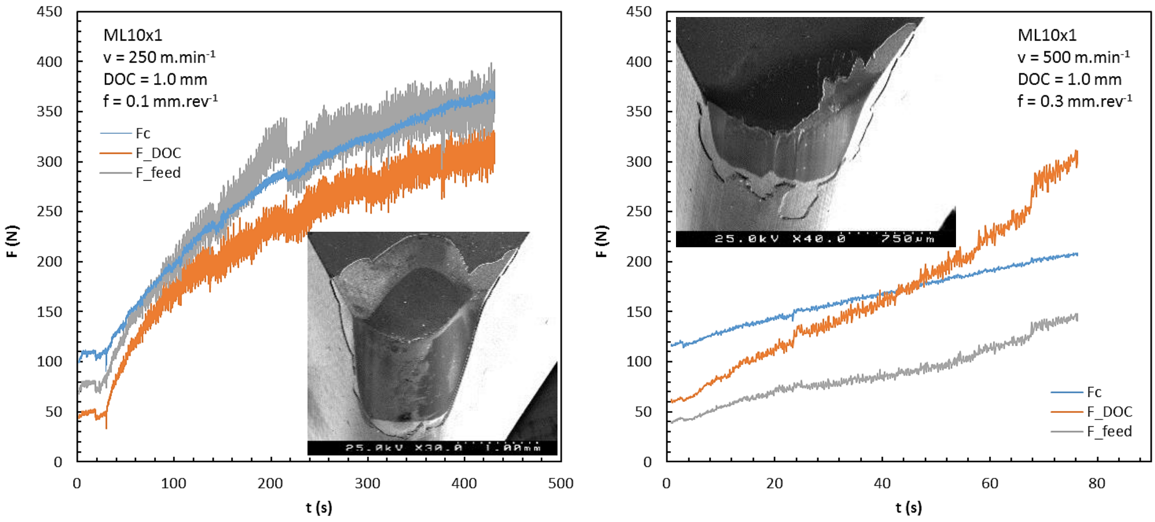

(a) (b)

Figure 58. Evolution of the three components of the cutting force with time when turning the MMC with ML10x1 insert at DOC = 1 mm. a) v = 250 m.min^{-1}, f = 0.1 mm.rev^{-1}; b) v = 500 m.min^{-1}, f = 0.3 mm.rev^{-1}. Insets: SEM micrographs of the cutting tip after cleaning the built up edge material.

Due to the early fracture of the ML10x1 cutting inserts, only a limited analysis can be made regarding the effects of the cutting parameters on the cutting force in the machining of 15 vol.% Al_2O_3 MMCs with these inserts. Therefore, just the initial values of the force for each test were thus used to assess how this cutting geometry compares with others from literature, where that information is available. With both DOC and feed values fixed, the effect of cutting speed on the cutting force is small, although with a slight tendency for a reduction, as it was also observed in the machining of MMCs with 30 µm [95] and 6 µm [101] CVD thick diamond coatings. This reduction occurs irrespectively of the thickness of the coated tool or of the turning geometry. The larger effects on all components of the cutting force are observed when significant increases are made to the DOC or to feed. The increase is linear with both these parameters. This is exemplified by the chart of Figure 59a, relative to the effect of feed on the initial values of F_c. Data–points collected from the literature fit the results obtained in the present work for both ML10x1 and ML10x2 coatings, with a general constant of 640 N per mm.rev^{-1}. An interesting finding that comes from this comparative analysis is that there is also little sensitivity towards the type (Al_2O_3 or SiC) or amount (10% to 20%) of reinforcing particles in what respects the absolute values of the cutting force, unlike wear rates. Data from a work of turning with PCD tools also fit the current work results despite the differences in cutting geometry and the use of lubrication [64]. Unlike this, and in a different work, quite smaller values for F_c and with very little sensitivity towards feed values were recorded [66] and are not considered here.

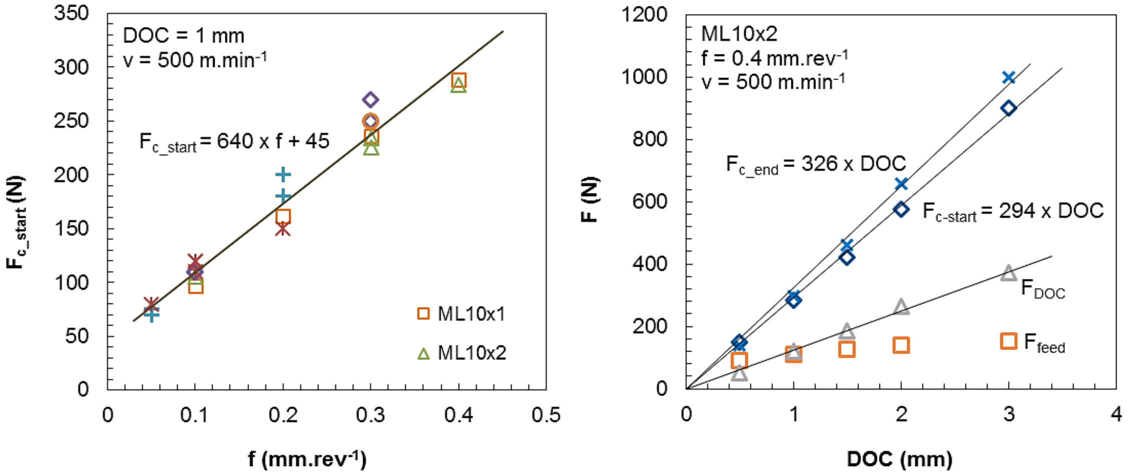

(a) (b)

Figure 59. a) Variation of the initial values of the main cutting force with feed (f), at fixed DOC and cutting speed. ✚ – CVD [95]; ◇ – [101]; ○ – [59]; ✱ – [64]. b) Effect of depth of cut in the initial values of cutting force for the ML10x2 inserts and end values of F_c, for fixed feed and speed.

For the ML10x2 inserts, data presented in Figure 59b illustrates the effect of DOC on the initial values of force components at fixed cutting speed and feed, where a constant of about 294 N.mm^{-1} of DOC was obtained for the initial F_c values. It is also clear that, as expected, the radial component, F_{DOC}, increases more rapidly than the axial F_{feed}, surpassing it for depth of cut values above one millimetre. As shown above, delamination, fracture and wear of the ML10x1 inserts have as consequence the increase in all components of the cutting force. A slow increase of wear of the cutting tip should result in corresponding low increases of the cutting force throughout the turning operation. This was observed for the ML10x2 inserts, where, when studying the effects of the DOC, the linear constant increased only to 326 N.mm^{-1} from the value of 294 N.mm^{-1}, as shown in Figure 59b.

There were a few cases where the ML10x2 tools could not withstand the mechanical stresses imposed by the dry turning within the range of defined conditions. For the fixed speed of 500 m.min^{-1} and DOC of 1.0 mm, there was never delamination of the diamond coating for feed values in the range 0.1–0.3 mm.rev^{-1}. For the same speed but with a fixed feed of 0.4 mm.rev^{-1}, the tool coatings failed for DOC values above 1.5 mm, Figure 60a. That is, for main cutting forces equal to or higher than 400 N there is failure of the tool due to delamination of the coating. However, the tool keeps cutting without loss of dimensional tolerance of the workpiece, a parameter followed throughout the turning tests. Despite the increased value of flank wear of the exposed substrate material due to the rubbing of the corner and flank of the insert against the very abrasive MMC, Figure 60a, the presence of the 21–24 µm thick layer of diamond at the cutting edge is enough for the tool to keep cutting well.

Finally, for fixed values of DOC (1.0 mm) and feed (0.4 mm.rev^{-1}), the cutting tip did not withstand the highest cutting speed of 1000 m.min^{-1}. In the SEM micrograph of Figure 60b, it can be seen that a small area of coating delaminated from part of the tool face next to the cutting edge and not just from the flank and the corner. It is also clear from Figure 60b that the remaining diamond film on the face shows extensive cracking what contributes to a faster failure of the tool. The delamination of the flank is limited to the region around the corner of the tool, as most of the cutting edge did not delaminate. This also takes place even if high DOC values are used (3 mm) as depicted in Figure 60c. These post–mortem observations confirmed the data obtained from the evolution of the cutting force and dimensional tolerance of the workpiece: only where there is delamination from the tool face the cutting forces will increase more abruptly and the machined diameter will be out of specification due to recession of the cutting edge.

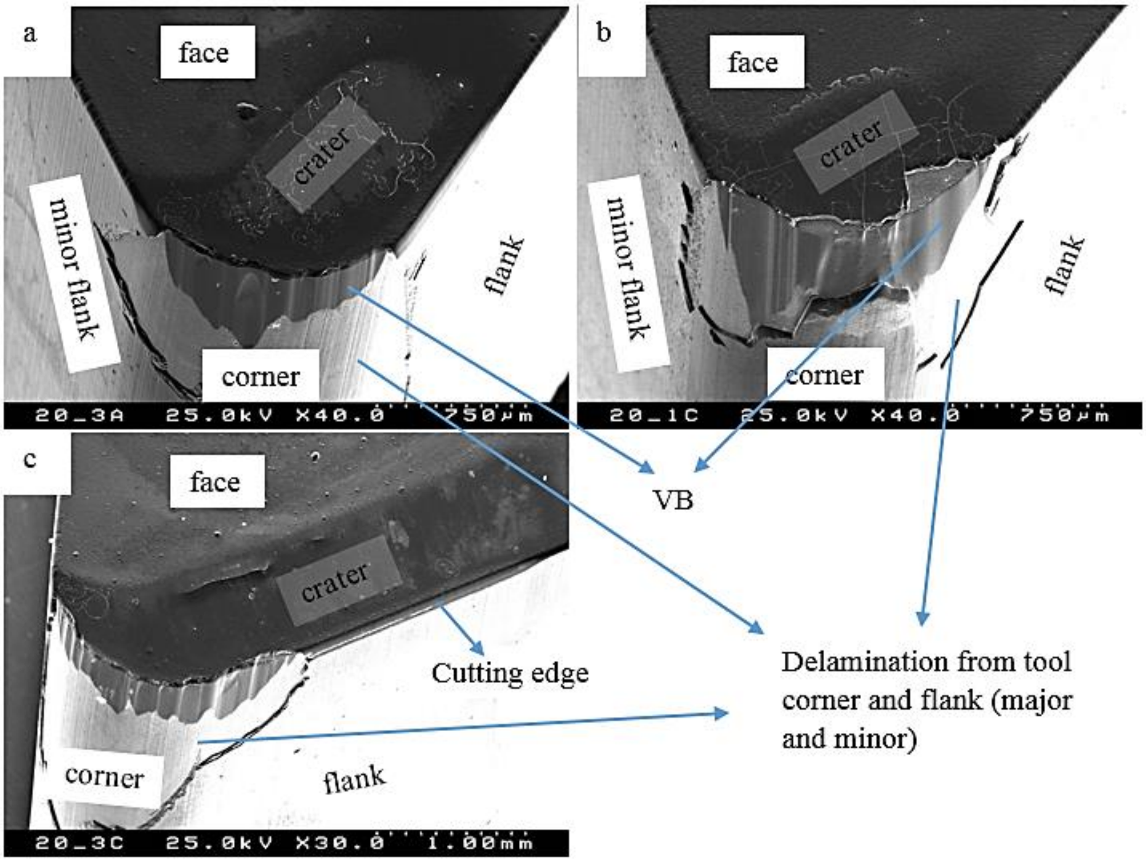

Figure 60. SEM micrographs of the ML10x2 cutting inserts after machining with a fixed feed, f = 0.4 mm.rev^{-1}: a) v = 500 m.min^{-1}, DOC=1.5 mm, L = 395 m; b) v = 1000 m.min^{-1}, DOC = 1.0 mm, L = 415 m; c) v = 500 m.min^{-1}, DOC = 3.0 mm, L = 375 m.

One should also bear in mind that the cutting geometry used in the present work relies on negative tool normal rake and tool cutting edge inclination (of –6°), this resulting in a strong rubbing of the turning chips on the tool face with the resulting crater being also visible on the micrographs of Figure 60. It is worth mentioning that in the conditions of Figure 60c, high DOC (3 mm) and medium speed (500 m.min^{-1}) the crater area is large but without delamination from the face. Crater wear is seldom, if ever, mentioned in the turning of MMCs with CVD diamond, indicating that most tools are used with a positive tool normal rake and tool cutting edge inclination or that they fail by delamination.

From the results of the present work and from the others already mentioned, there are a set of cutting conditions where the diamond coated inserts can be used. These parameters are dependent upon the workpiece material and the substrate/diamond system, including here all the possible surface treatments and deposition methods. For the ML10x2 inserts, these limits are: DOC values below 1.5 mm for feeds of 0.4 mm.rev^{-1}; maximum speeds of 750 m.min^{-1}; and feeds up to 0.4 mm.rev^{-1}. Within these boundaries, there is no delamination and the inserts wear out at the flank and corner forming a wear land that increases progressively with time, just as for PCD inserts. The SEM micrographs in Figure 61, of the cutting tips after cleaning the built up edge, illustrate this behaviour. DOC notch is absent from the major cutting edge due to the negative tool lead angle and it is almost negligible in the minor cutting edge, Figure 61a. As said previously, the cutting geometry, namely the negative tool normal rake, affects the wear behaviour of the tool face: crater wear is seldom, if ever, mentioned in the turning of MMCs, indicating that most tools are used with a positive tool normal rake. In the present work, and despite the short serrated chips produced for all cutting conditions (see inset micrographs in Figure 61), there is a marked evidence of the formation of a crater. From the SEM micrographs of the cutting tips it is also clear that some cracks appear at the surface layer of the face or may even cross several layers. Despite this, overall tool integrity was kept, even if the upper layer was removed partially, as can be seen for the 750 m.min^{-1} test, Figures 61c and 61d.

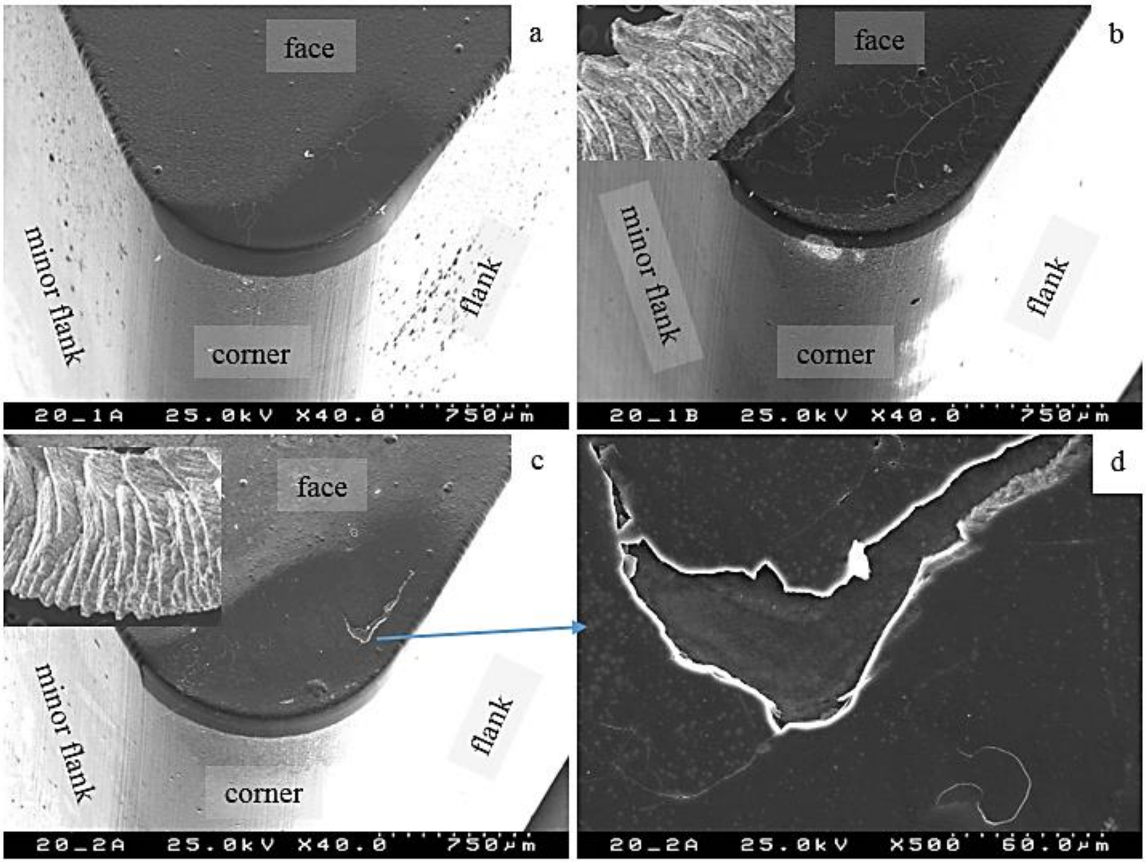

Figure 61. SEM micrographs of ML10x2 cutting inserts after machining at v = 500 m.min^{-1} and DOC=1.0 mm: a) f = 0.1 mm.rev^{-1}, L = 1708 m; b) f = 0.4 mm.rev^{-1}, L = 422 m. After machining at v = 750 m.min^{-1}, DOC = 1.0 mm, f = 0.4 mm.rev^{-1}, L = 413 m (c and d). Inset SEM micrographs of turning chips (chip width close to DOC values).

The multi–pass tests, done under dry and lubricated conditions, returned worn cutting tips after machining longer lengths than the above reported, Figure 62. The multilayer structure of the coating becomes obvious in the flank, and more pronounced craters are also formed, particularly in lubricated test, Figure 62c and 62d. The latter two SEM micrographs illustrate clearly the benefits of this multilayer strategy for the diamond coating, as fractures in the tool face propagate in steps along the NCD/MCD interfaces, to the nearest interface, resulting in successive partial delamination. This mechanism delays total delamination of the diamond coating from the substrate, unlike what would happen with monolayer coatings. This gradual loosening of material without total film spallation was already observed in erosion tests of multilayer diamond coatings with SiC particles [50]. In that work, the multilayer films presented a much improved erosion relatively to the mono–layer coatings of MCD and NCD that suffered from faster wear with substrate exposure.

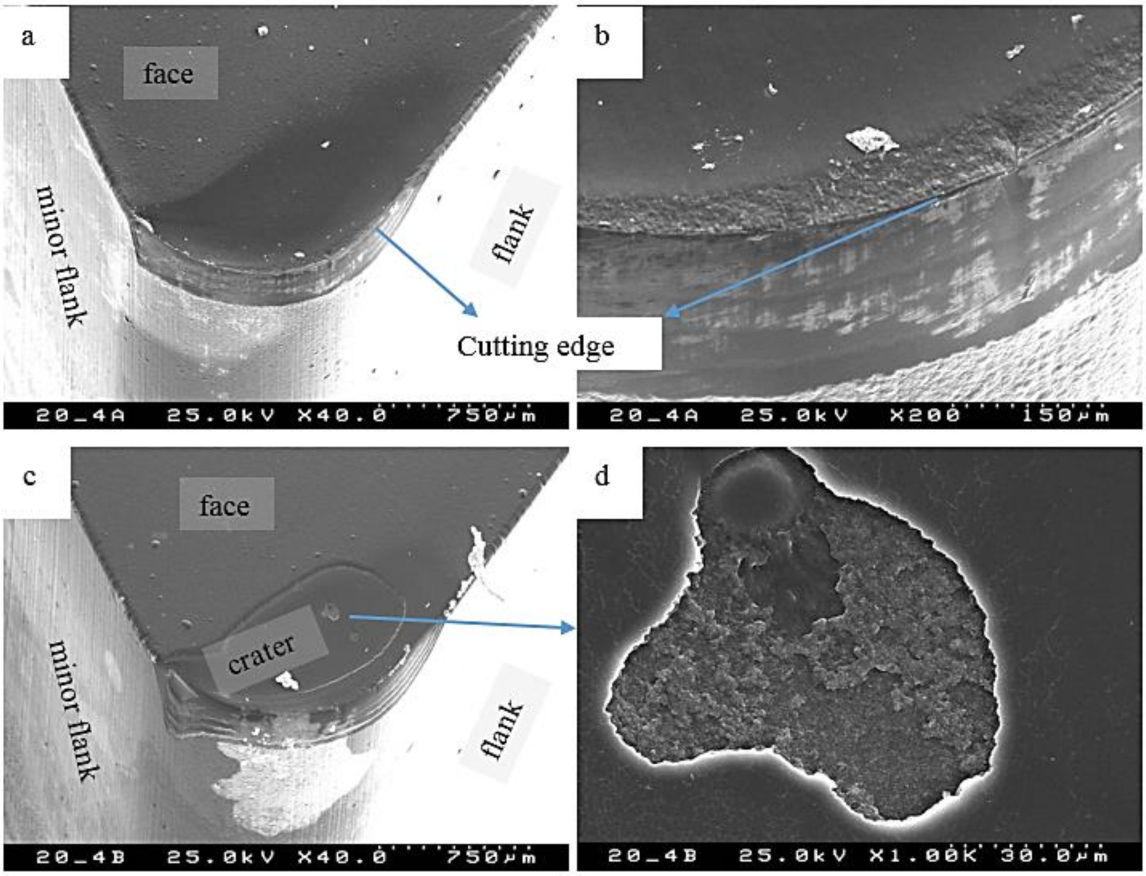

Figure 62. SEM micrographs of the ML10x2 cutting inserts after machining at $v = 500$ m.min^{-1}, DOC=1.0 mm, $f = 0.3$ mm.rev^{-1}: a, b) L = 1975 m (4 pass, dry); c, d) L = 1878 m (4 pass with lubrication).

The worn surfaces shown in the SEM micrographs of Figures 61 and 62 are very smooth, being polished by the action of the hard Al_2O_3 reinforcing particles of the MMC material. Wear should thus occur by a micro–scale abrasive wear mechanism. The microstructural observation in Figure 62c also shows that the notch formation occurs at the minor cutting edge and not only at the major cutting edge due to the –3° tool lead angle imposed by the tool holder.

Under non–fracture conditions, the tool life, as determined by a given width of the flank wear land (VB), is a function of the cutting conditions which conducts to highly disperse data. To make even more difficult a comparison between the results of different works, it is evident that the tool material, be it uncoated hardmetal, CBN, PCD, thick CVD or diamond coatings, strongly affects the outcome of tool life assessment. This approach also excludes all the tests where failure of the tool occurs by fracture of the cutting edge or, in the case of CVD diamond coatings, when there is delamination during the test. For the latter type of tool material, the maximum value of VB is limited by the thickness of the coating, for the cutting geometry used. In the case of the present work, the 6° tool normal clearance, –6° tool normal rake and a thickness of 24 µm for the multilayer diamond coating of the ML10x2 inserts, result in a VB maximum value of approximately 250 µm before the base material of the cutting edge is exposed, and this is an indication of the end of tool usefulness. Nevertheless, as was already seen, the exposure of the base material of the substrate is not by itself an indication of the end of the tool performance, since the diamond at the tool face keeps cutting even if the substrate is exposed. So, if no delamination or fracture of the cutting edge are observed, the usual standard tool life criterion of a fixed average VB value of 0.3 mm [162] is here used to compare literature and the present work data. As for the ML10x1 inserts, there was delamination for all tests, so they were excluded from this analysis, while for the ML10x2 inserts that did not delaminate, the VB values are below the threshold value for substrate exposure.

Qin et al. [59] tested NCD and MCD coatings on hardmetal substrates on the machining of a A359/SiC–20p composite at 240 m.min^{-1}, 480 m.min^{-1} with 0.15 and 0.30 mm.rev^{-1} at a fixed DOC value of 1.0 mm. The lifetime of the tools was much shorter than the values here reported as, unlike the results of the present work, the coating seemingly just delaminated after a certain amount of turning time without a gradual increase in VB. This was observed in other works [95] and for the ML10x1 inserts, showing that either the adhesion strength of the 25–30 µm thick CVD diamond coatings in those particular works is worse than that of the ML10x2 inserts or that the amount and nature of the reinforcing particles has to be taken into account. In fact it was found that higher amounts of reinforcing material are much more aggressive towards the inserts than lower fractions of hard particles [68]. In most of the works lubrication is used, although it was early reported that the main effects of its use are the reduction of the built–up–edge, without any significant change in the duration of the tool [163].

The data points in the chart of Figure 63 were collected from different works in the machining of MMCs at speeds around 500 m.min^{-1}, using PCD, CVD diamond coated tools and one with thick CVD diamond tip, and are compared with the wear behaviour of the surviving ML10x2 inserts used in the present work. Since the wear mode presented by all the tools shown in the graphic is gradual wear of the cutting edge and flank, the tool life is translated into the cutting length. This gives a more accurate view of the abrasive effects at the contact between tool and workpiece. Despite being at the lower end of the graph in Figure 63, the tendency shown by the inserts used in the present work is within that of the best CVD diamond coated tools tested, behaving better than most. PCD tools have dissimilar behaviour relatively to CVD tools as some excel while others are at the same level or behave worse than CVD coated ones.

In Figure 63, data taken from the work of Durante et al. [68] revealed the little influence of the nature of the abrasive particles on tool life (see points PCD [68] 20%A and PCD [68]

20%SiC), despite the fact that the hardness of SiC particles is about 1.7 times higher than that of Al_2O_3 [101]. The same authors showed that if MMCs contain higher fractions of filler particles (see points PCD [68] 10%A and PCD [68] 20%A), their abrasive effect is clear in the tool life of PCD inserts in the machining of Al–Al_2O_3 composites [68].

Very important is also the fact that the inserts have three usable cutting tips per deposition, while PCD tools have a single block brazed to one tip. So, the useful tool life of the ML10x2 triangular CVD diamond coated inserts will be three times the values recorded for a single cutting tip. The dotted line in Figure 63 corresponds to the extrapolation of the results of the present work to larger values of VB. They could be achieved if thicker coatings were used, e.g. a 38 µm thick coating would yield a maximum VB of 0.4 mm without substrate exposure. This places the tool life of the presently used inserts in the range of 6000 m per corner and thus of about 18000 m per insert. As a concluding remark, the present system, under correct machining conditions, performs as well or better than most of the systems using CVD diamond coatings and is as good as most PCD tools analysed by different authors.

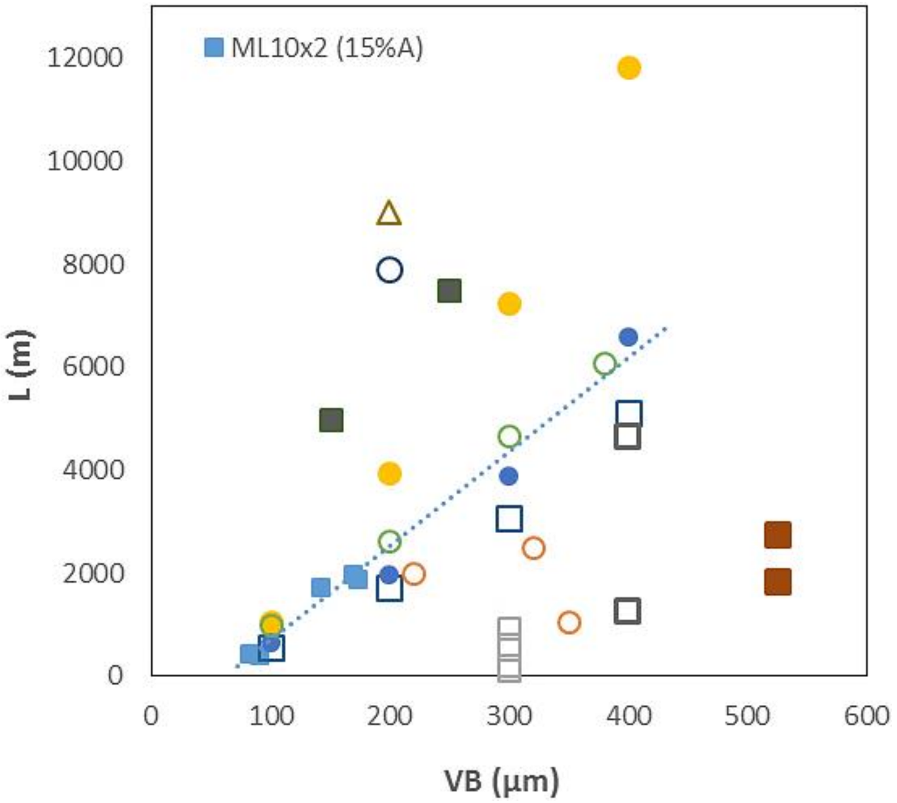

Figure 63. Tool machining length given as a function of flank wear of diamond tools (squares for CVD coated inserts, circles for PCD inserts and triangle for brazed thick CVD; filled symbols– workpiece material contains Al_2O_3; open symbols– reinforcing particles are SiC; dotted line corresponds to an extrapolation of ML10x2 results (filled blue squares). ■ – CVD/10%Al_2O_3 [98] ; ■ – CVD/10%Al_2O_3 [67]; □ – CVD/20%SiC [59]; □ – CVD/20%SiC [68]; □ – CVD/20%SiC [67]; ● – PCD/10%Al_2O_3 [68] ;● – PCD/20% Al_2O_3 [68]; ○ – PCD/20%SiC [68]; ○ – PCD/20%SiC [67]; △ – Thick CVD/20%SiC [67].

5.2. Multilayered diamond coated rings for self–mated mechanical seals

5.2.1. Characterization of pristine surfaces of SL and ML coated seal rings

Figure 64 shows SEM micrographs of diamond coated upper and lower Si_3N_4 mechanical seal rings: (a), (b) monolayer MCD (SL type) and (c), (d) multilayer MCD/NCD (ML type).

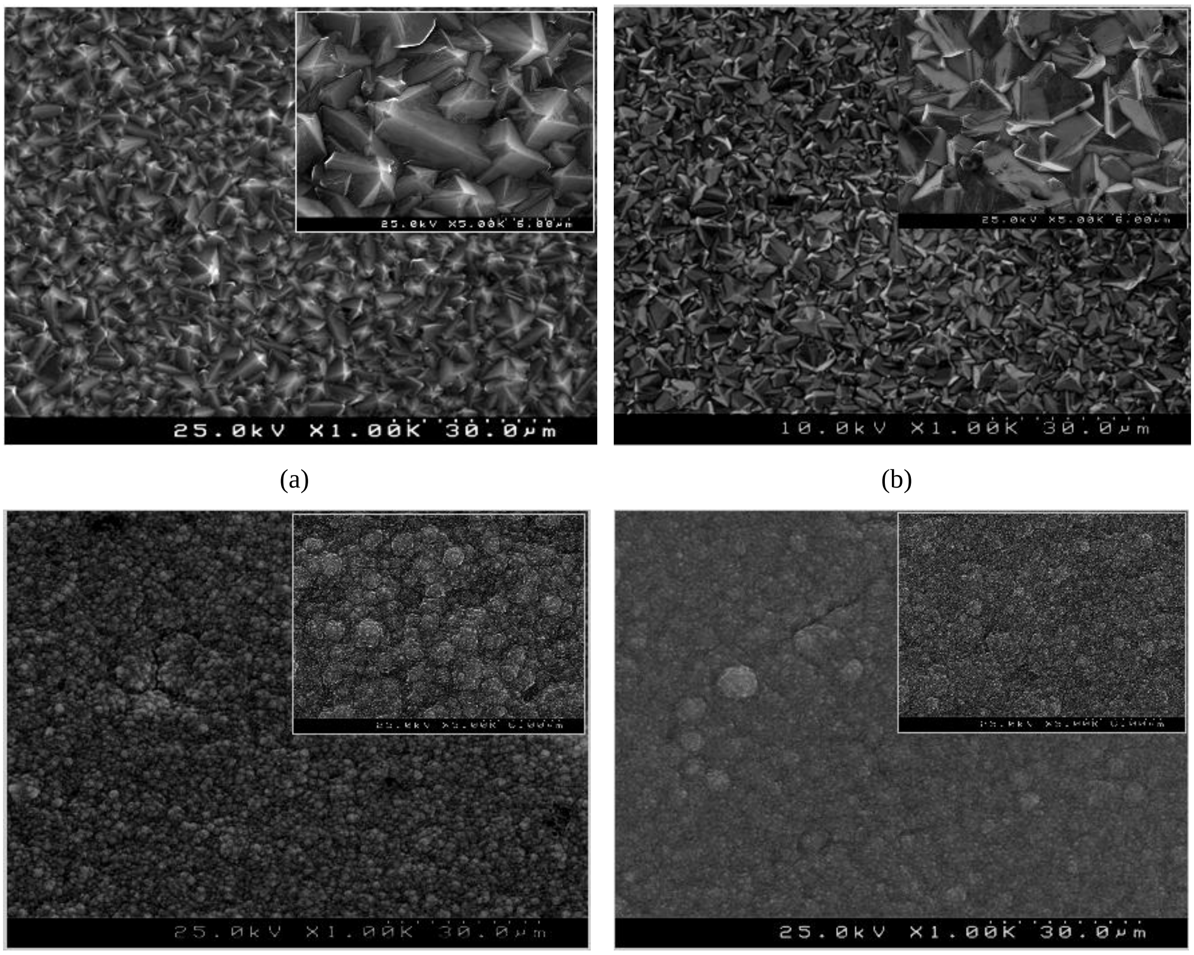

(a) (b)

(c) (d)

Figure 64. SEM micrographs of diamond coated upper (a,c) and lower (c,d) Si_3N_4 mechanical seal rings: (a), (b) SL type and (c), (d) ML type.

The MCD (SL) coating is coarse–grained, having pyramid–like shape diamond crystals, contrarily to the multilayer (ML) coated seal rings that have a top layer of NCD. Tables 18 and 19 contain the mean surface roughness (S_a), and root mean square surface roughness (S_q), respectively, of all the tested seal rings measured using 3D optical profilometry.

Table 18. Mean surface roughness, S_a (nm), for monolayer MCD (SL rings) and multilayer MCD/NCD (ML rings) seal rings measured in different regions of the surfaces.

Seal ring	External edge	Center	Internal edge	Center
SL1–U	535	187	455	
SL1–L				231
SL2–U	481	305	382	
SL2–L				206
ML1–U	261	132	196	
ML1–L				99
ML2–U	198	144	126	
ML2–L				115

U: upper (dynamic) ring & L: lower (static) ring
SL1 and SL2 pairs: Monolayer microcrystalline diamond (MCD) coating
ML1 and ML2 pairs: Multilayer micro/nanocrystalline diamond (MCD/NCD) coating

Table 19. Root mean square roughness, S_q (nm), for monolayer MCD (SL rings) and multilayer MCD/NCD (ML rings) seal rings measured in different regions of the surfaces.

Seal ring	External edge	Center	Internal edge	Center
SL1–U	682	247	575	
SL1–L				308
SL2–U	659	428	519	
SL2–L				270
ML1–U	416	199	333	
ML1–L				124
ML2–U	285	201	176	
ML2–L				150

U: upper (dynamic) ring & L: lower (static) ring
SL1 and SL2 pairs: Monolayer microcrystalline diamond (MCD) coating
ML1 and ML2 pairs: Multilayer micro/nanocrystalline diamond (MCD/NCD) coating

As given in these tables, MCD coatings have, as expected, higher surface roughness than the multilayered coatings. In the larger, upper, MCD coated seal rings there is some lack of uniformity between the borders and the center of the surface due to most likely to the edge effect during CVD that results in larger growth rates in those regions [87]. In the case of the smoother NCD top coating this effect is much reduced.

5.2.2. Tribological behaviour of diamond coated mechanical seal rings under biodiesel lubrication

Table 20 contains the maximum and steady state values of the friction coefficient measured under increasing P.V values in the runs of SL1 seal rings tested under biodiesel lubrication. Both the COF maximum and the COF steady state values are independent of the

P.V values and no modification of the sliding behaviour was observed until the end of the entire set of tests identified in Table 5 where a cumulative running distance of 152.2 km was reached. However, and despite the small COF values, it must be stressed that each individual run had to be stopped due to the increase of the biodiesel temperature. This occurred because the tests were done under biodiesel lubrication, at ambient pressure, without cooling of the test fluid, contrarily to real operating conditions, where the fluid is continuously renewed.

Table 20. Values of maximum and steady state friction coefficients obtained at increasing P.V product for SL1 seal rings under biodiesel lubrication.

P.V (MPa.ms^{-1})	COF (Max)	COF (Steady)
0.12	0.20	0.08
0.20	0.14	0.07
0.28	0.07	0.06
0.36	0.13	0.07
0.44	0.19	0.08
0.52	0.19	0.07
0.60	0.19	0.07
0.68	0.07	0.07
0.72	0.14	0.07

Figures 65(a) and (b) show representative coefficient of friction evolution versus distance for the above tests of the SL1 pair. The curves illustrate that there is an initial maximum peak, followed by a running in region (clearly observed in Figure 65b) and steady–state regions, similarly to what was described for the reciprocating testing with much smaller samples with the same type of MCD coating in Chapter 4 (Figure 55).

In the longer single run test performed with the SL2 pair (Table 7) under intermediate conditions of P.V = 0.30 MPa.ms^{-1}, the values of the COF measured are the same as for the consecutive tests with the SL1 pair. Figure 65(c) shows the evolution of COF in the first 4 km of this long test under biodiesel lubrication.

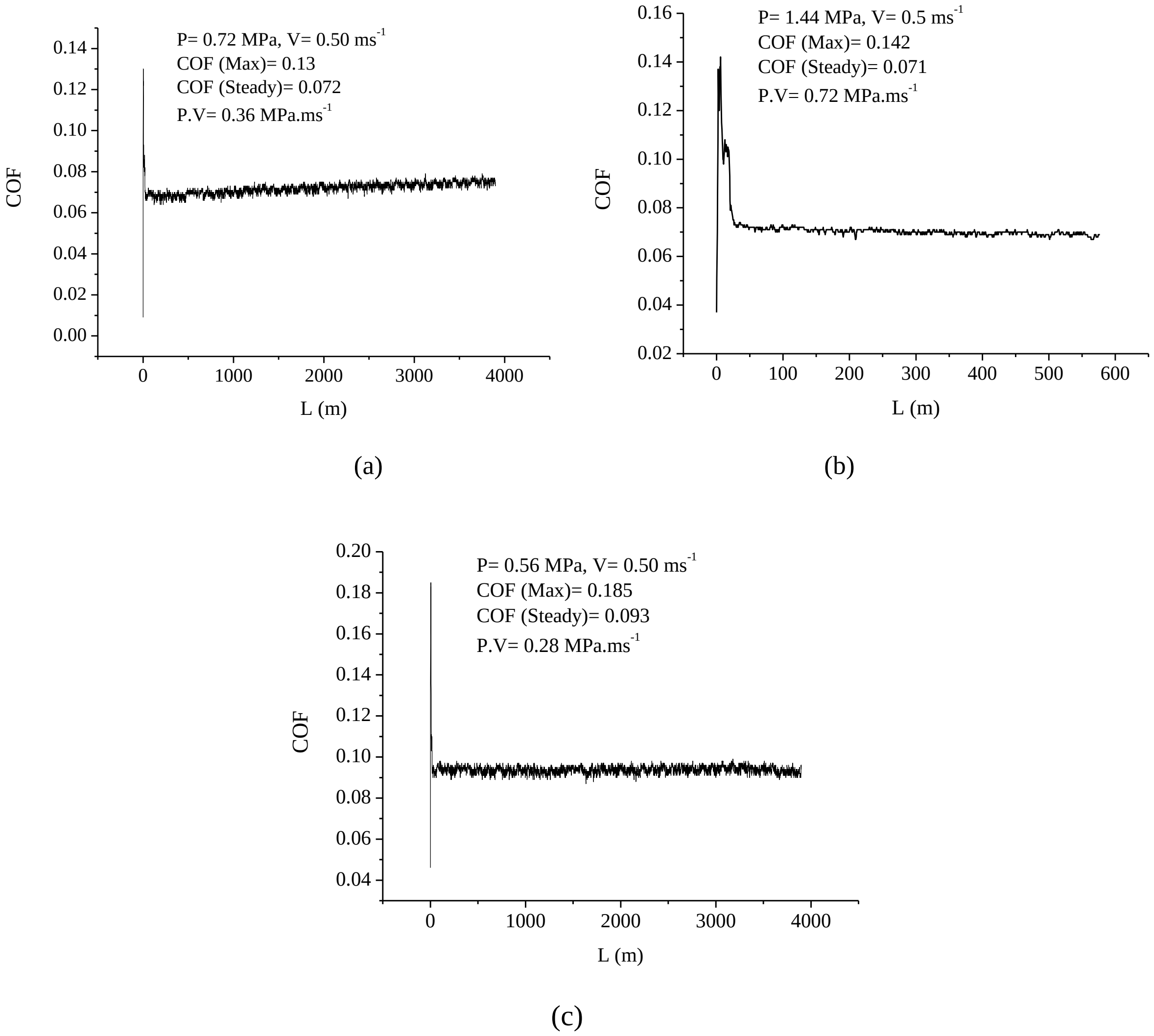

Figure 65. Coefficient of friction (COF) evolution versus working distance (L) for monolayer microcrystalline diamond–coated Si_3N_4 seal ring face under biodiesel lubrication. (a) short and b) long runs under different P.V conditions; c) long run.

For the multilayered MCD/NCD coated seal pair ML1 numerous runs were performed (Table 6) that showed average steady state COF of ~ 0.12, a value slightly higher than the ones measured for the SL1 and SL2 seal ring pairs. As discussed in Chapter 4 with respect to Figure 55, this higher COF(Steady) is probably due to the lower ability of the NCD top surface to retain the lubricant, unlike SL where it may remain in the valleys between the polished microcrystalline diamond grains. Figure 66 shows a typical friction coefficient curve for the first 4 km of a run. Again, in the complete set of runs up to a cumulative running distance of 394 km (Table 6) some heating of the fluid was detected (~50°C) preventing further increases in the P.V, either by increasing the speed or the load.

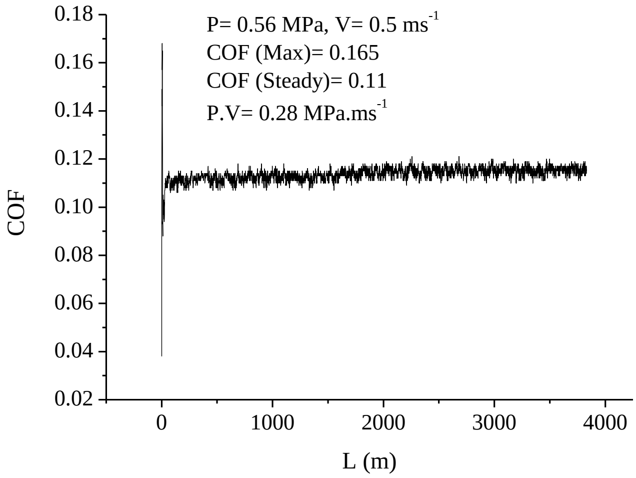

Figure 66. Coefficient of friction (COF) evolution versus distance (L) for a multilayer micro/nanocrystalline diamond coated Si_3N_4 seal face under biodiesel lubrication.

Figure 67 illustrates the surface topography of the worn SL1–L and SL1–U rings, before and after the complete set of runs (152.2 km) under biodiesel lubrication.

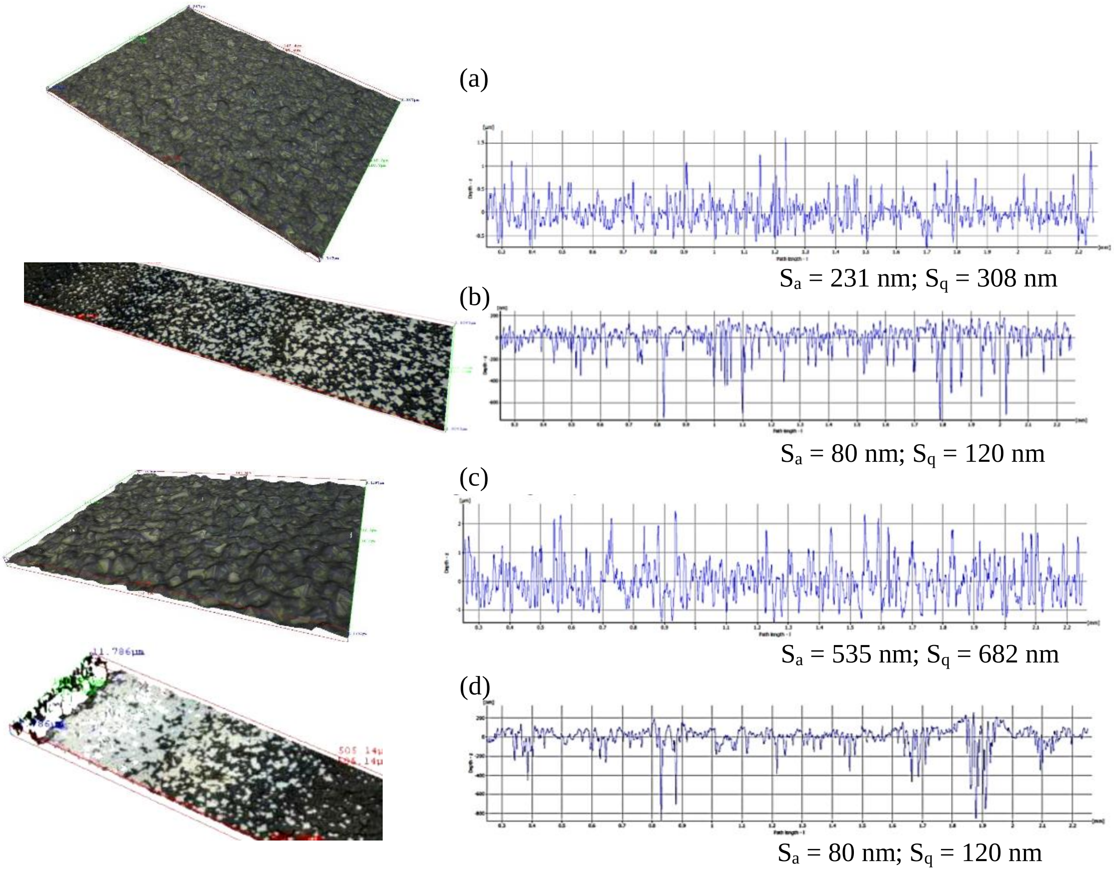

Figure 67. Optical profilometer images and surface roughness parameters of SL1–L and SL1–U seal rings: a) center of pristine surface of SL1–L; b) worn surface of SL1–L; c) outer edge of pristine SL1–U ring; d) worn surface of SL1–U ring.

As shown in Figure 67, after ring–on–ring testing, the surface roughness values of the dynamic and static seal rings decrease in the worn areas (bright contrast zones), but are still somewhat high when compared to a fully polished surface. The main wear mechanism is abrasion between the rough microcrystalline diamond surfaces (Figure 67(a) and (c)), which starts with the truncation of the pyramid–shaped diamond crystals and continues with the flattening [113–117], resulting in the bright contrast areas in the profilometer images of Figure 67(b) and 67(d). Interestingly, the final S_q roughness parameter matches that of the reciprocating test, $R_q = 130$ nm (Chapter 4, Figure 53). Despite the much longer sliding distance of the ring–on–ring tests, the resulting surface condition is similar to that of the reciprocating tests, due to the much lower contact pressures when comparing to the large Hertzian stresses of the latter.

Figure 68 illustrates the surface topography and surface roughness of the ML1, multilayer coated MCD/NCD mechanical seal ring pair after the complete set of tests under biodiesel lubrication. Regarding the reduction of the surface roughness of the worn surface, this system has a similar behaviour, with a large reduction of S_q down to values equivalent to those of polished surfaces (below 50 nm). This condition is a result of the smaller starting surface roughness when comparing to SL rings and to the longer sliding distances that reached 394 km in this ML1 system. Again, as for the SL rings, the final S_q roughness parameter matches that of the reciprocating test, $R_q = 17$ nm (Chapter 4, Figure 53).

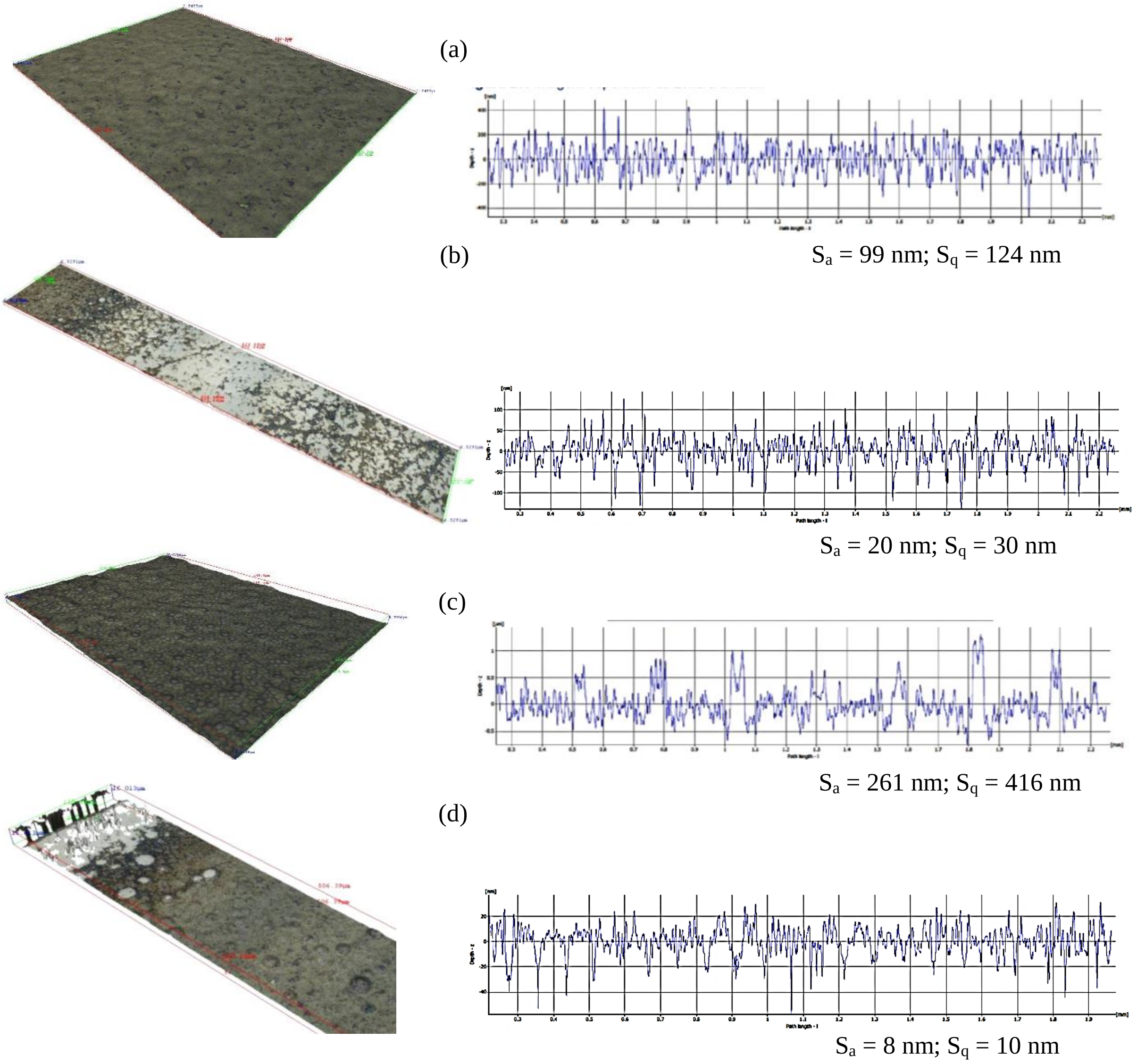

(a)

S_a = 99 nm; S_q = 124 nm

(b)

S_a = 20 nm; S_q = 30 nm

(c)

S_a = 261 nm; S_q = 416 nm

(d)

S_a = 8 nm; S_q = 10 nm

Figure 68. Optical profilometer images and surface roughness parameters of ML1–L and ML1–U seal rings: a) center of pristine surface of ML1–L; b) worn surface of ML1–L; c) outer edge of pristine ML1–U ring; d) worn surface of ML1–U ring.

SEM was also used to characterize the morphology of the above seal ring pairs after sealing tests, as shown in Figure 69, for a more detailed characterization. Comparing to the corresponding pristine surfaces in Figure 64, the ML rings (Figures 69(c,d)) are almost fully polished inside the wear tracks while the SL rings still show plateau/valley morphology, characteristic of MCD abraded surfaces.

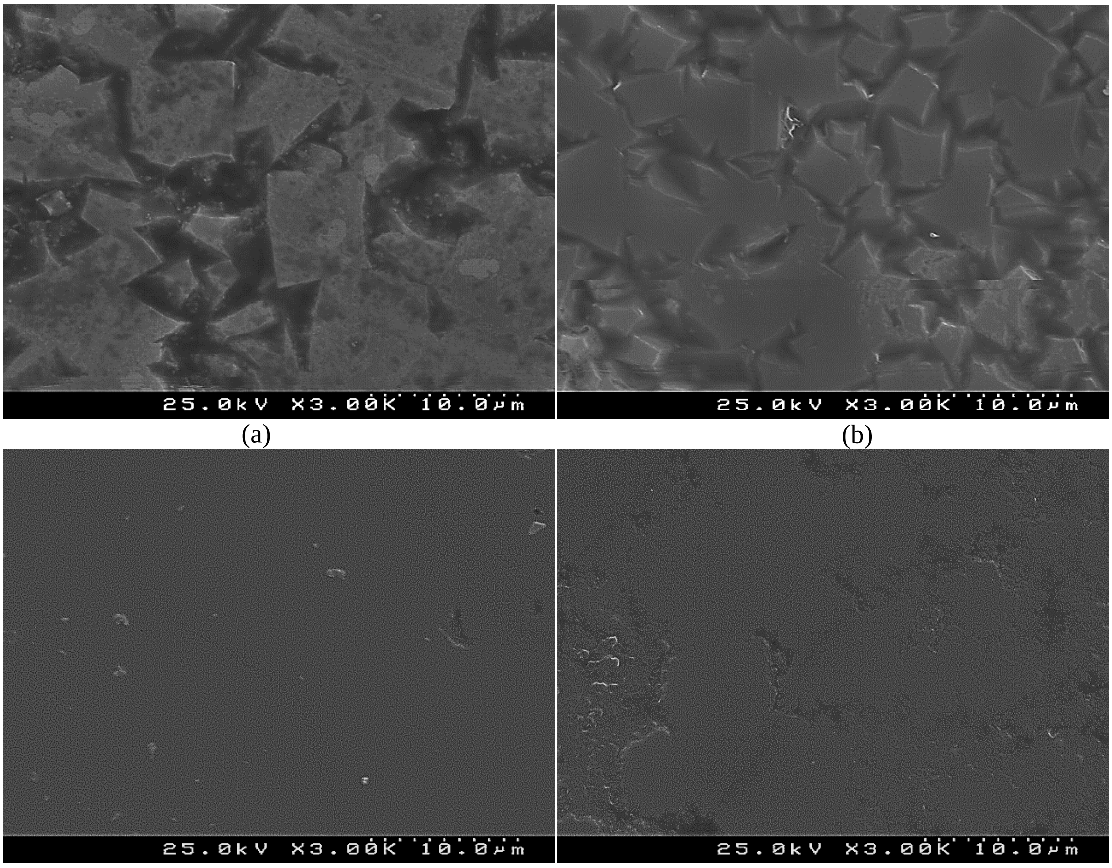

(a) (b)

(c) (d)

Figure 69. SEM micrographs of the worn diamond coated mechanical seal rings: (a) SL1–U; (b) SL1–L; (c) ML1–U; (d) ML1–L.

.

5.2.3. Sealing performance of diamond coated mechanical seal rings in water–lubricated conditions

Ring–on–ring tests were performed in pressurized water lubrication (2 bars) to find the sealing performance of the SL microcrystalline diamond (MCD) and ML micro/nanocrystalline diamond (MCD/NCD) coated Si_3N_4 mechanical seal rings. In a first set of experiments with the objective of determining the P.V sealing conditions, the angular speed was kept constant at 250 rpm (V= 0.50 ms^{-1}) and increasing effective pressures were assessed, Tables 7 and 8 (Chapter 2). For the SL pair of seal rings, the P.V value for sealing is P.V= 0.80 $MPa.ms^{-1}$ while for the ML pair, the value is slightly lower, P.V= 0.72 $MPa.ms^{-1}$. The evolution of the friction coefficient of runs performed under these sealing conditions is presented in Figures 70(a) and 70(b) for the SL and ML pairs of rings, respectively. The steady state COF values in both tribosystems are similar but are half those reached under biodiesel lubrication, as depicted in Figures 65 and 66.

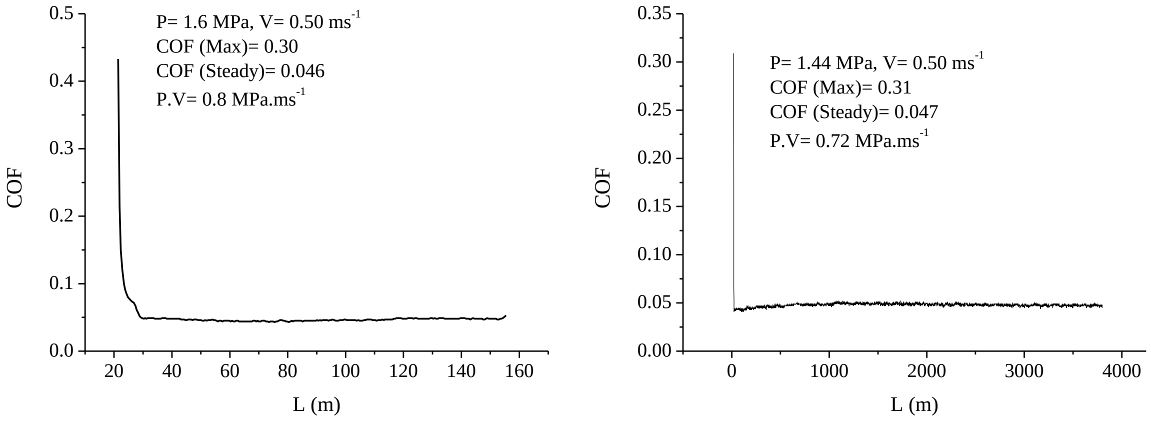

(a) (b)

Figure 70. Coefficient of friction (COF) evolution versus distance (L) at P.V sealing conditions of pressurized water using: a) self–mated single layer MCD (SL); b) self–mated multi–layered (ML) seal rings.

In addition, sealing tests were performed at the linear velocity of V= 3.9 ms^{-1} (ω= 2000 rpm) in pressurized water (2 bars) to find the maximum P.V condition of the ML seal rings as described in Table 10 (Chapter 2). The maximum P.V= 5.3 MPa.ms^{-1} was achieved at P= 1.36 MPa (F= 850 N). The tribological performance of the ML system at this linear velocity, namely the evolution of the COF up to the P.V limit, Figure 71(a), is similar to that observed at V = 0.50 ms^{-1} (Figure 70(b)). At the P.V limit, the coefficient of friction starts to show instability of the steady–state regime and increases to values higher than those of the P.V sealing conditions, Figure 71(b). Moreover, slight vibration on the sealing system took place. The continuation of the sealing test in this situation can lead to the delamination and spalling–off the diamond coating. The breakdown of the diamond coating in these conditions is attributed to the seizure mechanism of the diamond–coated seal faces [114,116,117]. Both the P.V sealing and the P.V limit conditions obtained in this work are very similar to the results of other studies with CVD diamond coated seal rings [113,114,164,165]. By contrast, bare Si_3N_4 self–mated systems could not provide efficient sealing of a mixture of 20 vol.% of hydrogen peroxide in deionised water, in PV conditions varying between 0.8 and 5.2 MPa.ms^{-1} [108].

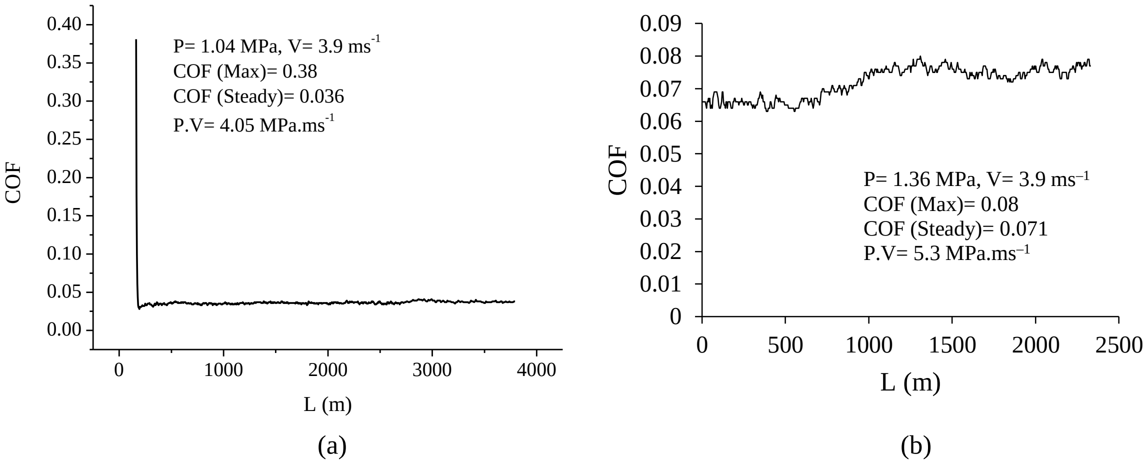

Figure 71. Coefficient of friction (COF) evolution versus distance (L) for MCD/NCD coated ML seal rings in pressurized water: a) below the P.V limit condition; b) at the P.V limit condition.

5.2.4. Evaluation of the wear coefficients by confocal optical profilometry

The quantification of the wear coefficient of diamond coated seal rings is seldom done due to the limitations of conventional techniques (weighing, AFM) for evaluating the very low wear rates of this type of tribological system and of large dimension specimens. With the capability of the 3D optical profilometer of high vertical resolution (down to 3 nm in confocal mode), this is now a feasible high precision task.

Figures 72 to 74 present 3D surface images obtained by optical profilometry in confocal mode, together with an example of a topographic profile across the wear tracks. The comparison of the wear tracks under biodiesel lubrication shows that the lower MCD coated ring (SL1–L, Figure 72) depicts a narrower and deeper profile that the multi–layered MCD/NCD lower ring (ML1–L, Figure 73). This is due to the more pronounced edge effect in the counterface upper ring characteristic of microcrystalline diamond growth, as already discussed concerning Tables 18 and 19. It must be pointed out that the depth of the wear tracks did not surpass 1.5 µm even in the system where the highest wear was observed (ML2–L, Figure 74).

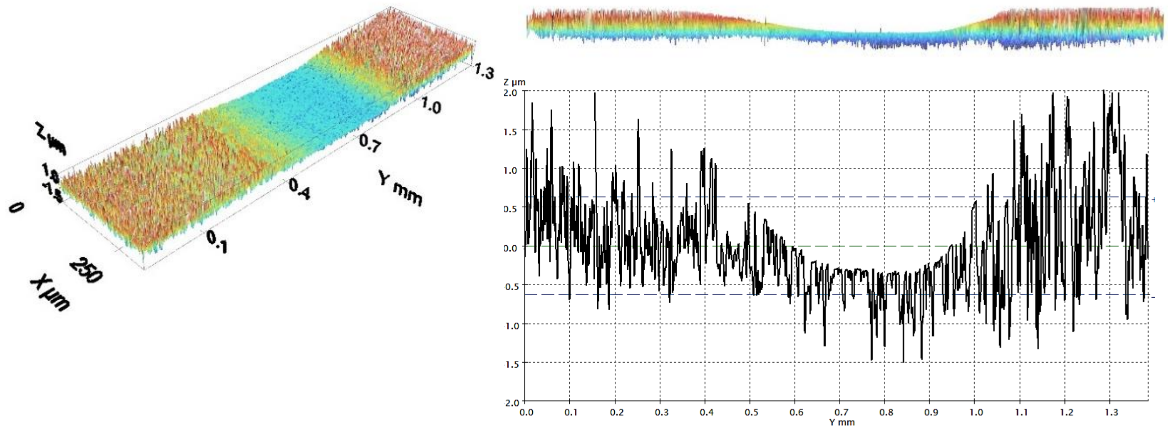

Figure 72. 3D image and topographic profile of the wear track of the ring SL1–L after testing under biodiesel lubrication.

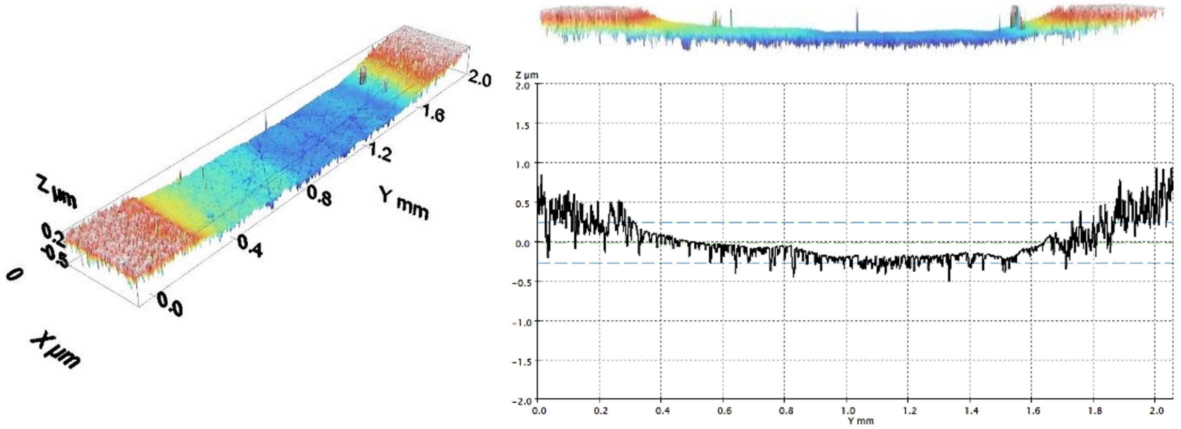

Figure 73. 3D image and topographic profile of the wear track of the ring ML1–L after testing under biodiesel lubrication.

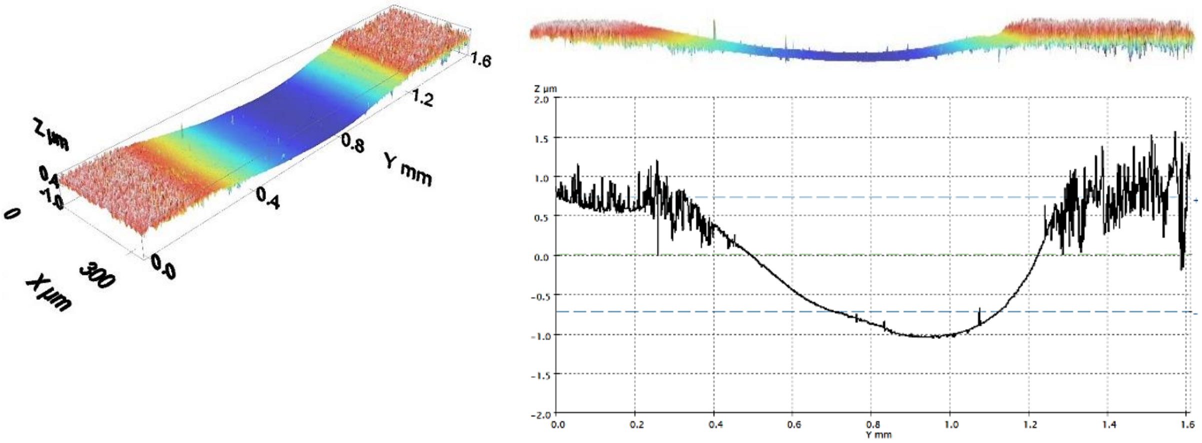

Figure 74. 3D image and topographic profile of the wear track of the ring ML2–L after sealing test of pressurized water.

The wear coefficient values of these lower, static, rings were obtained by taking four 3D images for each circular wear track at angle shifts of 90°. The total wear volume (mm^3) is obtained by multiplying the perimeter (mm) of the circular wear track by the average value of the projected cross section worn areas (mm^2). Finally, this volume was divided by the total sum of F.L products from all the runs of each condition as given in Table 5 (ML1–L), Table 6 (SL1–L) and Table 10 (SL2–L). The calculated wear coefficient values are given in Table 21, revealing that there are no significant differences between the behaviour of either the coatings or the tested fluids. It is worth noting that this calculation is done here for the first time in diamond coated mechanical seal rings.

Table 21. Wear coefficient values of the lower rings tested in different conditions

Coating	Fluid	k ($mm^3N^{-1}m^{-1}$)
Single layer (SL) MCD coating	Biodiesel lubrication	5.5×10^{-10}
Multilayered (ML) MCD/NCD coating	Biodiesel lubrication	4.1×10^{-10}
Multilayered (ML) MCD/NCD coating	Water sealing	6.0×10^{-10}

Comparing to the values obtained for biodiesel lubrication in reciprocating sliding ball–on–flat experiments in Section 4.3 ($k = 1.5 \times 10^{-7}$ $mm^3N^{-1}m^{-1}$ for SL and $k = 5 \times 10^{-8}$ $mm^3N^{-1}m^{-1}$ for ML), the seal rings present much lower wear rates, by about two to three orders of magnitude. Also, the k value estimate in water sealing is two orders of magnitude lower than the values found in the literature for ball–on–flat reciprocating experiments [42,43]. This can be explained by the huge difference between the linear test speeds (V) and contact pressures:

i) speeds are in the 0.5–3.9 ms^{-1} range (Tables 6 to 10, Chapter 2) in the seal ring characterization while for the reciprocating tests they are in the 12–16 $mm.s^{-1}$ range (Chapter 2);

ii) contact pressures (P) fall in the range 0.24–1.60 MPa (Tables 6 to 10, Chapter 2) while the apparent contact pressures in the reciprocating tests go from the initial Hertzian contact stress values (3–5.8 GPa range, Chapter 4) down to 200–1200 MPa, when considering the final diameter of the wear scars of the balls.

In the ring–on–ring tests, the combined effect of a much larger speed with a lower contact pressure, translates into a V/P ratio of the Stribeck parameter that is at least five orders of magnitude higher than that of the reciprocating ball–on–flat tests. As a consequence, during the operation of the mechanical seal rings system, lubrication is effective for preserving the internal part of the rings while in the ball–on–flat contact, boundary lubrication or even no lubrication conditions are established, increasing the wear coefficient.

Chapter 6

Conclusions and future work

This chapter introduces the main conclusions of the PhD study. Suggestions for future work are also here presented.

The present PhD study dealt with the development and applications of tribosystems based on multilayered micro/nanocrystalline diamond (MCD/NCD) coatings grown on silicon nitride (Si_3N_4) ceramic substrates using the hot–filament CVD deposition technique. Several geometries for distinct applications were coated: discs and balls for tribological lab–scale testing, mechanical seal rings and cutting inserts for in–service testing. The conclusions of the present PhD study can be grouped in six main categories:

1. The semi–industrial hot–filament CVD reactor used in this work allowed full diamond coating of silicon nitride ceramic samples and tools having different geometries and sizes. Tenfold multilayered diamond coatings were achieved by the deposition of alternate rough microcrystalline diamond and smooth fine–grained diamond layers, allowing simultaneously a smoother surface and an enhancement of the adhesion strength. The multilayered strategy allows a reduction of the RMS to one third relatively to that of MCD single layer coatings, while the threshold delamination load increases from 600 N and 800 N for the single layer NCD and MCD coatings, respectively, to 900 N.

2. At room temperature, in the 10–90% relative humidity (RH) range there is no clear trend for the evolution of both the static friction coefficient and the steady–state friction coefficient, which show average values of $\bar{\mu}_{\mathrm{Max}} = 0.32$ and $\bar{\mu}_{\mathrm{Steady}} = 0.09$, respectively. The intrinsic roughness of the pristine diamond surfaces explains the starting friction peaks.

Regarding the wear coefficient of the discs, a valley–shaped evolution is observed within the 10% to 90% RH range, with a minimum of about 1.7×10^{-7} $mm^3N^{-1}m^{-1}$. The increment of the wear coefficient for high RH can be attributed to fatigue enhancement by the increased critical loads, while the absence of adsorbed water, and thus reduced lubrication, at low RH accounts for the high k values. Gradual truncation and smoothening of the nanocrystalline ballas–shaped diamond top layer is observed. Wear progresses by second–body and third–body action, inducing a fine scale self–polishing wear mechanism. The balls have consistently lower values of k than the discs, this being normally attributed to fatigue effects on the plate that is submitted to loading–unloading cycles, contrarily to the continuously loading on the ball. The wear coefficients of the discs and balls are in the vicinity of ~ 10^{-7} $mm^3N^{-1}m^{-1}$ indicative of a mild wear regime while the balls are in the mild to very mild wear regime, with some values entering the ~ 10^{-8} $mm^3N^{-1}m^{-1}$ range.

Interestingly, the most net effect of humidity was found on the value of the critical load (i.e. the load above which there is detachment of the diamond coating) that triples from 40 N at 10% RH to 120 N at 90% RH. The formation of a water layer between the two surfaces induces a load bearing effect by extending the contact area during the sliding.

When studying the effect of temperature in the range 50–250°C, a higher average value of $\overline{\mu}_{\text{Max}}$ = 0.64 is observed, probably due to the dryer environment and thus to the reduced lubricious effect of humidity between the sliding surfaces. Regarding the wear coefficient (k) values in the range 50–100ºC the k_{Disc} are around $2\text{x}10^{-7}$ $\text{mm}^3\text{N}^{-1}\text{m}^{-1}$ while k_{Ball} are about half that value.

The clearest difference between the RH and temperature experiments is observed for the critical loads. The values achieved in the tests with temperature are limited to the range 40–55 N, while at room temperature a value of 120 N was reached. However, the critical loads at high temperature are similar to those attained under dry conditions (≤ 25% RH) highlighting the absence of water as the load bearing medium. Regarding the sliding wear tests performed in circular configuration at 150°C–250°C, delamination occurred in all the tested tribopairs at minimum loads of 40 N.

3. The substitution of conventional steel materials used in biodiesel lubricated systems, namely the injection pumps and seals of internal combustion engines, by CVD diamond coated materials offers two main advantages: (i) lower friction coefficient values of 0.07 as the minimum, instead of those observed for steels, higher than 0.10; and (ii) the very mild wear regime ($k \sim 10^{-8}$ $\text{mm}^3\text{N}^{-1}\text{m}^{-1}$) observed in lubricated sliding is similar to that observed in dry tests, thus protecting the system even when running in lubricant starved condition, which is not the case of steels.

Among the tested diamond coating types, the single layer MCD and the multilayered, the former tribopair presents a higher initial friction coefficient peak (0.30 to 0.35 with MCD against 0.15 with multilayered) due to the intrinsic higher surface roughness of MCD. However, once running–in is attained, the MCD leads to an optimal friction performance with its surface presenting plateaus and valleys capable to interact positively with the lubricant. A pre–polishing would reduce dramatically both k and initial friction coefficient.

Although the Si_3N_4 material used as the substrate for the diamond coatings also demonstrates better tribological performance than steel at the tested condition, this ceramic shows an adverse load effect affecting both friction and wear, not seen in the tests with the CVD diamond coated samples. More than that, the bare Si_3N_4 material could not satisfactorily operate in the absence of lubrication.

4. Turning of an Al–based metal matrix composite (Al–MMC) containing 15 vol.% Al_2O_3 particles, was achieved with Si_3N_4 inserts coated with tenfold multilayered CVD diamond films. The measured cutting forces match closely those reported in the literature. This behaviour was observed independently of the type of geometry, tool type, lubrication or even workpiece material, being mostly dependent on the turning conditions, increasing linearly with feed (~ 640 N per mm.rev^{-1} of feed). The main cutting force increases with depth of cut (DOC) at a rate of 294 N per mm of DOC.

Inserts with the thinner 12 µm thick multilayer diamond coating did not withstand the usual turning conditions of MMCs, always failing by fracture of the cutting tip following early delamination of the diamond film. The thicker coating (21–24 µm thick) performs well within the following limits: DOC values below 1.5 mm for feeds of 0.4 mm.rev^{-1}; maximum speeds of 750 m.min^{-1}; and feeds up to 0.4 mm.rev^{-1}.

For delamination–free turning conditions, the wear of the flank and corner occurs progressively, with the worn surfaces having a smooth appearance, typical of a micro–scale abrasive wear mechanism. Crater wear is also present, due to the negative tool normal rake, and for the longer machining tests, some surface cracks may appear. Crater wear occurs by successive wear of the layers, delaying total delamination of the diamond coating from the substrate, unlike what would happen with monolayer coatings.

The tool life of the 24 µm multilayer MCD/NCD film was compared with a wide set of literature data on turning of MMCs with different nature of reinforcing particles (SiC and Al_2O_3) and different amounts (10, 15 and 20 vol.%). Within the limits of the working parameters, the multilayer diamond coated inserts behave better than most reported CVD diamond systems and as well as most reports using PCD tools, especially when considering the existence of three tips per tool, as opposed to one for PCD.

5. For multilayered MCD/NCD coated mechanical seal rings tested under biodiesel lubrication $\overline{\mu}_{\mathrm{Steady}}$~ 0.12, a value slightly higher than the ones measured for the MCD seal ring pairs. This is probably due to the lower ability of the NCD top surface to retain the lubricant, unlike in MCD where it may remain in the valleys between the polished microcrystalline diamond grains, as was observed in the ball on disc reciprocating tests. For both types of coatings, each individual run of the total sliding distance had to be stopped due to the increase of the biodiesel temperature to values above 50°C.

In the multilayered system the surface roughness endures a larger reduction of S_q to values equivalent to those of polished surfaces (below 10–30 nm). The resulting surface condition of the ring–on–ring tests is similar to that of the reciprocating tests due to the much lower contact pressures when comparing to the large Hertzian stresses of the latter. The seal rings present wear rates ($4.1x10^{-10}$ $mm^3N^{-1}m^{-1}$) that are lower by two orders of magnitude when comparing to the values obtained in reciprocating sliding ball–on–flat experiments also under biodiesel lubrication ($k = 5 \times 10^{-8}$ $mm^3N^{-1}m^{-1}$).

6. The minimum full sealing P.V conditions of MCD single layer and multilayered diamond–coated Si_3N_4 seal rings of water pressurized at 2 bar are P.V= 0.80 $MPa.ms^{-1}$ and P.V= 0.72 $MPa.ms^{-1}$, respectively. The maximum P.V condition (5.3 $MPa.ms^{-1}$) before seizure of the multilayered CVD diamond coated seal rings was reached at a load of F= 850 N for a linear velocity of V= 3.9 ms^{-1}. These results demonstrate that the multilayered CVD diamond coatings strongly enhance the sealing performance relatively to the bare Si_3N_4 mechanical seal rings.

The k value estimated in water sealing ($6.0x10^{-10}$ $mm^3N^{-1}m^{-1}$) is two orders of magnitude lower than the values for ball–on–flat reciprocating experiments obtained under water lubrication. The combined effect of a much larger speed with a lower contact pressure, translates into a V/P ratio of the Stribeck parameter that is at least five orders of magnitude higher than that of the reciprocating ball–on–flat tests. Lubrication is thus effective, unlike in the ball–on–flat contacts where boundary lubrication or even no lubrication conditions are established.

For future work, the application of CVD multilayer micro/nanocrystallline diamond on the well–established hardmetal substrates, also considering modifications in the number and thickness of MCD and NCD layers. Machining processes such as drilling, milling and grinding of difficult–to–cut materials, like MMCs, Al–Si alloys, CFRP, GFRP, pre–sintered and sintered hardmetal, should also be exploited.

Concerning future evolutions in the seal rings, two issues should be addressed: i) minimizing the edge effect in the growth of CVD diamond; ii) develop texturing strategies in the seal ring face to ensure that there will always exist lubricant reservoirs.

References

[1] P.W. May, Diamond thin films: a 21st century material, Philosophical Transactions of the Royal Society of London, Series A: Mathematical, Physical and Engineering Sciences 358(1766) (2000) 473–495.

[2] S. Tong Lee, Z. Lin, X. Jiang, CVD diamond films: nucleation and growth, Materials Science and Engineering R: Reports 25(4) (1999) 123–154.

[3] A. Rizzo, M.A. Signore, D. Valerini, PVD protective multilayer coatings for tribological applications, EAI (Energia, Ambiente e Innovazione) 3 (2012) 102–108.

[4] G. Abadias, A. Michel, C. Tromas, C. Jaouen, S.N. Dub, Stress, interfacial effects and mechanical properties of nanoscale multilayered coatings, Surface and Coatings Technology 202 (2007) 844–853.

[5] B. Ramamoorthy, B.C. Yeldose, An investigation into the adhesion strength of diamond like carbon multilayer coating, Intelligent Information Management 1 (2009) 179–194.

[6] C. Donnet, A. Erdemir, Historical developments and new trends in tribological and solid lubricant coatings, Surface and Coatings Technology 180 (2004) 76–84.

[7] P.C. Yashar, W.D. Sproul, Nanometer scale multilayered hard coatings, Vacuum 55(3) (1999) 179–190.

[8] K.K. Shih, D.B. Dove, Ti/Ti–N Hf/Hf–N and W/W–N multilayer films with high mechanical hardness, Applied Physics Letters 61(6) (1992) 654–656.

[9] J.K. Park, Y.J. Baik, The crystalline structure, hardness and thermal stability of AlN/CrN superlattice coating prepared by DC magnetron sputtering, Surface and Coatings Technology 200(5) (2005) 1519–1523.

[10] K. Holmberg, H. Ronkainen, A. Matthews, Tribology of thin coatings, Ceramics International 26 (2000) 787–795.

[11] H. Holleck, V. Schier, Multilayer PVD coatings for wear protection, Surface and Coating Technology 76–77 (1995) 328–336.

[12] M. Vojs, M. Vesely, R. Redhammer, J. Janik, M. Kadlecikova, T. Danis, M. Marton, M. Michalka, P. Sutta, Double bias HF CVD multilayer diamond films on WC–Co cutting tools, Diamond and Related Materials 14 (2005) 613–616.

[13] P. Hess, The mechanical properties of various chemical vapor deposition diamond structures compared to the ideal single crystal, Journal of Applied Physics 111 (2012) 051101–15.

[14] S. Takeuchi, S. Oda, M. Murakawa, Synthesis of multilayer diamond film and evaluation of its mechanical properties, Thin Solid Films 398–399 (2001) 238–243.

[15] M. Kadlecikova, M. Vojs, J. Breza, M. Vesely, Z. Frgala, M. Michalka, J. Matejkova, A. Vojackova, T. Danis, M. Marton, Microwave and hot filament chemical vapour deposition of diamond multilayers on Si and WC–Co substrates, Microelectronics Journal 38 (2007) 20–23.

[16] H.J. Lee, H. Li, H. Jeon, W.S. Lee, Some novel aspects of nanocrystalline diamond nucleation and growth by direct current plasma assisted chemical vapor deposition, Diamond and Related Materials 19(11) (2010) 1393–1400.

[17] D. Zhou, D.M. Gruen, L.C. Qin, T.G. McCauley, A. R. Krauss, Control of diamond film microstructure by Ar additions to CH_4/H_2 microwave plasmas, Journal of Applied Physics 84(4) (1998) 1981–1989.

[18] A. Erdemir, G.R. Fenske, A.R. Krauss, D.M. Gruen, T. McCauley, R.T. Csencsits, Tribological properties of nanocrystalline diamond films, Surface and Coatings Technology 120–121 (1999) 565–572.

[19] A.R. Krauss, O. Auciello, D.M. Gruen, A. Jayatissa, A. Sumant, J. Tucek, D.C. Mancini, N. Moldovan, A. Erdemir, D. Ersoy, M.N. Gardos, H.G. Busmann, E.M. Meyer, M.Q. Ding, Ultrananocrystalline diamond thin films for MEMS and moving mechanical assembly devices, Diamond and Related Materials 10 (2001) 1952–1961.

[20] C.S. Abreu, M.S. Amaral, F.J. Oliveira, Tribological testing of self–mated nanocrystalline diamond coatings on Si_3N_4 ceramics, Journal of Surface and Coatings Technology 200(22–23) (2006) 6235–6239.

[21] X. Lu, Q. Yang, C. Xiao, Synthesis and field electron emission characteristics of diamond multilayer films grown by graphite etching, Journal of Physics D: Applied Physics 40 (2007) 4010–4014.

[22] J.L. Luo, X.T. Ying, P.N. Wang, L.Y. Chen, Growth and optical properties of nanocrystalline/microcrystalline diamond multilayer film, Journal of the Korean Physical Society 46 (2005) 224–228.

[23] C.S. Abreu, F.J. Oliveira, M. Belmonte, A.J.S. Fernandes, R.F. Silva, J.R. Gomes, Grain size effect on self–mated CVD diamond dry tribosystems, Wear 259 (2005) 771–778.

[24] M. Belmonte, A.J.S. Fernandes, F.M. Costa, F.J. Oliveira, R.F. Silva, Adhesion behaviour assessment on diamond coated silicon nitride by acoustic emission, Diamond and Related Materials 12 (2003) 733–737.

[25] F.A. Almeida, M. Amaral, F.J. Oliveira, A.J.S. Fernandes, R.F. Silva, Nano to micrometric HFCVD diamond adhesion strength to Si_3N_4, Vacuum 81 (2007) 1443–1447.

[26] A. R. Konicek, D. S. Grierson, A. V. Sumant, T. A. Friedmann, J. P. Sullivan, P.U.P.A. Gilbert, W. G. Sawyer, R. W. Carpick, Influence of surface passivation on the friction and wear behavior of ultrananocrystalline diamond and tetrahedral amorphous carbon thin films, Physical Review B 85 (2012) 155448.

[27] I.P. Heyward, I.L. Singer, L.E. Seitzman, Effect of roughness on the friction of diamond on CVD diamond coatings, Wear 157 (1992) 215–227.

[28] D. Rats, L. Vandenbulckea, C. Boherbx, G. Farges, Tribological study of diamond coatings on titanium alloys, Surface and Coatings Technology 91–95 (1997) 555–560.

[29] L. Vandenbulcke, M.I. De Barros, Deposition, structure, mechanical properties and tribological behavior of polycrystalline to smooth fine–grained diamond coatings, Surface and Coatings Technology 146 –147 (2001) 417–424.

[30] T. Grogler, A. Franz, D. Klaffke, S.M. Rosiwal, R.F. Singer, Tribological optimization of CVD diamond coated Ti–6Al–4V1, Diamond and Related Materials 7 (1998) 1342–1347.

[31] N. Sharma, N. Kumar, S. Dhara, S. Dash, Ashok Bahuguna, M. Kamruddin, A.K. Tyagi, B. Raj, Tribological properties of ultra nanocrystalline diamond film–effect of sliding counterbodies, Tribology International 53 (2012) 167–178.

[32] E. Zeiler, D. Klaffke, K. Hiltner, T. Grögler, S.M. Rosiwal, R.F. Singer, Tribological performance of mechanically lapped chemical vapor deposited diamond coatings, Surface and Coatings Technology 116–119 (1999) 599–608.

[33] K. Miyoshi, M. Murakawa, S. Watanabe, S. Takeuchi, R.L.C. Wu, Tribological characteristics and applications of superhard coatings: CVD diamond, DLC, and c–BN, NASA/TM–1999–209189 (1999) 1–6.

[34] S.E. Grillo, J.E. Field, The friction of natural and CVD diamond, Wear 254 (2003) 945–949.

[35] J.E. Field, C.S.J. Pickles, Strength, fracture and friction properties of diamond, Diamond and Related Materials 5 (1996) 625–634.

[36] S.E. Grillo, J.E. Field, The friction of CVD diamond at high Hertzian stresses: the effect of load, environment and sliding velocity, Journal of Physics D: Applied Physics 33 (2000) 595–602.

[37] S.E. Grillo, J.E. Field, High reduction of diamond friction by oxygen containing liquids, Diamond and Related Materials 9 (2000) 185–190.

[38] S.J. Bull, P.R. Chalker, C. Johnston, V. Moore, The effect of roughness on the friction and wear of diamond thin films, Surface and Coatings Technology 68–69 (1994) 603–610.

[39] X. Lei, B. Shen, S. Chen, L. Wang, F. Sun, Tribological behaviour between micro– and nano–crystalline diamond films under dry sliding and water lubrication, Tribology International 69 (2014) 118–127.

[40] C.S. Abreu, M. Amaral, A.J.S. Fernandes, F.J. Oliveira, R.F. Silva, J.R. Gomes, Friction and wear performance of HFCVD nanocrystalline diamond coated silicon nitride ceramics, Diamond and Related Materials 15 (2006) 739–744.

[41] C.S. Abreu, M. Amaral, F.J. Oliveira, A.J.S. Fernandes, J.R. Gomes, R.F. Silva, Enhanced performance of HFCVD nanocrystalline diamond self–mated tribosystems by plasma pretreatments on silicon nitride substrates, Diamond & Related Materials 15 (2006) 2024–2028.

[42] C.S. Abreu, E. Salgueiredo, F.J. Oliveira, A.J.S. Fernandes, R.F. Silva, J.R. Gomes, CVD diamond water lubricated tribosystems for high load planar sliding, Wear 265 (2008) 1023–1028.

[43] C.S. Abreu, M. Amaral, F.J. Oliveira, J.R. Gomes, R.F. Silva, HFCVD nanocrystalline diamond coatings for tribo–applications in the presence of water, Diamond and Related Materials 18 (2009) 271–275.

[44] L. Schafer, M. Hofer, R. Kroger, The versatility of hot–filament activated chemical vapor deposition, Thin Solid Films 515 (2006) 1017–1024.

[45] S.A. Catledge, P. Baker , J.T. Tarvin, Y.K. Vohra, Multilayer nanocrystalline/microcrystalline diamond films studied by laser reflectance interferometry, Diamond and Related Materials 9 (2000) 1512–1517.

[46] F. Sun, Y. Ma, B. Shen, Z. Zhang, M. Chen, Fabrication and application of nano–microcrystalline composite diamond films on the interior hole surfaces of Co cemented tungsten carbide substrates, Diamond and Related Materials 18 (2009) 276–282.

[47] E. Salgueiredo, F.A. Almeida, M. Amaral, A.J.S. Fernandes, F.M. Costa, R.F. Silva, F.J. Oliveira, CVD micro/nanocrystalline diamond (MCD/NCD) bilayer coated odonatological drill bits, Diamond and Related Materials 18 (2009) 264–270.

[48] N. Jiang, K. Sugimoto, K. Nishimura, Y. Shintani, A. Hiraki, Synthesis and structural study of nano/micro diamond overlayer films, Journal of Crystal Growth 242 (2002) 362–366.

[49] B. Shen, F. Sun, Deposition and friction properties of ultra–smooth composite diamond films on Co–cemented tungsten carbide substrates, Diamond and Related Materials 18 (2009) 238–243.

[50] E. Salgueiredo, F.A. Almeida, M. Amaral, M.A. Neto, F.J. Oliveira, R.F. Silva, A multilayer approach for enhancing the erosive wear resistance of CVD diamond coatings, Wear 297 (2013) 1064–1073.

[51] F.A. Almeida, M.M. Maru, M. Shabani, F.J. Oliveira, R.F. Silva, C.A. Achete, Enhancing the tribological performance under biodiesel lubrication using CVD diamond coated parts, Wear 302 (2013) 1370–1377.

[52] E. Salgueiredo, C.S. Abreu, M. Amaral, F.J. Oliveira, J.R. Gomes, R.F. Silva, Self–mated tribological systems based on multilayer micro/nanocrystalline CVD diamond coatings, Wear 303 (2013) 225–234.

[53] E. Salgueiredo, M. Amaral, F.A. Almeida, A.J.S. Fernandes, F.J. Oliveira, R.F. Silva, Mechanical performance upgrading of CVD diamond using the multilayer strategy, Surface and Coatings Technology 236 (2013) 380–387.

[54] N. Chen, B. Shen, G. Yang, F. Sun, Tribological and cutting behavior of silicon nitride tools coated with monolayer– and multilayer–microcrystalline HFCVD diamond films, Applied Surface Science 265 (2013) 850–859.

[55] R. Dumpala, M. Chandran, N. Kumar, S. Dash, B. Ramamoorthy, M.S. Ramachandra Rao, Growth and characterization of integrated nano– and microcrystalline dual layer composite diamond coatings on WC–Co substrates, International Journal of Refractory Metals and Hard Materials 37 (2013) 127–133.

[56] http://www.makino.com/about/news/cutting tools and market trends in the USA/175.

[57] G. Byrne, D. Dornfeld, B. Denkena, Advancing Cutting Technology, CIRP Annals–Manufacturing Technology 52(2) (2003) 483–507.

[58] R. Teti, Machining of composite materials, CIRP Annals–Manufacturing Technology 51(2) (2002) 611–634.

[59] F. Qin, J. Hu, Y.K. Chou, R.G. Thompson, Delamination wear of nano–diamond coated cutting tools in composite machining, Wear 267(5) (2009) 991–995.

[60] P. Philbin, S. Gordon, Characterization of the wear behavior of polycrystalline diamond (PCD) tools when machining wood–based composites, Journal of Materials Processing Technology 162 (2005) 665–672.

[61] X. Xiao, L.C. Lev, M.J. Lukitsch, Material transfer during machining of aluminum alloys with polycrystalline diamond cutting tools, Journal of Materials Processing Technology, 209(17) (2009) 5760–5765.

[62] http://www.glendower.co.uk/diamond–tipped–tooling.html.

[63] J.T. Lin, D. Bhattacharyya, C. Lane, Case study–machinability of a silicon carbide reinforced matrix composite aluminum metal, Wear 181–183 (1995) 883–888.

[64] J.P. Davim, A. Monteiro Baptista, Relationship between cutting force and PCD cutting tool wear in machining silicon carbide reinforced aluminum, Journal of Materials Processing Technology103 (2000) 417–423.

[65] N. Muthukrishnan, M. Murugan, K. Prahlada Rao, Machinability issues in turning of Al–SiC (10p) metal matrix composites, International Journal of Advanced Manufacturing Technology 39 (2007) 211–218.

[66] M. El–Gallab, M. Sklad, Machining of Al/SiC particulate metal–matrix composites Part I: Tool performance, Journal of Materials Processing Technology 83 (1998) 151–158.

[67] G.E. D'Errico, R. Calzavarini, Turning of metal matrix composites, Journal of Materials Processing Technology 119 (2001) 257–260.

[68] S. Durante, G. Rutelli, F. Rabezzana, Aluminum–based MMC machining with diamond–coated cutting tools, Surface and Coatings Technology 94–95 (1997) 632–640.

[69] K.D. Bouzakis, N. Michailidis, G. Skordaris, E. Bouzakis, D. Biermann, R. M'Saoubi, Cutting with coated tools: Coating technologies, characterization methods and performance optimization, CIRP Annals–Manufacturing Technology 61 (2012) 703–723.

[70] A. Shokrani, V. Dhokia, S.T. Newman, Environmentally conscious machining of difficult–to–machine materials with regard to cutting fluids, International Journal of Machine Tools and Manufacture 57 (2012) 83–101.

[71] M. Schwander, K. Partes, A review of diamond synthesis by CVD processes, Diamond and Related Materials 20(9) (2011) 1287–1301.

[72] J.P. Davim, F. Mata, Chemical vapor deposition (CVD) diamond coated tools performance in machining of PEEK composites, Materials and Design 29(8) (2008) 1568–1574.

[73] Q. Liang, Y.K. Vohra, R.G. Thompson, High speed continuous and interrupted dry turning of A390 Aluminum/Silicon Alloy using nanostructured diamond coated WC–6 wt.% cobalt tool inserts by MPCVD, Diamond and Related Materials 17(12) (2008) 2041–2047.

[74] J.Y. Sheikh–Ahmad, J.S. Stewart, H. Feld, Failure characteristics of diamond–coated carbides in machining wood–based composites, Wear 255(7) (2003) 1433–1437.

[75] D. Zhang, B. Shen, F. Sun, Study on tribological behavior and cutting performance of CVD diamond and DLC films on Co–cemented tungsten carbide substrates, Applied Surface Science 256(8) (2010) 2479–2489.

[76] J. Hu, Y.K. Chou, R.G. Thompson, On stress analysis of diamond coating cutting tools, Transactions of the North American Manufacturing Research Institute of SME 35 (2009) 177–184.

[77] S. Hogmark, S. Jacobson, M. Larsson, Design and evaluation of tribological coatings, Wear 246 (2000) 20–33.

[78] http://www.sp3diamondtech.com/products.php.

[79] R.P. Martinho, F.J.G. Silva, A.P.M. Baptista, Cutting forces and wear analysis of Si_3N_4 diamond coated tools in high speed machining, Vacuum 82(12) (2006) 1415–1420.

[80] N. Chen, F. Sun, Cutting performance of multilayer diamond coated silicon nitride inserts in machining aluminium–silicon alloy, Transactions of Nonferrous Metals Society of China 23 (2013) 1985−1992.

[81] A. Kopf, S. Feistritzer, K. Udier, Diamond coated cutting tools for machining of non–ferrous metals and fiber reinforced polymers, International Journal of Refractory Metals and Hard Materials 24 (2006) 354–359.

[82] R. Dumpala, M. Chandran, S. Madhavan, B. Ramamoorthy, M.S. Ramachandra Rao, High wear performance of the dual–layer graded composite diamond coated cutting tools, International Journal of Refractory Metals and Hard Materials 48 (2015) 24–30.

[83] F.A. Almeida, A.J.S. Fernandes, R.F. Silva, F.J. Oliveira, Re–sharpenable thick CVD diamond–coated Si_3N_4 tools for hardmetal turning, Surface and Coatings Technology 201 (2006) 1776–1782.

[84] F.A. Almeida, A.J.S. Fernandes, F.J. Oliveira, R.F. Silva, Semi–orthogonal turning of hardmetal with CVD diamond and PCD inserts at different cutting angles, Vacuum 83 (2009) 1218–1223.

[85] G. Castro, F.A. Almeida, F.J. Oliveira, A.J.S. Fernandes, J. Sacramento, R.F. Silva, Dry machining of silicon–aluminum alloys with CVD diamond brazed and directly coated Si_3N_4 ceramic tools, Vacuum 82 (2008) 1407–1410.

[86] F.A. Almeida, F.J. Oliveira, M. Sousa, A.J.S. Fernandes, J. Sacramento, R.F. Silva, Machining hardmetal with CVD diamond direct coated ceramic tools: effect of tool edge geometry, Diamond and Related Materials 14 (2005) 651–656.

[87] F.A. Almeida, M. Amaral, F.J. Oliveira, R.F. Silva, Machining behavior of silicon nitride tools coated with micro–, submicro– and nanometric HFCVD diamond crystallite sizes, Diamond and Related Materials 15 (2006) 2029–2034.

[88] Z.P. Luo, Y.G. Song, S.Q. Zhang, A TEM study of the microstructure of SiC_p/Al composite prepared by pressureless infiltration method, Scripta Materialia 45 (2001) 1183–1189.

[89] K.N. Tandon, Z.C. Feng, X.Y. Li, Wear behavior of SiC particulate reinforced aluminum composites sliding against steel balls under dry and lubricated conditions, Tribology Letters 6 (1999) 113–122.

[90] S.A. Sajjadia, H.R. Ezatpoura, M. Torabi Parizib, Comparison of microstructure and mechanical properties of A356 aluminum alloy/Al_2O_3 composites fabricated by stir and compo–casting processes, Materials and Design 34 (2012) 106–111.

[91] L. Iuliano, L. Settineri, A. Gatto, High–speed turning experiments on metal matrix composites, Composites Part A 29 (1998) 1501–1509.

[92] J.P. Davim, Diamond tool performance in machining metal–matrix composites, Journal of Material Processing Technology 128 (2002) 100–105.

[93] P. K. Jain, S.C. Soni, P.V. Baredar, Review on machining of aluminum metal matrix composites, Material Science Research India 11(2) (2014) 114–120.

[94] Y. Sahin, M. Kok, H. Celik, Tool wear and surface roughness of Al_2O_3 particle–reinforced aluminum alloy composites, Journal of Materials Processing Technology 128 (2002) 280–291.

[95] Y.K. Chou, J. Liu, CVD diamond tool performance in metal matrix composite machining, Surface and Coatings Technology 200 (2005) 1872–1878.

[96] C.H. Shen, The importance of diamond coated tools for agile manufacturing and dry machining, Surface and Coatings Technology 86–87 (1996) 672–677.

[97] T.C.S. Vandevelde, K. Vandierendonck, M. Van Stappen, W. Du Mong, P. Perremans, Cutting applications of DLC, hard carbon and diamond films, Surface and Coatings Technology 113 (1999) 80–85.

[98] R. Polini, F. Casadei, P. D'Antonio, E. Traversa, Dry turning of alumina/aluminum composites with CVD diamond coated Co–cemented tungsten carbide tools, Surface and Coatings Technology 166 (2003) 127–134.

[99] K. Kanda, S. Takehana, S. Yoshida, R. Watanabe, S. Takano, H. Ando, F. Shimakura, Application of diamond–coated cutting tools, Surface and Coating Technology 73 (1995) 115–120.

[100] E.J. Oles, A. Inspektor, C.E. Bauer, The new diamond–coated carbide cutting tools, Diamond and Related Materials 5 (1996) 617–624.

[101] A. Kremer, A. Devillez, S. Dominiak, D. Dudzinski, M. El Mansori, Machinability of Al/SiC particulate metal–matrix composites under dry conditions with CVD diamond coated carbide tools, Machining Science and Technology 12 (2008) 214–233.

[102] B. Shen, F.H. Sun, The cutting performance of ultra–smooth composite diamond coated WC–Co inserts in dry turning Al/SiC–MMC, Advanced Materials Research 325 (2011) 400–405.

[103] http://www.pumpsandsystems.com.

[104] P.J. Kelly, R.D. Arnell, M.D. Hudson, A.E.J. Wilson, G. Jones, Enhanced mechanical seal performance through CVD diamond films, Vacuum 61(1) (2001) 61–74.

[105] M. Huebner, Material selection for mechanical seals, Proceedings of the 22nd International Pump Users Symposium, February 28–March 3; 2005, Houston, Texas, USA.

[106] W. Schuebl, Mechanical seals for high face speed applications, Proceedings of 12th turbomachinery symposium, November 1983, Texas, USA.

[107] K. Wakely, Mechanical seals–some improvements in face materials, Tribology International 19 (4) (1986) 198–203.

[108] J.M. Carrapichano, J.R. Gomes, F.J. Oliveira, R.F. Silva, Si_3N_4 and Si_3N_4/SiC composite rings for dynamic sealing of circulating fluids, Wear 255 (2003) 695–698.

[109] J. Wang, Q. Jia, X. Yuan, Sh. Wang, Experimental study on friction and wear behavior of amorphous carbon coatings for mechanical seals in cryogenic environment, Applied Surface Science 258 (2012) 9531–9535.

[110] J.M. Carrapichano, F.J. Oliveira, R.F. Silva, J.R. Gomes, Functionality diagrams for hybrid mechanical seals with silicon nitride Rings, Journal of the American Ceramic Society 88(8) (2005) 2177–2180.

[111] A.M. Kovalchenko, J.W. Elam, A. Erdemir, J.A. Carlisle, O. Auciello, J.A. Libera, M.J. Pellin, D.M. Gruen, J.N. Hryn, Development of ultra–nanocrystalline diamond (UNCD) coatings for multipurpose mechanical pump seals, Wear 270 (2011) 325–331.

[112] P. Hollman, H. Bjorkman, A. Alahelisten, S. Hogmark, Diamond coatings applied to mechanical face seals, Surface and Coatings Technology 105 (1998) 169–174.

[113] M.A. Tome, A.J.S. Fernandes, F.J. Oliveira, R.F. Silva, J.M. Carrapichano, High performance sealing with CVD diamond self–mated rings, Diamond and Related Materials 14 (2005) 617–621.

[114] F. Mubarok, J.M. Carrapichano, F.A. Almeida, A.J.S. Fernandes, R.F. Silva, Enhanced sealing performance with CVD nanocrystalline diamond films in self–mated mechanical seals, Diamond and Related Materials 17 (2008) 1132–1136.

[115] A.V. Sumant, A.R. Krauss, D.M. Gruen, O. Auciello, Ultrananocrystalline diamond film as a wear resistant and protective coating for mechanical seal applications, Tribology Transactions 48 (2005) 24–31.

[116] G.A. Jones, On the tribological behavior of mechanical seal face materials in dry line contact Part I. mechanical carbon, Wear 256 (2004) 415–432.

[117] G.A. Jones, On the tribological behavior of mechanical seal face materials in dry line contact Part II: bulk ceramics, diamond and diamond–like carbon films, Wear 256 (2004) 433–455.

[118] B.R. Lawn, A.G. Evans, D.B. Marshall, Elastic/plastic indentation damage in ceramics: the median/radial crack system, Journal of American Ceramic Society 63(9–10) (1980) 574–571.

[119] K. Niihara, R. Morena, D.P.H. Hasselman, Evaluation of K_{1C} of brittle solids by the indentation method with low crack–to–indent ratios, Journal of Materials Science Letters 1 (1982) 13–16.

[120] G.R. Anstis, P. Chantikul, B.R. Lawn, D.B. Marshall, A critical evaluation techniques for measuring fracture toughness: I, direct crack measurements, Journal of the American Ceramic Society 64(9) (1981) 533–538.

[121] A.G. Evans, E.A. Charles, Fracture toughness determination by indentation, Journal of the American Ceramic Society 59(7–8) (1976) 371–372.

[122] D.K. Shetty, I.G. Wright, P.N. Mincer, A.H. Clauer, Indentation fracture of WC–Co cermets, Journal of Materials Science 20 (1980) 1873–1882.

[123] Basic nomenclature and definitions for single–point cutting tools (American National Standard B94.50–1975) (1975).

[124] T. Honma, Y. Ukyo, Sintering process of Si_3N_4 with Y_2O_3 and Al_2O_3 as sintering additives, Journal of Materials Science Letters 18 (1999) 735–737.

[125] J.F. Yang, T. Ohji, Influence of Yttria–Alumina Content on sintering behavior and microstructure of silicon nitride ceramics, Journal of American Ceramic Society 83(8) (2000) 2094–2096.

[126] E.Y. Sun, P.F. Becher, K.P. Plucknett, Ch.H. Hsueh, K.B. Alexander, Sh. B. Waters, Microstructural design of silicon nitride with improved fracture toughness: II, effects of Yttria and Alumina additives, Journal of American Ceramic Society 81(11) (1998) 2831–2840.

[127] M.H. Bocanegra–Bernal, B. Matovic, Mechanical properties of silicon nitride–based ceramics and its use in structural applications at high temperatures, Materials Science and Engineering A 527(6) (2010) 1314–1338.

[128] S. Funfschilling, T. Fett, M.J. Hoffmann, R. Oberacker, T. Schwind, J. Wippler, T. Bohlke, H. Ozcoban, G.A. Schneider, P.F. Becher, J.J. Kruzic, Mechanisms of toughening in silicon nitrides: the roles of crack bridging and microstructure, Acta Materialia 59(10) (2011) 3978–3989.

[129] P.F. Becher, E.Y. Sun, K.P. Plucknett, K.B. Alexander, Ch.H. Hsueh, H.T. Lin, Sh. B. Waters, C.G. Westmoreland, Microstructural design of silicon nitride with improved fracture toughness: I, effects of grain shape and size, Journal of American Ceramic Society 81(11) (1998) 2821–2830.

[130] K. Komeya, Y. Haruna, T. Meguru, Oxidation behaviour of Si_3N_4–Y_20_3–Al_2O_3 system the sintered, Journal of Materials Science 27 (1992) 5727–5734.

[131] H. Miyazaki, H. Hyuga, Y. Yoshizawa, K. Hirao, T. Ohji, Crack profiles under a Vickers indent in silicon nitride ceramics with various microstructures, Ceramics International 36 (2010) 173–179.

[132] A. C. Ferrari, J. Robertson, Interpretation of Raman spectra of disordered and amorphous carbon, Physical Review B 61 (1999) 14095–14107.

[133] A. Kromka, J. Breza, M. Kadlecikova, J. Janik, F. Balon, Identification of carbon phases and analysis of diamond/substrate interfaces by Raman spectroscopy, Carbon 43 (2005) 425–429.

[134] A.C. Ferrari, J. Robertson, Origin of the 1150 cm^{-1} Raman mode in nanocrystalline diamond, Physical Review B 63 (2001) 1214051–1214054.

[135] A.C. Ferrari, J. Robertson, Raman spectroscopy of amorphous, nanostructured, diamond–like carbon, and nanodiamond, Philosophical Transactions of the Royal Society A 362 (2004) 2477–2512.

[136] F.H. Sun, Z.M. Zhang, M. Chen, H.S. Shen, Improvement of adhesive strength and surface roughness of diamond films on Co–cemented tungsten carbide tools, Diamond and Related Materials 12 (2003) 711–718.

[137] F.A. Almeida, F.J. Oliveira, R.F. Silva, D.L. Baptista, S.B. Peripolli, C.A. Achete, High resolution study of the strong diamond/silicon nitride interface, Applied Physics Letters 98 (2011) 171913.

[138] M. Nesladek, K. Vandierendonck, C. Quaeyhaegens, M. Kerkhofs, L.M. Stals, Adhesion of diamond coatings on cemented carbides, Thin Solid Films 270 (1995) 184–188.

[139] K. Mallika, R. Komanduri, Low pressure microwave plasma assisted chemical vapor deposition (MPCVD) of diamond coatings on silicon nitride cutting tools, Thin Solid Films 396 (2001) 145–165.

[140] D.M. Gruen, Nanocrystalline diamond films, Annual Review of Materials Science 29 (1999) 211–259.

[141] N. Kumar, R. Ramadoss, A.T. Kozakov, K.J. Sankaran, S. Dash, A.K. Tyagi, N.H. Tai, I–Nan Lin, Humidity–dependent friction mechanism in an ultrananocrystalline diamond film, J. Phys. D: Applied Physics 46 (2013) 275501(1)–275501(8).

[142] J.J. Mares, P. Hubik, J. Kristofik, J. Ristein, P. Strobel, L. Ley, Influence of ambient humidity on the surface conductivity of hydrogenated diamond, Diamond & Related Materials 17 (2008) 1356–1361.

[143] D.S. Grierson, A.V. Sumant, Tribochemistry and material transfer for the ultrananocrystalline diamond–silicon nitride interface revealed by x–ray photoelectron emission spectromicroscopy, Journal of Vacuum Science & Technology B 25(5) 1700–1705.

[144] X. Chen, T. Kato, M. Kawaguchi, M. Nosaka, J. Choi, Structural and environmental dependence of superlow friction in ion vapour–deposited a–C:H:Si films for solid lubrication application, J. Phys. D: Applied Physics 46 (2013) 255304(1)–255304(11).

[145] A. R. Konicek, D. S. Grierson, P. U. P. A. Gilbert, W. G. Sawyer, A.V. Sumant, R.W. Carpick, Origin of Ultralow Friction and Wear in Ultrananocrystalline Diamond, Physical Review Letters 100 (2008) 235502(1)–235502(4).

[146] A. Skopp, D. Klaffke, Aspects of tribological testing of diamond coatings, Surface and Coatings Technology 98 (1998) 1027–1037.

[147] A.R. Konicek, C. Jaye, M.A. Hamilton, W.G. Sawyer, D.A. Fischer, R.W. Carpick, Near–Edge X–ray absorption fine structure imaging of spherical and flat counterfaces of ultrananocrystalline diamond tribological contacts: a correlation of surface chemistry and friction, Tribology Letters 44 (2011) 99–106.

[148] B. Bhushan, A.V. Kulkarni, Effect of normal load on microscale friction measurements, Thin Solid Films 278 (1996) 49–56.

[149] C.S. Abreu, F.J. Oliveira, M. Belmonte, A.J.S. Fernandes, J.R. Gomes, R.F. Silva, CVD diamond coated silicon nitride self–mated systems: tribological behaviour under high loads, Tribology Letters, 21(2) (2006) 141–151.

[150] M. Amaral, C.S. Abreu, A.J.S. Fernandes, F.J. Oliveira c, J.R. Gomes, R.F. Silva, Nanodiamond–based tribosystems, Surface & Coatings Technology 204 (2010) 1962–1969.

[151] M. Amaral, C.S. Abreu, F.J. Oliveira, J.R. Gomes, R.F. Silva, Biotribological performance of NCD coated Si_3N_4–bioglass composites, Diamond & Related Materials 16 (2007) 790–795.

[152] M. Amaral, C.S. Abreu, F.J. Oliveira, J.R. Gomes, R.F. Silva, Tribological characterization of NCD in physiological fluids, Diamond & Related Materials 17 (2008) 848–852.

[153] S.J. Bull, Tribology of carbon coatings: DLC, diamond and beyond, Diamond and Related Materials 4 (1995) 827–836.

[154] C. Wild, R. Kohl, N. Herres, W. Muller–Sebert, P. Koidl, Oriented CVD diamond films: twin formation, structure and morphology, Diamond and Related Materials 3 (1994) 373–381.

[155] M.I. De Barros, L. Vandenbulcke, J. Fontaine, G. Farges, M. Vayer, R. Erre, Tribological performance of diamond–coated Ti–6Al–4V alloy with respect to diamond characteristics, Surface and Coatings Technology 127 (2000) 193–202.

[156] I.A. Polonsky, T.P. Chang, L.M. Keer, W.D. Sproul, An analysis of the effect of hard coatings on near–surface rolling contact fatigue initiation induced by surface roughness, Wear 208 (1997) 204–219.

[157] C.P.O. Treutler, Industrial use of plasma–deposited coatings for components of automotive fuel injection systems, Surface and Coatings Technology 200 (2005) 1969–1975.

[158] Standard Test Method for Wear Testing with a Pin–on–Disk Apparatus, ASTM G 99–105.

[159] J.R Gomes, F.J Oliveira, R.F Silva, M.I Osendi, P Miranzo, Effect of α–/β Si_3N_4–phase ratio and microstructure on the tribological behaviour up to 700°C, Wear 239 (2000) 59–68.

[160] D. Klaffke, A. Skopp, Are thin hard coatings (TiN, DLC, diamond) beneficial in tribologically stressed vibrational contacts? – Effects of operational parameters and relative humidity, Surface and Coatings Technology 98 (1998) 953–961.

[161] M. V Ramesh, W.B. Lee, C.F. Cheung, K.C. Chan, A parametric analysis of cutting forces in single–point diamond turning of Al6061/SiCp metal matrix composites (MMCs) forces in single–point diamond turning, Mater. Manuf. Process. 16 (2001) 61–78.

[162] V.P. Astakhov, The assessment of cutting tool wear, International Journal of Machine Tools and Manufacture 44 (2004) 637–647.

[163] N.P. Hung, F.Y.C. Boey, K.A. Khor, Y.S. Phua, H.F. Lee, Machinability of aluminum alloys reinforced with silicon carbide particulates, Journal of Materials Processing Technology 56 (1996) 966–977.

[164] A. Schade, S.M. Rosiwal, R.F. Singer, Influence of surface topography of HF–CVD diamond films on self–mated planar sliding contacts in dry environments, Surface & Coatings Technology 201 (2007) 6197–6205.

[165] M. Perle, C. Bareiss, S.M. Rosiwal, R.F. Singer, Generation and oxidation of wear debris in dry running tests of diamond coated SiC bearings, Diamond & Related Materials 15 (2006) 749–753.